JAERI 1293

JAERI 1293

Models of Multi-rod Code FRETA-B for Transient Fuel Behavior Analysis (Final Version)

November 1984

日 本 原 子 力 研 究 所

Japan Atomic Energy Research Institute

JAERIレポートは，日本原子力研究所が研究成果編集委員会の審査を経て不定期に公刊している研究報告書です。

入手の問合わせは，日本原子力研究所技術情報部情報資料課（〒319-11茨城県那珂郡東海村）あて，お申しこしください。なお，このほかに財団法人原子力弘済会資料センター（〒319-11 茨城県那珂郡東海村日本原子力研究所内）で複写による実費頒布をおこなっております。

JAERI reports are reviewed by the Board of Editors and issued irregularly.

Inquiries about availability of the reports should be addressed to Information Division Department of Technical Information, Japan Atomic Energy Research Institute, Tokai-mura, Naka-gun, Ibaraki-ken 319-11, Japan.

編集兼発行　日本原子力研究所
印　　刷　いばらき印刷㈱

Models of Multi-rod Code FRETA-B for Transient Fuel Behavior Analysis (Final Version)

Masaaki Uchida and Naoaki Otsubo*

Department of Nuclear Safety Research
Tokai Research Establishment
Japan Atomic Energy Research Institute
Tokai-mura, Naka-gun, Ibaraki-ken, Japan

Received April 6, 1984

Abstract

This paper is a final report of the development of FRETA-B code, which analyzes the LWR fuel behavior during accidents, particularly the Loss-of-Coolant Accident (LOCA).

The very high temperature induced by a LOCA causes oxidation of the cladding by steam and, as a combined effect with low external pressure, extensive swelling of the cladding. The latter may reach a level that the rods block the coolant channel. To analyze these phenomena, single-rod model is insufficient; FRETA-B has a capability to handle multiple fuel rods in a bundle simultaneously, including the interaction between them. In the development work, therefore, efforts were made for avoiding the excessive increase of calculation time and core memory requirement.

Because of the strong dependency of the in-LOCA fuel behavior on the coolant state, FRETA-B has emphasis on heat transfer to the coolant as well as the cladding deformation. In the final version, a capability was added to analyze the fuel behavior under reflooding using empirical models.

The present report describes the basic models of FRETA-B, and also gives its input manual in the appendix.

Keywords: Fuel, Code, LOCA, Ballooning, Shell Model, Heat Transfer, Reflooding, Gas Flow, FRETA-B, Reactor Safety, LWR

* Century Research Center Corp.

複数燃料棒の過渡挙動解析コードFRETA-B (最終バージョン)の解析モデル

日本原子力研究所東海研究所安全工学部

内田　正明・大坪　直昭*

(1984年4月6日受理)

要　　旨

本報告は，冷却水喪失事故（LOCA）を中心とする軽水炉事故時における燃料挙動を解析するコードFRETA−Bの開発に関する最終報告である．

LOCA時に燃料被覆管は，通常時に比してきわめて高温状態に達する．このために水蒸気による酸化が起こると共に，外圧の低下に伴って大きなふくれが生じ，場合によっては，冷却材流路の閉塞に至る可能性がある．これらの現象を解析するには，単一の燃料棒で炉心またはバンドル全体を代表させる方法では不十分である．このためFRETA−Bにはバンドル（の一部）を構成する複数の燃料棒をそれらの相互作用を含めて同時解析する機能を持たせた．したがって開発にあたっては，これによる計算時間と記憶容量の増大を抑制することに注意を払った．

LOCA時の燃料挙動は，冷却材の状態に大きく依存する．このためFRETA−Bは，燃料棒の変形とならんで冷却材への伝熱を重点項目としている．最終バージョンでは，再冠水進行下の挙動も経験的モデルにより解析する機能を加えた．

本報告は，FRETA−Bのモデルを概説すると共に，入力マニュアルを付録として含めた．

* センチュリー・リサーチ・センター

CONTENTS

目　　次

List of Tables and Figures

1. Introduction

FRETA-B (Fuel Reliability Evaluation Code for Transients and Accidents - Bundle Geometry) is a computer code for analyzing the behavior of zircaloy-clad oxide fuel rods for light water reactors. It is specialized in the fuel behavior during accidents, particularly the Loss-of-Coolant Accident (LOCA).

The phenomena expected to be important during LOCA are roughly grouped into four: heat transfer, oxidation of cladding, fuel rod deformation, and internal gas pressure and flow. Some of these phenomena can be analyzed independently for each rod, whereas for some others rod-to-rod or rod-to-structural component interaction must be considered. Swelling of fuel rod due to reduced external pressure and high temperature (ballooning) is restricted by the contact with surrounding fuel rods or shroud. Even if the rod has ruptured before contact, hoop strain at rupture is determined by azimuthal temperature difference which is affected by rod-rod radiative heat transfer. Consideration of such multi-rod effect requires two-dimensional modeling for the phenomena in each rod.

The code first started as a single-rod, one-dimensional code FREG-3T[1]. At the time, famous US code FRAP-T had already existed, which remained single-rod code until the development was completed at FRAP-T6[2]. As integral multi-rod code, there exists, other than FRETA-B, only a British code MABEL[3] developed in AEE Winfrith. However, the two codes have taken different approaches to deal with the multi-rod effect. MABEL model is essentially a 'single rod sorrounded by eight rods' model. The heat transfer and deformation models for the central rod of 3 X 3 lattice is two-dimensional: azimuthal variation of state is evaluated at 12 azimuthal nodes.

On the other hand, in FRETA-B it was tried to deal with a bundle with arbitrary shape and size by combining subchannel elements. In exchange for the increased number of fuel rods for analysis, the number of azimuthal nodes was restricted to the minimum number, four, each of which faces different coolant subchannels (in ballooning model, 20 nodes are used whose temperatures are interpolated from the four-node results of thermal analysis). To supress the increase of running time, use of two-dimensional model in each fuel rod was restricted to heat conduction and ballooning; for other phenomena, one-dimensional models are independently applied at four azimuthal nodes. Other measures taken to save running time are summarized in Chapter 7.

Figure 1 lists main subroutines of FRETA-B with brief description of their functions. It shows how they are arranged in the time and space loops.

The basic models of FRETA-B have been described in the previous report[4]. Considerable updating of the code have been made since then. Important changes are solution of heat conduction equation by the method of weighted residuals in place of the finite difference method (3.6), incorporation of rod-rod contact model (5.7), and of reflood heat transfer model (3.8). The present report is intended as the final report of the code development. It describes the analytical models of the code. Experiences of code assessment are summarized in Chapter 7. Input manual is given in Appendix A.

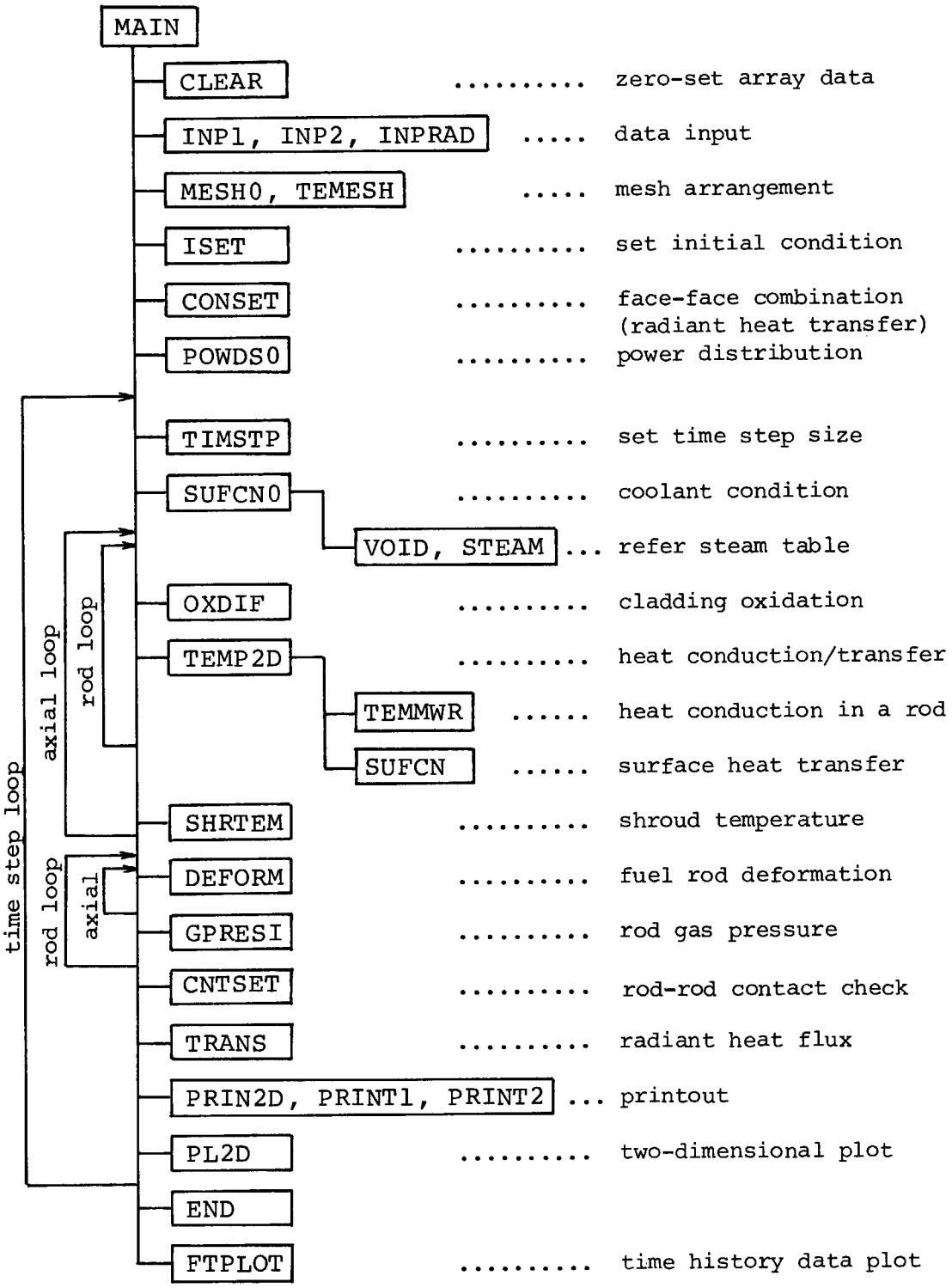

Fig. 1 Main subroutines of FRETA-B.

2. Geometrical Model and Time Step

The solid components of a fuel bundle considered in FRETA-B are fuel rod, empty tube in fuel rod position, and (shroud) plate in inter-rod position; the code has no model for grid spacers. The effects of such components as water rod or guide tube on the fuel behavior can be approximated by substituting such components with the empty tube model of which thermal properties can be assigned by input.

From the coolant side, the basic unit of geometry is a subchannel bounded by four fuel rods. The geometry of a bundle comprising many fuel rods is defined by specifying which rods bound which subchannel.

Each fuel rod is divided into axial segments; each segment is then divided into four azimuthal sectors; finally the state of each sector is evaluated at radial nodes. Fuel states in a bundle vary both in axial and transverse directions. But the gradient of any state variable takes quite different values in the two directions: for example, it can occur under postulated LOCA that a cladding temperature difference of 50 K is found over 0.5 m interval axially, while the same difference is realized between two opposite sides of a rod cross section, 12 mm apart. It means that when two-dimensional modeling is to be made, it must be made in the transverse directions, neglecting the axial change of state.

In FRETA-B whose analytical models are at most two-dimensional, two principal coordinates are radial and azimuthal. Division of a bundle into axial segments is principally for independent calculation of axial state changes (an exception is gas flow in the fuel-cladding gap for which all axial segments must be considered simultaneously). In other words, FRETA-B grasps a bundle geometry primarily through its transverse cross section and regards the whole bundle as a stack of such cross sections (**Fig. 2**).

Various shapes of subchannel model are prepared to simulate various parts of a bundle (cross section). As an example, **Fig. 3** shows how an imaginary 2 X 2 rod bundle can be defined by a combination of six subchannels of four different types. Each subchannel is bounded by face elements which comprise both actual solid surfaces and imaginary faces. The code does not realize the shape of the entire bundle; the only informations necessary for calculation are such as that, in **Fig. 3** example, subchannels 2 and 4 share a face element 21 and hence they are adjacent to each other, or, sector 4 of rod 1 faces subchannel 2, and so forth. Subchannels 1 and 4 in **Fig. 3** are special types that are prepared for reducing the geometry for analysis utilizing symmetry relationship. The actual procedure of defing a bundle geometry using these elements is described in detail in Appendix A.

FRETA-B analyzes the transient fuel state changes which occur in a relatively small time period, typical period for postulated LOCA being several hundred seconds. Time zero is set to be the onset of transient at which time fuel is normally on power. The actual power history before the time zero is too long to accurately follow by a transient code. FRETA-B therefore postulates an imaginary power ramp period starting from -100 s. Power is hypothetically raised to the initial steady level in one second and then the resultant transient fuel state changes such as temperature or gas pressure are calculated following time steps until time zero. Since the time constants for reversible fuel state changes are smaller than 10 s, a steady state is realized before time zero. If the fuel for analysis had received long-term irradiation, the fuel state changes before the transient should be calculated by separate fuel codes and the results be input as room-temperature conditions.

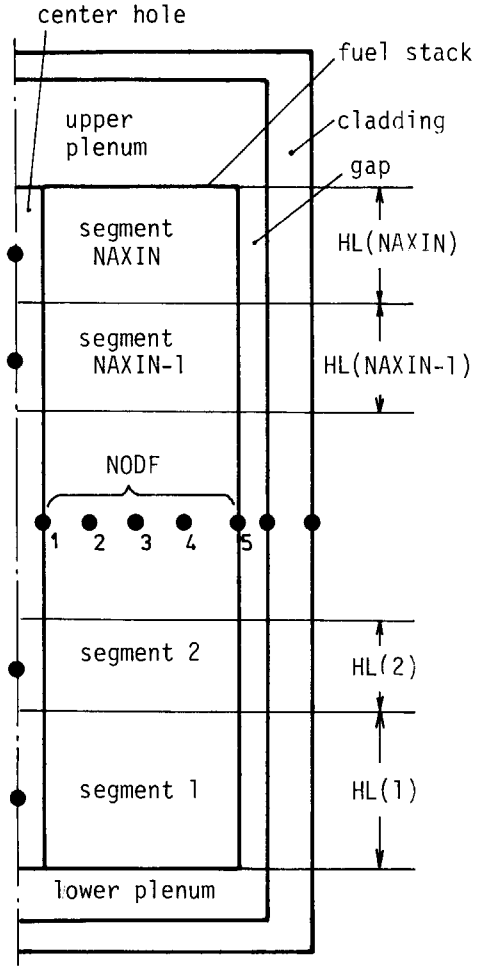

Fig. 2 Axial and radial nodes (fuel state is evaluated at the dots).

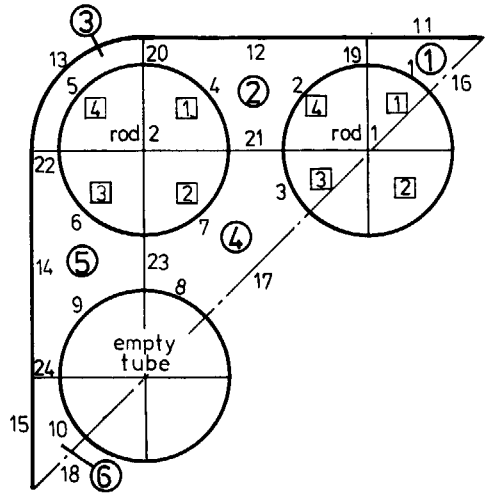

Fig. 3 Sample bundle geometry with rod number, channel number and face element number.

To suppress the increase of running time due to multi-rod modeling, FRETA-B manages time step in two ways. The first is automatic time step redivision which is applied to the entire time step loop. Fuel temperature jump in a time step is monitored at all nodes of the bundle and when it is found to have exceeded the input-specified limiting value, all calculation results in the step are cancelled and the step size is reduced from the input value according to the fraction of the excess. Thus user can specify coarse time step size expecting the code to modify it where necessary, at least from the viewpoint of thermal stability (**Fig. 4**).

The second measure is the use of local time step. Some phenomena can proceed very rapidly without much influencing other phenomena. A typical example is the last stage of ballooning: just before rupture, cladding can swell at a rate greater than 10^3 %/s. Thermal state is virtually frozen during such a fast transient. In such a case, reduced local time step is applied for calculating the deformation and gas flow in the rod in problem, and rod-rod contact sheck. Similar treatment is also made for following the stress relaxation in the cladding induced by pellet-clad interaction.

Within each time step, no iteration is made between the calculation results of different subcodes: for example, mechanical subcode is called after thermal subcode and the calculated deformations are not reflected to the thermal state of the present step, but to the state in the next step. It does not cause any serious problem in calculating a transient because by far the most important parameter governing any fuel state change is temperature and the time step size is so controled as to keep the temperature jump small enough.

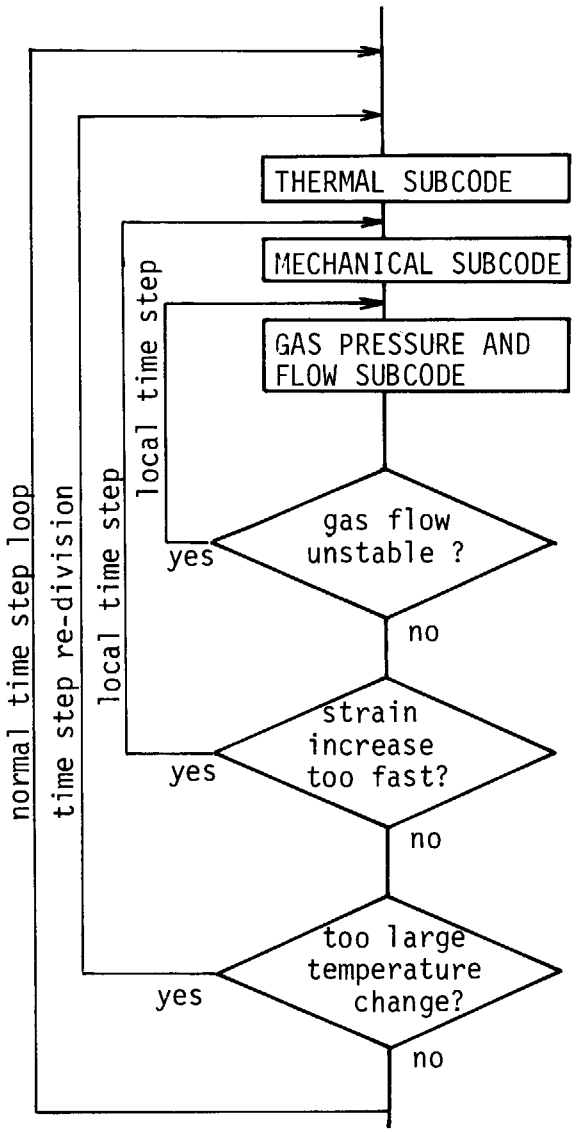

Fig. 4 Time step loops.

3. Thermal Models

3.1 Scope

The thermal calculation of FRETA-B can either be limited to the heat conduction within each rod, or extended to include a simplified treatment of coolant enthalpy rise along the fuel rods. A key input parameter MODSHT determines the scope of thermal calculation and necessary boundary conditions:

MODSHT = 1 heat conduction within each rod is calculated with input cladding temperature history,

= 2 rod surface heat transfer (conductive and radiative) is calculated with input axially-uniform coolant enthalpy and mass flux,

= 3 local coolant state is calculated from input inlet or outlet coolant condition data,

= 4 cladding temperature is calculated using input local coolant temperature and heat transfer coefficient,

= 5 same as MODSHT = 2, but local coolant data are input.

Two-dimensional heat conduction in each fuel rod is calculated under all the above five options. Radiative and conductive heat transfer at rod surface is calculated under options 2, 3, and 5. When reflooding process is included in the transient, a special empirical model can be used under the option MODSHT = 3, detail of which is described in 3.8. Simplified heat transfer models are provided also for such heat sinks as external shroud, water rod, and control rod guide tube; the models are described in 3.9.

3.2 Heat Source Terms

Heat sources considered in FRETA-B are, 1) prompt fission heat, 2) delayed fission heat, 3) decay heat after shutdown, and 4) metal-water reaction heat in the cladding. The last one is described in Chapter 4. For the first three, three input options are provided:

1) total power history table is input,
2) delayed fission heat is calculated and used together with the ANS 1978 standard table for the decay heat[5] after 10^{13} s irradiation,
3) the ANS standard table is used alone with a multiplication factor of 1.2.

Delayed fission power is given as a fraction to the initial prompt fission power P_0 by

$$P_n(t)=P_1\sum_i^6 [A_i \exp(-0.693\, t/\tau_i)] \tag{3.1}$$

$$\frac{P_1}{P_0}=\frac{\beta}{\beta+\rho_{sm}} \tag{3.2}$$

where $P_n(t)$ is delayed fission heat, β is the fraction of total delayed neutron (0.007). Scram reactivity ρ_{sm} differs from reactor to reactor and can be input. The terms A_i and τ_i are the fraction and half life(s), respectively, of the i-th precurser nuclide and stored in the code.

Heat generation rate from the above sources is expressed in the form

$$P(n,\theta,r,z,t)=\overline{P}_0(n)\cdot f(\theta,n)\cdot g(r)\cdot h(z)\cdot p(t) \tag{3.3}$$

where n is rod number; θ represents azimuthal sectors; r is radius; z is axial elevation (segments) and t is time. $\overline{P_0}(n)$ is the average linear heat rating of rod n at time zero. Equation (3.3) means that sectorwise power fraction can be given independently in each rod, but that axial and radial power shapes (relative) are common to all rods and also the time dependency is common to every local power.

3.3 Coolant Conditions

When local coolant enthalpy is to be calculated from the input inlet enthalpy under the option MODSHT = 3, some hydraulic calculations are inevitable. However, since FRETA-B is a fuel behavior code, general modeling of hydraulic process is out of the scope: coolant flow state is considered to the extent that it makes a significant effect on fuel temperature. The present model is essentially a slight modification of the stationary heat balance model.

The following approximations are made:

1) in each time step, flow state is assumed to be stationary, and hence mass flow rate be uniform from inlet to outlet,
2) all subchannels are either regarded as independent conduits, or assumed to have same enthalpy by option,
3) when the input mass velocity is very small (less than 3 kg/m^2 s), hydraulic calculation is not made; local coolant temperature is simply set equal to the average of surrounding rod surface temperatures in the previous time step. It is nearly equal to assuming an adiabatic boundary condition for heat conduction in each rod.
4) pressure is everywhere uniform.

For the ease of description in this section, the concept of fuel axial segment is extended to include coolant channels, and its axial boundary is called 'node', as illustrated in **Fig. 5**. Noting a subchannel, local enthalpy is expressed as a function of elevation z (m) and time $t(s)$ as $H(z,t)$ (J/kg), and given by

$$H(z,t)=H(o,t_{in})+\int_{t_{in}}^{t}\frac{V(z')Q(z')}{S(z')}\,d\tau \tag{3.4}$$

where $H(o,t)$ is inlet (outlet when flow is reversed) enthalpy; t_{in} is the time at which the coolant left the inlet; V (specific volume, m^3/kg), Q (total heat inflow to the unit length of subchannel, W/m), and S (flow area, m^2) are functions of the elevation z' which is the instantaneous location of the coolant as it flows from the inlet to elevation z.

If we notice the flow of coolant from the beginning of the present time step t_o to the end of the step $t_o+\Delta t$, then we get, instead of (3.4),

$$H(z,t_o+\Delta t)=H(z_o,t_o)+\int_{t_o}^{t_o+\Delta t}\frac{V(z')Q(z')}{S(z')}\,d\tau \tag{3.5}$$

where z_o is the elevation at which the coolant located at time t_o. Enthalpy $H(z,t_o+\Delta t)$ is evaluated at the center of each axial segment. The starting point z_o at time t_o is somewhere upstream of z, generally off the center of an segment. Denoting the segments to which elevations z and z_o belong as j and k, the time step span is divided as

$$\Delta t=\delta t_k+\delta t_{k+1}+\cdots\cdots+\delta t_{j-1}+\delta t_j \tag{3.6}$$

where δt_i is the time span during which the coolant was flowing in segment i.

Then the relation (3.5) is written numerically as

$$H_j(t_o+\Delta t)=H_o(t_o)+\sum_{i=k}^{j}\frac{V_i Q_i}{S_i}\,\delta t_i \tag{3.7}$$

in which positions z and z_o are indicated by subscripts j and o. If the time step size Δt is sufficiently long, the original segment k is the lowermost (uppermost for reversed flow) segment, and $H_o(t_o)$ is inlet (outlet) enthalpy at the beginning of the time step. In general cases, the original segment k and the elevation z_o in the segment are unknowns that must be determined first.

The subdivided time span δt_i is related to local velocity u_i (m/s) and segment length ΔL_i (m) as

$$\delta t_i=\frac{\Delta L_i}{u_i}=\frac{\Delta L_i}{G_i V_i}=\frac{S_i \Delta L_i}{W V_i} \tag{3.8}$$

where G_i is mass flux (kg/m^2 s), and W is mass flow rate in the subchannel (kg/s) which is assumed to be uniform from bottom to the top of the bundle. Inserting the last expression of (3.8) into (3.7) we get

$$H_j(t_o+\Delta t)=H_o(t_o)+\sum_{i=k}^{j}\frac{Q_i \Delta L_i}{W}\ . \tag{3.9}$$

The axial span ΔL_i is generally equal to segment length except for the top and bottom segments j and k, and is given as a function of elevation x_i (m) of node i (bottom end of segment i) as

$$\Delta L_i=\begin{cases}\dfrac{x_{j+1}-x_j}{2} & \text{for } i=j,\\ x_{i+1}-x_i & \text{for } k\neq i\neq j,\\ x_{k+1}-z_o & \text{for } i=k.\end{cases} \tag{3.10}$$

If the elevation of the starting point z_o and hence its segment number k are determined, and if it is not the inlet (outlet), the previous-step enthalpy at the point $H_o(t_o)$ is determined from the previous-step enthalpies at nodes as

$$H_o(t_o)=H_k^{(b)}(t_o)+[H_{k+1}^{(b)}(t_o)-H_k^{(b)}(t_o)]\frac{z_o-x_k}{x_{k+1}-x_k} \tag{3.11}$$

where $H_k^{(b)}(t)$ is the enthalpy evaluated at node k (bottom of segment k : superscript (b) means 'bottom').

In order to calculate $H_j(t_o+\Delta t)$ using (3.9) and (3.10), unknowns k and z_o must be determined, but they have dependency on V_i, specific volume of the coolant, and hence on the enthalpies in the present time step. What is done in the code is an iteration: first using the previous step enthalpies, positional parameters ΔL_i and z_o are determined by (3.6), (3.8) and (3.10). Then using (3.9) and (3.11), enthalpies at time $t_o+\Delta t$ are calculated. Then using the new enthalpies, specific volume V_i is updated (by reference to steam table) for insertion into (3.8).

This procedure is repeated only twice without further iteration for convergence. It is because the present model is not aimed at determining the instantaneous coolant condition in every time step exactly, but intended for defining boundary condition for thermal analysis in fuel rods. As stated in Chapter 2, the time step size is so controled to keep any fuel temperature jump within the step below a threshold value. Moreover, fuel rods have generally greater heat capacity per unit axial length than coolant. Therefore, even if the calculated coolant condition is one time step behind the actual change, it is sufficient for defining thermal boundary condition.

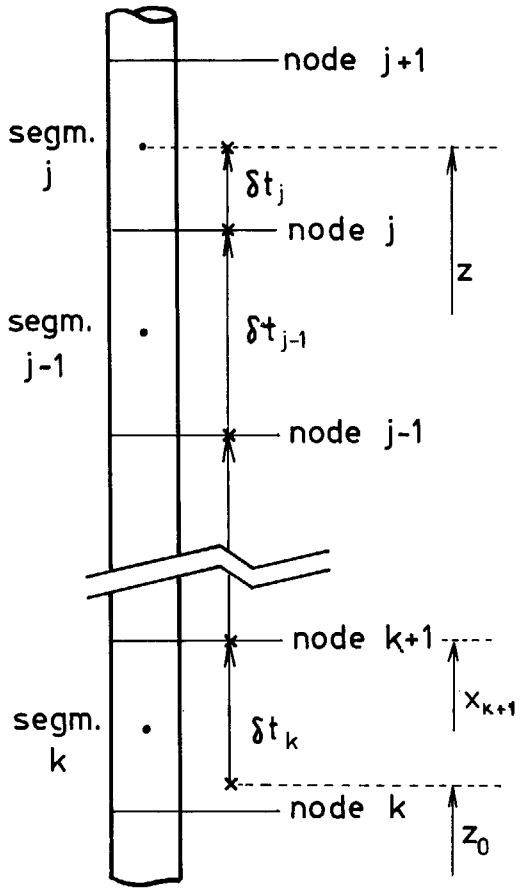

Fig. 5 Coolant enthalpy rise model.

Assumption 3), skip of enthalpy calculation under very low flow rate, was made for the same reason, though the threshold mass flux of 3 kg/m^2 s was determined arbitrarily by experience. Under low flow rate, coolant temperature becomes nearly equal to local solid surface temperature except very near the inlet losing the effect as coolant. On the other hand, it requires very small time step size to continue coolant enthalpy calculation under such conditions.

3.4 Convective Heat Transfer

The classification of heat transfer modes and use of a heat transfer correlation in each mode are basically from the RELAP-5 models[6] with some modifications. **Figure 6** schematically shows the heat transfer regimes in the $\Delta T_{sat}-x$ (quality) plane. Following correlations are prepared for these regimes. Nomenclature is given together at the end of the correlations.

MODE 1 single-phase forced convection (Dittus-Boelter)

$$\phi = h(T_W - T_B) \tag{3.12}$$

$$h = 0.023 \frac{k}{De} Re^{0.8} Pr^{0.4} \tag{3.13}$$

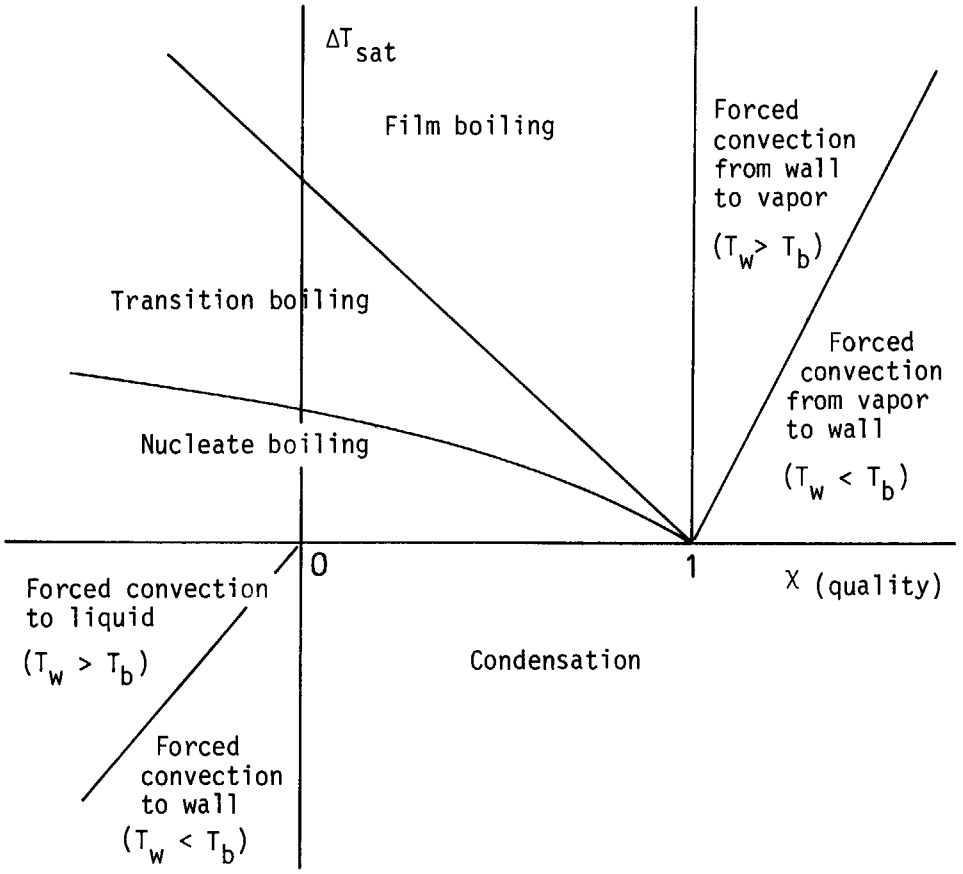

Fig. 6 Heat transfer regimes in temperature-quality space.

MODE 2 nucleate boiling (Chen)

$$\phi = h_{mic}\,\Delta T_{sat} + h_{mac}(T_W - T_B) \tag{3.14}$$

$$h_{mic} = 0.00122 \frac{k_f^{0.79} c_{pf}^{0.45} \rho_f^{0.49}}{\sigma^{0.5} \mu_f^{0.29} H_{fg}^{0.24} \rho_g^{0.24}} \Delta T_{sat}^{0.24}\, \Delta P \tag{3.15}$$

$$h_{mac} = 0.023 \frac{k_f}{De} Re_f^{0.8}\, Pr_f^{0.4}\, F \tag{3.16}$$

S and F are correction factors, for detail see ref. (6).

MODE 3 high-flow transition boiling (Modified Condie-Bengston)

$$\phi_{TB} = (\phi_{DNB} - \phi_{FB}|_{\Delta T_{DNB}}) \exp\left(\frac{\Delta T_{DNB}}{2} - \sqrt{\frac{\Delta T_{sat}}{2}}\right) \frac{\Delta T_{sat}}{\Delta T_{DNB}} \tag{3.17}$$

where ΔT_{DNB} is ΔT_{sat} at departure from nucleate boiling (DNB), and $\phi_{FB}|_{DNB}$ is film boiling heat flux at DNB.

MODE 4 high-flow film boiling (Condie-Bengston)

$$h_{FB} = 0.081033 \frac{k_g^{0.4376} Pr_w^{2.307} Re_g^{[0.6004 + 0.2456\, ln(1 + Xe)]}}{De^{0.7842} (1 + x_e)^{2.59028}} - 13.89471 \exp(1.450 \times 10^{-7} P \cdot Pr_w) \tag{3.18}$$

MODE 5 low-flow post-CHF transition and film boiling

$$\phi=\phi_{liq}+\phi_{vap} \tag{3.19}$$

$$\phi_{vap}=h_v(T_w-T_f)=\alpha h_c(T_w-T_f) \tag{3.20}$$

$$h_c=\max\begin{cases}3.15144\dfrac{k_{film}}{De}(Gr\,Pr_{film})^{0.25}\\[2ex] 0.73817\dfrac{k_{film}}{De}(Gr\,Pr_{film})^{0.33}\end{cases} \tag{3.21}$$

$$Gr=g\left(\frac{De}{2}\right)^3\beta_{film}(T_w-T_f)\left(\frac{\rho}{\mu}\right)^2_{film} \tag{3.22}$$

$$\phi_{liq}=\begin{cases}(h_{TB}+h_{FB})T_{sat}(0.96-\alpha) & \left(\Delta T_{sat}>\dfrac{1}{B}\right)\\[2ex] \phi_{DNB} & \left(\Delta T_{sat}\le\dfrac{1}{B}\right)\\[2ex] 0 & (\alpha\ge 0.96)\end{cases} \tag{3.23}$$

$$\phi_{TB}=2.71\left[B(\phi_{DNB}-\phi_{vap})-(0.96-\alpha)h_{FB}\Big|_{\Delta T_{sat}=\frac{1}{B}}\right]e^{-B\Delta T_{sat}} \tag{3.24}$$

$$h_{FB}=5.527\left(\frac{De}{\lambda_c}\right)^{0.172}\left[\frac{k_g^3\rho_g(\rho_f-\rho_g)H_{fg}g}{De\,\mu_g\Delta T_{sat}}\right]^{0.25} \tag{3.25}$$

$$\lambda_c=\left[\frac{\sigma}{g(\rho_f-\rho_g)}\right]^{0.5} \tag{3.26}$$

$$B=\begin{cases}\text{ln-ln interpolation}\\ B=0.01368\ \text{K}^{-1}\ \text{at}\ P=413700\ \text{Pa}\\ B=0.01476\ \text{K}^{-1}\ \text{at}\ P=620550\ \text{Pa}\end{cases}$$

MODE 6 condensation

$$h=\max(h_{laminar},\,h_{turbulent}) \tag{3.27}$$

$$h_{laminar}=0.296\left[\frac{\rho_f(\rho-\rho_g)g\,H_{fg}k_f^3}{De\,\mu_f(T_{sat}-T_w)}\right]^{0.25} \tag{3.28}$$

$$h_{turbulent}=9.858\times10^{-3}\sqrt{\frac{k_f\rho_f c_{pf}\mu_g v_g}{\mu_f De}} \tag{3.29}$$

Nomenclatures are

- ϕ : heat flux (W/m^2)
- h : heat transfer coefficient (W/m^2 K)
- μ : dynamic viscosity (kg/m s)
- H_{fg} : latent heat of vaporization (J/kg)
- ρ : density (kg/m^3)
- p : pressure (N/m^2)
- De : hydraulic diameter (m)
- x_e : quality
- α : void fraction

g : acceleration of gravity (9.8 m/s^2)
β : thermal expansion coefficient (K^{-1})
ΔP : difference of vapor pressures at T_w and T_{sat} (N/m^2)
v : velocity (m/s)
c_p : specific heat (J/kg)
σ : surface tension (N/m) .

Subscripts denote sat : saturated condition; f : liquid; g : vapor; w : wall; B :bulk; $film$ denotes film temperature $\left(=\frac{T_w+T_B}{2}\right)$.

The primary deviation from the original RELAP-5 model exists in that the Dittus-Boelter equation is used both for subcooled water and superheated steam in FRETA-B. Second difference is the definition of high and low flow conditions. The FRETA-B logic is due to Bjornard and Griffith[7] in which, as in RELAP-5, flow velocity is normalized to the velocity of rising bubbles as

$$j_g^*=Gx_e[\,gDe\rho_g(\rho_f-\rho_g)]^{-\frac{1}{2}}\,, \tag{3.30}$$

$$j_f^*=G(1-x_e)[gDe\rho_f(\rho_f-\rho_g)]^{-\frac{1}{2}}\,. \tag{3.31}$$

High and low flow conditions are determined as

$$\begin{cases} j_g^{*\frac{1}{2}}+j_f^{*\frac{1}{2}}\leq j_{crit} & \text{low flow} \\ j_g^{*\frac{1}{2}}+j_f^{*\frac{1}{2}}> 1.2\times j_{crit} & \text{high flow} \\ \text{interpolation between } j_{crit} \text{ and } 1.2\times j_{crit} & \end{cases} \tag{3.32}$$

where j_{crit} is 1.36 and 3.5 for normal and reverse flow conditions, respectively.

A third difference is that radiative heat transfer term in the low-flow post-CHF correlation was omitted in the FRETA-B model because radiative heat transfer is considered separately in more detail.

For critical heat flux, the following three correlations are used:

1. high flow subcooled (Tong's W-3 correlation)

In SI unit,

$$\begin{aligned}\phi_{DNB}=3.154\times10^6\times[&2.022-6.2379\times10^{-8}P \\ &+(0.1722-1.4268\times10^{-8}P)\exp\{(18.18-5.99\times10^{-7}P)x_e\}] \\ &\times[(0.148-1.60x_e+0.173x_e|x_e|)G/1356+1.037]\times[1.157-0.869x_e] \\ &\times[0.266+0.836\exp(-124.1De)]\times[0.826+3.413\times10^{-7}(H_f-H_{in})]\end{aligned} \tag{3.33}$$

2. high flow saturated (Hsu and Beckner)

$$\phi=\phi_{DNB,w-3}\Big|_{\substack{x_e=0\\H_f=H_{in}}}\sqrt{1.76(0.96-\alpha)} \tag{3.34}$$

where $\phi_{DNB,w-3}$ is critical heat flux given by (3.33) and H_{in} is inlet enthalpy.

3. low flow (Modified Zuber)

$$\phi_{DNB}=0.232H_{fg}(0.96-\alpha)[\sigma g(\rho_f-\rho_g)]^{0.25}\left[\frac{\rho_f\rho_g}{\rho_f+\rho_g}\right]^{0.5} \tag{3.35}$$

3.5 Radiative Heat Transfer

Radiative heat transfer in the coolant subchannels is calculated under the following assumptions:

1) temperature and emissivity are uniform over each fuel sector surface and shroud element,
2) axial segments are sufficiently long, so that net axial flow of radiative energy can be neglected,
3) emissivity is independent of spectrum,
4) emission, reflection and absorption of radiation on a face are isotopic.

First, rod-to-rod heat transfer is formulated assuming subchannels to be vacuum, and then rod-to-coolant heat transfer is considered as a correction term to the former. Assumption 2) reduces the problem to two-dimensional radiative heat transfer problem. If we regard subchannel boundaries as completely absorptive 'face', then each subchannel can be considered as a closed space. For two-dimensional radiative heat transfer in a space enclosed by discrete face elements, an elegant method known as Hottel's method[8] is available. The models in this section are for the most part according to his model.

In order to calculate inter-subchannel heat transport using the view factors within each subchannel, however, a fifth assumption is made in FRETA-B:

5) radiation flux traveling across the boundary from a subchannel to an adjacent one is isotropic (in half sphere).

This assumption is not valid when the emissivities of solid surfaces are high, hence when direct beams are dominant over reflected ones. But its use is almost inevitable when radiative heat transfer in a bundle with arbitrary size and complexity must be analyzed in a subcode of fuel behavior analysis code.

(1) View Factors in Vacuum

In two-dimensional radiative heat transfer problem, geometrical view factor for direct beams between two discrete face elements is easily obtained from a simple geometrical relationship known as cross-string method[8]. When two face elements (two arcs in two-dimensional problem) AB and CD are facing each other, see **Fig. 7**, product of geometrical view factor and surface area (perimeter) is given by diagonal minus lateral chord lengths as

$$A_i F_{ij} = \frac{1}{2}[(AD+BC)-(AC+BD)] \tag{3.36}$$

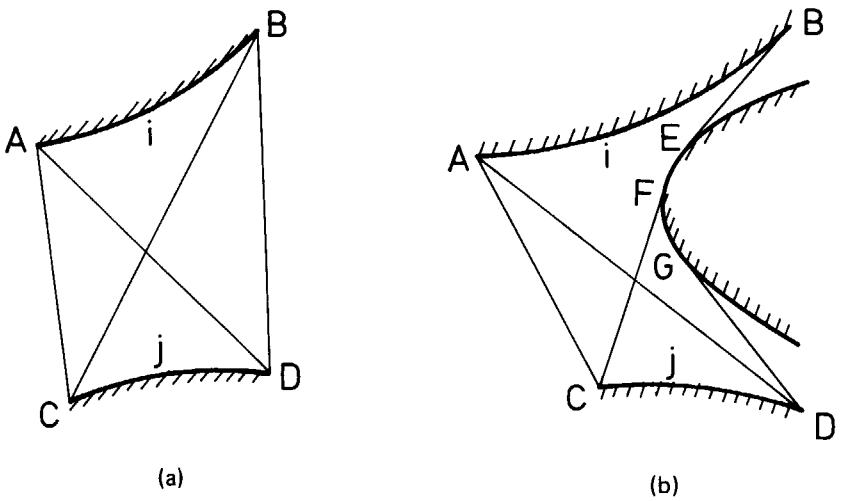

Fig. 7 Cross-string method for geometrical view factors.

where A_i is area (per unit axial length) of face i (m) and F_{ij} is geometrical view factor. A reciprocal relationship exists between the view factors:

$$A_i F_{ij} = A_j F_{ji} \ . \tag{3.37}$$

We can regard a subchannel a closed space by including the channel boundary into the enclosing faces. Then 'modified view factors' which accounts also for reflected beams in a subchannel can be calculated from the geometrical view factors by the Hottel's method.

The modified view factor ψ_{ij} can be defined in terms of total energy transfer E_{ij}(W/m) as follows:

$$\begin{aligned} E_{ij} &= \varepsilon_i \varepsilon_j \sigma T_i^4 A_i F_{ij}^* \\ &= \sigma T_i^4 A_i \psi_{ij} \end{aligned} \tag{3.38}$$

where ε is emissivity (= absorptivity), σ is Stefan-Boltzman constant (5.67×10^{-8} J/m^2 s K^4) and T is temperature (K). In (3.38), the term F_{ij}^* has the same meaning as F_{ij} except that reflection is considered, but the definition of ψ_{ij} includes the emissivities ε_i and ε_j of the emitting and absorbing faces.

In a closed space, the following relationship exist for the summation of the view factors from a face to all faces in the space:

$$\sum_j F_{ij} = 1, \tag{3.39}$$

$$\sum_j \psi_{ij} = \varepsilon_i . \tag{3.40}$$

The reciprocal relationship of (3.37) applies to F_{ij}^* and ψ_{ij} too.

For calculating the modified view factor ψ_{ij}, another quantity R_{ij} is defined as follows:

R_{ij} = the energy flux leaving face j, when energy flux ε_i from face i (equals the emissivity) is the only radiation source in the space.

From this definition, the following relation between R_{ij} and ψ_{ij} is deduced:

$$A_i \psi_{ij} = A_i R_{ij} \frac{\varepsilon_j}{1-\varepsilon_j} \ . \tag{3.41}$$

Then noting only the radiation originally emitted from face i, and considering the energy balance between incident, absorbed and reflected energies on face j, the following equation is obtained:

$$(1-\varepsilon_j)[\varepsilon_i A_i F_{ij} + \sum_n (A_n R_{in} F_{nj})] = A_j R_{ij} \tag{3.42}$$

where the summation in the braket is made over all reflective faces in a unit cell. The first term in the braket means direct incidence from face i to face j. Then still fixing the original emission source to face i, a similar energy balance equation is obtained on the next reflective face $(j+1)$.

Thus, if the number of reflective faces (total minus boundary faces) in the cell is N', N' equations are obtained with N' unknown variables R_{ij}, R_{in} etc. Solving these equations for R_{ij}, and applying (3.41) to the results, the modified view factors ψ_{ij} are derived for combinations of face i and the solid faces. For boundary faces on which reflective flux is zero, the following equation is used instead of (3.41):

$$A_i \psi_{im} = \varepsilon_i A_i F_{im} + \sum_n (R_{in} A_n F_{nm}) \ . \tag{3.43}$$

Then the original emission from face $i+1$ is considered, and the same procedure is repeated. The emissions from boundary faces are considered but the symmetry faces are excluded.

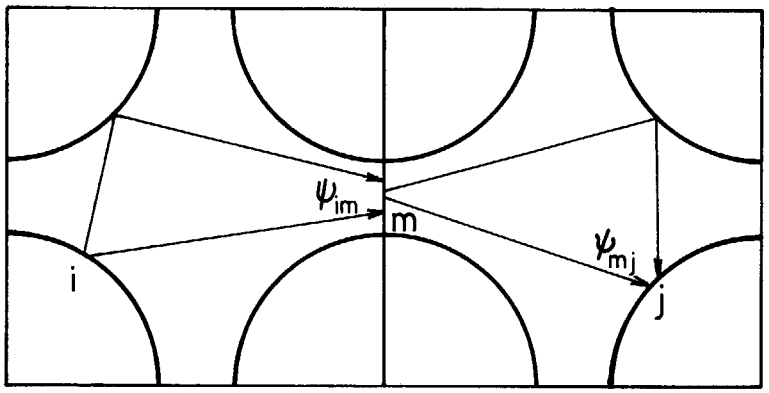

Fig. 8 Connection of modified view factors across boundary faces.

Thus modified view factors are determined for all combinations of solid and boundary faces in a unit cell. Using assumption 5), these factors can be easily expanded to the combination of two faces in different unit cells. Let i and j be two solid face elements in two adjacent unit cells having a common boundary face m. Since $A_i\psi_{im}$ is the part of emission from face i that was 'absorbed' at the boundary face m, the flux $A_i\psi_{im}/A_m$ can be regarded as the source term in the next cell (**Fig. 8**). Hence,

$$A_i\psi_{ij}=(A_i\psi_{im}/A_m)\,A_m\psi_{mj}=A_i\psi_{im}\psi_{mj}\ . \tag{3.44}$$

Here the afore-mentioned assumption 5) has been used. The radiation flux from a particular face has generally a directionality when it travels across the boundary into the next cell. For applying the Hottel's method to this flux in the next cell, this approximation, neglect of directionality, is necessary.

Similarly, if faces i and j are separated by two boundary faces m and n,

$$A_i\psi_{ij}=A_i\psi_{im}\psi_{mn}\psi_{nj}\ . \tag{3.45}$$

Practically, however, this cell to cell migration chain cannot be traced until the original emission decays completely. In the code, the number of the chain is limited to two: that is, migrations into adjacent cells and into the third cells, including the back reflection into the original cell, are considered.

(2) Emission and Absorption by the Coolant

In the foregoing descriptions, the space between solid faces has been assumed to be vacuum. In fact, water absorbs and emits radiation energy even in the steam phase. When the coolant is in the two-phase state, scattering of light by water droplets poses difficult problems. The FRETA-B treatment of the coolant effect is essentially that for the single-phase steam: the two-phase state is treated simply as an interpolation between steam and completely absorptive fluid states.

When a lump of water vapor exists, an emissivity can be defined for its surface. But different from solid surface case, the emissivity of a vapor lump is not an interinsic surface property; it depends also on the mass of vapor behind the surface. Several correlations for vapor emissivity have been proposed, out of which FRETA-B uses Schack's equation[9]:

$$\varepsilon_g=\frac{4.5\times10^3\,(P\cdot L)^{0.8}}{T_g-273} \tag{3.46}$$

where P is pressure (MPa), T_g is temperature (K), and L is the representative dimension of the

vapor lump (m).

Emissivity of the two-phase mixture with quality X is approximated by the interpolation between unity (complete absorption) at $X=0$, and the emissivity of the vapor saturated at the pressure $\varepsilon_g(P)$ as

$$\varepsilon=1+(\varepsilon_g(P)-1)X \ . \tag{3.47}$$

As on solid surfaces, emissivity and absorptivity of a vapor lump are identical and complementary to transmissivity:

$$\varepsilon_g=a_g=1-\tau_g \ . \tag{3.48}$$

For each travelling of radiation from face i to j, the fraction of the energy lost in the coolant is given by $(a_g)_{ij}$ (equals $(\varepsilon_g)_{ij}$), which is derived from (3.46) taking the representative distance L to be the distance between the centers of the two face elements. Thus the geometrical view factor F_{ij} is replaced by

$$F'_{ij}=F_{ij}(\tau_g)_{ij} \ . \tag{3.49}$$

Using F'_{ij} instead of F_{ij}, the procedure of calculating the modified view factors between face elements also applies to the case with the absorption by the coolant. The factors naturally take smaller values than in the vacuum case. Thus instead of (3.40),

$$\sum_j \psi_{ij}<\varepsilon_i \ . \tag{3.50}$$

The difference means the energy absorbed by the coolant, so that modified view factor to or from the coolant can be defnined as

$$A_i\cdot\psi_{ik}=A_k\cdot\psi_{ki}=A_i\cdot\varepsilon_i-\sum_j A_i\cdot\psi_{ij} \tag{3.51}$$

where k represents k-th subchannel of the bundle, in which faces i and j are located. It means that the vapor (or two-phase fluid) lump in each subchannel can be treated just as solid face elements. The energy transfer in the opposite direction, emission by the coolant and absorption at a solid face, is also given by (3.38), using $A_k\psi_{ki}$ of (3.51) and taking T_i to be the coolant temperature. The 'connection' of the view factors across boundary faces is made in the same way as between solid faces.

(3) Method of Numerical Calculation

Net radiation energy leaving face i is given by

$$Q_i=\varepsilon_i\sigma A_iT_i^4-\sum_j(\sigma T_j^4 A_j\psi_{ji}) \tag{3.52}$$

where summation is made over all relevant solid face elements and vapor lumps (subchannels). Equation (3.52) is not solved simultaneously with the equations of convective heat transfer and fuel rod internal heat conduction; instead radiation energy Q_i is calculated using the temperatures that were derived from convective heat transfer and internal heat conduction (and radiative heat in the previous step), and added as heat source term in the next time step.

It is because 1) (3.52) has temperatures of all fuel sector surfaces and subchannels as unknown terms of fourth power, 2) on each fuel sector surface, choice of one convective heat transfer correlation from the six modes in 3.4 involves some trial-and-error process comparing the temperatures calculated by correlations for different modes (some of the correlations are highly nonlinear), and 3) solution process of internal heat conduction equation described in 3.6 is also fairly complex.

These circumstances make simultaneous solution of all heat transfer equations almost impossible. The present explicit treatment of radiative heat transfer, however, has not made at least any numerical instability problem in application to practical problems. It is because the energy carried by radiation is generally small compared with heat capacity of fuel rods, and also because automatic time step control is made as described in 2.

The modified view factors in fact take different values at different cross sections of a bundle, and they also change with the change of fuel and coolant states. To save running time, however, the following approximations are made:

1) the effect of fuel rod deformation is neglected;
2) the view factors determined at an elevation of bundle (normally neat the center) are used to calculate radiative heat transfer at all elevations;
3) emissivity of solid surface is assumed to be independent of temperature.

On the other hand, change of coolant emissivities with time cannot be neglected because emissivity of vapor has strong dependency on temperature and pressure and the both parameters change widely during LOCA. In FRETA-B, view factors are renewed when the coolant condition has changed appreciably from the condition at the last renewal:

1) when the coolant temperature at a monitoring point has changed more than 50 K,
2) when pressure has changed more than 2 MPa (above 4 MPa), or 1 MPa (below 4 MPa).

3.6 Heat Conduction in Fuel Rod

Transient heat conduction equation in a fuel rod is written in general form as

$$\rho C_p \frac{\partial T}{\partial t} = \nabla \cdot (k \nabla T) + P \tag{3.53}$$

where ρ is density (kg/m^3), C_p is specific heat (J/kg·K), k is thermal conductivity (W/m·K), and P is heat generation rate in unit volume (W/m^3). Neglecting the axial heat flow and also the azimuthal variation of thermal conductivity in the cylindrical geometry, (3.53) becomes

$$\rho C_p \frac{\partial T}{\partial t} = \frac{1}{r} \frac{\partial}{\partial r} \left(kr \frac{\partial T}{\partial r} \right) + \frac{k}{r^2} \frac{\partial^2 T}{\partial \theta^2} + P \quad . \tag{3.54}$$

The above equation applies to the heat flows both in fuel pellet and the cladding. But the former requires much more careful numerical procedure than the latter because of larger temperature difference in pellet and the resultant larger difference of thermal conductivity. Similarly, the radial derivative term in (3.54) is much more important than the azimuthal derivative term.

In order to save running time, therefore, different numerical methods are applied to different modes of heat flow in different parts of fuel rod according to their importance and complexity:

1) method of weighted residuals (MWR) for the radial heat flow in pellet,
2) explicit finite difference approximation for the azimuthal heat flow both in fuel pellet and the cladding, and
3) implicit finite difference method for the radial heat flow in the cladding.

The resultant set of numerical equations are solved simultaneously with the surface heat transfer equation as a boundary condition.

(1) Radial Heat Flow in Fuel Pellet

Since FRETA-B must analyze many fuel rods, and since heat conduction in fuel pellet is merely one out of diverse phenomena to be considered, its numerical procedure must be a

fast-running one. The method of weighted residuals (MWR)[10] answers this requirement though, as a semi-analytical method, it cannot be applied to a region having discontinuity (hence the heat conduction in the cladding was separately handled by the finite difference method). The point collocation method was chosen for its simplicity out of the various methods grouped into MWR. It is a method similar to the least-square fitting of experimental data to a trial function: a series of functions with unknown numerical constants is used to express the unknown temperature distribution and inserted into the differential equation, and then the unknown constants are evaluated from the conditions at selected collocation points.

This technique has been applied in COBRA-IV code[11] to the radial heat flow in fuel pellet using polynominals as trial functions. Use of polynominals, however, needs very high order of terms in such a complex analysis as that sudden strong cooling is given at the surface. In FRETA-B, a series of modified Bessel functions was chosen as trial functions. Since modified Bessel function gives rigorous solution to a simple diffusion equation in cylindrical coordinate, its use as trial function is adequate.

First, to remove the non-linearity of (3.54) due to the temperature dependency of thermal conductivity, the following transformation is made:

$$\theta=\frac{1}{k_o}\int_{T_o}^{T}k(T)dT=G(T) \tag{3.55}$$

where T_o is a reference temperature and k_o is the thermal conductivity at T_o . Inversely, T can be expressed as a function monotonically increasing with θ :

$$T=H(\theta) \ . \tag{3.56}$$

Then replacing the temperature T in the radial and time derivatives of (3.54) with the new variable, and also normalizing the radius with the pellet outer radius b as

$$x=\frac{r}{b} \ , \tag{3.57}$$

we have

$$\frac{k_o\rho C_p}{k}\frac{\partial\theta}{\partial t}=\frac{k_o}{b^2}\left[\frac{\partial^2\theta}{\partial x^2}+\frac{1}{x}\frac{\partial\theta}{\partial x}\right]+\frac{k}{r^2}\frac{\partial^2 T}{\partial\theta^2}+P \ . \tag{3.58}$$

If the heat generation term and the azimuthal term are absent, (3.58) has a general solution of the form

$$\theta=C\exp\left(\frac{\mu^2 kt}{b^2\rho C_p}\right)[AI_o(\mu x)+BK_o(\mu x)] \tag{3.59}$$

where I_o and K_o are modified Bessel function and Kelvin function, respectively. Now with $P\neq 0$, it is tried to solve eqn. (3.58) by the method of weighted residuals using the trial function of the form:

$$\theta=A_o(t)+\sum_{m=1}^{M}\left\{A_m(t)\frac{I_o(\mu_m x)}{I_o(\mu_m)}+B_m(t)\frac{K_o(\mu_m x)}{K_o(\mu_m)}\right\} \ . \tag{3.60}$$

When there is no center hole in the pellet,

$$\left.\frac{\partial T}{\partial r}\right|_{r=0}=\left.\frac{\partial\theta}{\partial x}\right|_{x=0}=0 \tag{3.61}$$

hence $B_m=0$ in (3.60), and

$$\theta=A_o(t)+\sum_{m=1}^{M}A_m(t)\frac{I_o(\mu_m x)}{I_o(\mu_m)} \ . \tag{3.62}$$

Here, the total number of terms M and the numerical constants μ_m for each term are predetermined so that, with small number of collocation points (nodes), (3.62) may be able to express the temperature distributions expected to occur during a LOCA and preferably also RIA (reactivity insertion accident). After some comparison tests with the results of finite difference method, the series was determined as $\mu_m = 0, 3, 5, 7, 9, 11$, by which use of four terms (up to 7) was found adequate for most normal operation and LOCA conditions.

Expressing the azimuthal heat flow term in (3.58) by the temperatures in the previous time step (explicit method), and making finite difference approximation to time derivative, we have

$$\frac{k_0 b^2 \rho C_p}{k_{i,l}} \frac{\Theta^{n+1}-\Theta^n}{\Delta t} = k_o\left(\frac{\partial^2}{\partial x^2}+\frac{1}{x}\frac{\partial}{\partial x}\right)\Theta^{n+1}+b^2P+\frac{b^2 k_{i,l}}{\Delta y_i^2}(T^n_{i,l-1}+T^n_{i,l+1}-2T^n_{i,l}) \tag{3.63}$$

where superscripts $n+1$ and n represent the present and the last time steps, respectively, and subscripts i and l denote radial and azimuthal nodes, respectively. Since the number of azimuthal nodes is four,

$$\Delta y_i = \frac{2\pi r_i}{4} = \frac{\pi}{2} r_i. \tag{3.64}$$

Using the Bessel function expansion of (3.62) in the radial derivative term of (3.58) and with an abreviation

$$\lambda_i = \frac{k_0 b^2 \rho C_p}{k_{i,l}\Delta t} \tag{3.65}$$

differential equation (3.58) as evaluated at a collocation point x_i becomes

$$\lambda_i \Theta_i^{n+1} - \sum_{m=1}^{M} k_0 \mu_m^2 \frac{I_0(\mu_m x_i)}{I_0(\mu_m)} A_m(t) = b^2 P_i + \lambda_i \Theta_i^n + \frac{b^2 k_{i,l}}{\Delta y_i^2}(T^n_{i,l-1}+T^n_{i,l+1}-2T^n_{i,l}) \tag{3.66}$$

in which Θ^{n+1} and $A_m(t)$ are unknowns to be determined.

(2) Boundary Condition at the Pellet Surface and Heat Conduction in the Cladding

From the continuity of heat flow at the pellet-clad gap,

$$-\frac{k_0}{b}\frac{\partial \Theta}{\partial x}\Big|_{x=1} = -k\frac{\partial T}{\partial r}\Big|_{r=b} = \frac{r_g}{b} h_g (T_{po}-T_{ci}) \tag{3.67}$$

where subscripts g, po and ci denote gap, pellet surface and cladding inner surface, respectively, and h_g is gap heat transfer coefficient (W/m^2 K). Since the temperature distribution in pellet is described by Θ, not T, the pellet outer surface temperature T_{po} in (3.67) must be expressed as a function of Θ_{po}^{n+1} Since Θ is a temperature weighted by the fuel thermal conductivity (**Fig. 9**), linear transformation gives a good approximation within a small temperature range:

$$\Theta_{po} = cT_{po} + d \tag{3.68}$$

$$T_{po} = \alpha \Theta_{po} + \beta \tag{3.69}$$

where the coefficients are determined from the temperature distribution in the last time step. Then using (3.62) and (3.69), the continuity equation (3.67) transforms into

$$-\omega\alpha\Theta_{po}^{n+1} - k_0 \sum_{m=1}^{M} \frac{\mu_m I_1(\mu_m)}{I_0(\mu_m)} A_m(t) + \omega T_{ci}^{n+1} = \omega\beta \tag{3.70}$$

where an abbreviation $\omega=r_g h_g$ was made.

The heat flow in the cladding is evaluated at only two radial nodes, i.e. inner surface and outer surface. Finite difference approximation of (3.54) at the cladding inner surface leads to

$$\frac{\rho C_p}{\Delta t}\frac{r_{cm}^2-r_{ci}^2}{2}(T_{ci}^{n+1}-T_{ci}^{n})=\omega(T_{po}^{n+1}-T_{ci}^{n+1})+r_{cm}k_{cm}\frac{T_{co}^{n+1}-T_{ci}^{n+1}}{r_{co}-r_{ci}}+r_{ci}Q_{R1}$$
$$+\frac{k_{ci}(r_{cm}-r_{ci})}{\Delta y_{ci}}(T_{ci,l-1}^{n}+T_{ci,l+1}^{n}-2T_{ci,l}^{n})/2\pi \qquad (3.71)$$

where Q_{R1} is metal-water reaction heat at the inside surface (W/m^2) and the subscript cm denotes the cladding midplane. Using (3.69) for removing T_{po}^{n+1} in (3.71), and arranging the equation in terms of unknown variables we have

$$-\Delta t\,\omega\alpha\Theta_{po}^{n+1}+\left\{\rho C_p\frac{r_{cm}^2-r_{ci}^2}{2}+\Delta t\omega+\frac{\Delta t\,r_{cm}k_{cm}}{r_{co}-r_{ci}}\right\}T_{ci}^{n+1}-\frac{\Delta t\,r_{cm}k_{cm}}{r_{co}-r_{ci}}T_{co}^{n+1}$$
$$=\rho C_p\frac{r_{cm}^2-r_{ci}^2}{2}T_{ci}^{n}+\Delta t\{r_{ci}Q_{R1}+\omega\beta\}+\frac{r_{cm}-r_{ci}}{2\pi}\frac{k_{ci}}{\Delta y_{ci}}(T_{ci,l-1}^{n}+T_{ci,l+1}^{n}-2T_{ci,l}^{n})\Delta t. \qquad (3.72)$$

Finally at the cladding outer surface, the radial and azimuthal heat flows are balanced with temperature rise, the reaction heat at the outside surface Q_{R2}, and the surface heat flux to the coolant. Surface heat flux is divided into radiative and convective parts:

$$\phi=\phi_c+\phi_{rad} \qquad (3.73)$$

and only the convective part is incorporated into the simultaneous solution of heat conduction equation; radiative heat flux is considered as a heat source term in the next time step. Then the resultant heat balance equation is, with unknowns in the left side,

$$-\frac{\Delta t\,r_{cm}k_{cm}}{r_{co}-r_{ci}}T_{ci}^{n+1}+\left\{\rho C_p\frac{r_{co}^2-r_{cm}^2}{2}+\frac{\Delta t\,r_{cm}k_{cm}}{r_{co}-r_{ci}}\right\}T_{co}^{n+1}+\Delta t\,r_{co}\phi_c$$
$$=\rho C_p\frac{r_{co}^2-r_{cm}^2}{2}T_{co}^{n}+\Delta t\,r_{co}(Q_{R2}-\phi_{rad})$$
$$+\frac{r_{co}-r_{cm}}{2\pi}\frac{k_{co}}{\Delta y_{co}}(T_{co,l-1}^{n}+T_{co,l+1}^{n}-2T_{co,l}^{n})\Delta t. \qquad (3.74)$$

(3) Numerical Solution Procedure

If J radial nodes are set in a fuel pellet (node J is pellet surface), and the MWR equation (3.66) is evaluated at $J-1$ nodes from 1 (innermost node) to $J-1$. then $J-1$ sets of eqn. (3.66) added with (3.70), (3.72) and (3.73) constitute $J+2$ sumultaneous equations. The unknown varibles are Θ_1^{n+1} to Θ_J^{n+1}, T_{ci}^{n+1}, T_{co}^{n+1}, $A_1(t)$ to $A_M(t)$ and ϕ_c, whose total number is $J+M+3$. If we take $M+1$ equals $J-1$, equation (3.62) can be solved for $A_m(t)$:

$$A_m(t)=C_m+\sum_{j}^{J-1}D_j\Theta_j^{n+1}. \qquad (3.75)$$

Thus, replacing (3.75) into (3.66) and (3.70), we have $J+2$ equations with $J+3$ unknowns Θ_1^{n+1} to Θ_J^{n+1}, T_{ci}^{n+1}, T_{co}^{n+1} and ϕ_c. Applying the Gauss elimination method to the matrix equation from the interior node ($j=1$) outward, we get finally an equation of the form:

$$E\,T_{co}^{n+1}+F=\phi_c. \qquad (3.76)$$

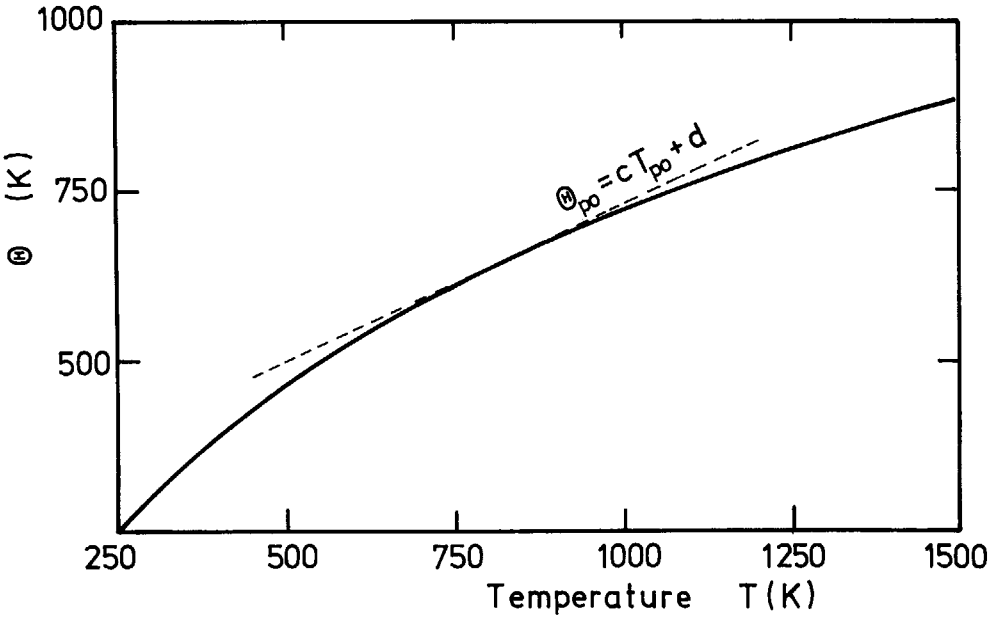

Fig. 9 Thermal conductivity-weighted temperature (Lyons equation[15] for UO_2 is used with T_0 = 298 K).

Another equation relating T_{co}^{n+1} to ϕ_c is available from the surface heat transfer correlations described in 3.4, which is written either as

$$h(T_{co}^{n+1}-T_{cool})=\phi_c\,, \tag{3.77}$$

or in a more complex form for boiling heat transfer:

$$\phi_c=f(T_{co}^{n+1},\ T_{sat})\,. \tag{3.78}$$

Either (3.77) or (3.78) is solved simultaneously with (3.76) for the unknowns T_{co}^{n+1} and ϕ_c. Then tracing backward the elimination process, a complete set of unknowns, θ_1^{n+1} to θ_f^{n+1}, T_{ci}^{n+1} and T_{co}^{n+1} is determined.

At the collocation points in fuel pellet, temperatures can be directly obtained by inserting the θ^{n+1} values into (3.56). For the other points which include fuel center, however, the coefficients of the Bessel functions $A_m(t)$ are determined first by inserting the θ^{n+1} values at the collocation points into (3.75), and then the θ^{n+1} values at the other points are obtained by (3.62). The actual form of the function f in (3.78), and the actual process of choosing one correlation out of six correlations in 3.4 are very complex. This complexity is the reason why the Gauss elimination process is not made to include all equations, but stopped at (3.74) expressing the result by the two coefficients E and F in (3.76). It is also the reason why radiative heat transfer equation is not solved simultaneously: simultaneous consideration of radiative heat transfer equation necessitates simultaneous execution of the above complex procedure in all sectors of all rods.

(4) Hollow Pellet Case

Denoting the pellet inner radius by a, and using the boundary condition

$$\left.\frac{\partial\theta}{\partial x}\right|_{x=\frac{a}{b}}=0\,, \tag{3.79}$$

the thermal conductivity integral is expressed by the following trial function:

$$\theta = A_0(t) + \sum_1^M A_m(t) \left\{ \frac{I_0(\mu_m x)}{I_0(\mu_m)} - \frac{I_1\left(\mu_m \frac{a}{b}\right)}{K_1\left(\mu_m \frac{a}{b}\right)} \frac{K_0(\mu_m x)}{I_0(\mu_m)} \right\} \tag{3.80}$$

The heat balance equations take correspondingly a little more complex form, but they can be solved by fundamentally the same procedure.

(5) Accuracy and Running Time

A new point of the present numerical method for solving heat conduction equation is the use of MWR with Bessel functions as trial functions for the radial heat flow in pellet. Accuracy check was, therefore, made on whether these trial functions can well express the radial temperature distribution in steady axisymmetric problems. The other parts of the present model, i.e. technique of variable separation for treating transient change and explicit finite difference approximation for azimuthal heat flow, are merely conventional methods.

As a sample problem, a fuel rod operating at uniform power density was postulated and the radial temperature distribution was calculated first by the code. Then using the cladding outer surface temperature and gap heat transfer coefficient values obtained from the code, temperature distributions in the cladding and fuel pellet were calculated by the analytical method and compared with the code results. The comparison is made in **Table 1**. It shows about 1% relative error in the temperature rise from the cladding inner surface to pellet center. This level of accuracy is marginal for application to normal operation conditions, but is sufficient for accident conditions in which sources of much greater error are unavoidable in all other models and input data.

Merit of the present method exists in the reduction of running time compared with the finite difference method. It is achieved primarily through the reduction of the number of nodes (collocation points) by using trial functions that are most suitable for expressing the expected temperature distribution. The above check calculation was made using five nodes in fuel pellet. Finite difference analysis requires eight to ten nodes to keep the same level of accuracy. Second point in the smaller running time is that, in MWR equation (3.66), majority of the terms needs definition only once at the beginning of a transient analysis: Bessel functions need not be called every time step. These two points contribute to suppress the running time by MWR to approximately less than one-half of that by the finite difference method.

Table 1 Comparison of fuel temperatures calculated by FRETA-B with analytical results (steady, axisymmetric, flat-power condition)

		FRETA-B	analytical
clad outer temperature	(K)	532	532 *
clad inner temperature	(K)	580	580
fuel outer temperature	(K)	842	837
fuel center temperature	(K)	1639	1628

* Clad outer temperature and gap conductance values were taken from the code results.

3.7 Gap Conductance Model and Material Properties

Heat transfer coefficient across fuel-clad gap (gap-conductance) is evaluated by the modified Ross-Stoute model. The original Ross-Stoute model[12] was applicable only to closed-gap case. In GAPCON-THERMAL code[13] it was modified to consistently include open-gap case. FRETA-B has adopted the GAPCON-THERMAL modification of the Ross-Stoute model except for a FRETA-B original model for relocation of pellet fragments.

The gap state is classified in terms of nominal hot gap size t_g (m), which is the cladding inner radius minus pellet radius, and arithmetic mean roughnesses R_f for fuel and R_c for cladding (m), as

$$\text{open gap if} \quad t_g > 1.98(R_f+R_c), \tag{3.81}$$

and otherwise as closed gap.

Gap conductances for the two cases are given by

$$h_g=\frac{k_g}{t_g+(g_1+g_2)}+h_r \qquad \text{(open gap)}, \tag{3.82a}$$

$$=\frac{0.2\,k_m P_i}{R^{0.5}H}+\frac{k_g}{t_0+(g_1+g_2)}+h_r \qquad \text{(closed gap)} \tag{3.82b}$$

where
- h_g : gap conductance (W/m^2 K),
- k_g : thermal conductivity of the gap gas (W/m^2 K),
- H : Mayer hardness of the cladding (Pa),
- P_i : contact pressure between pellet and cladding (Pa),
- h_r : radiative contribution to gap conductance (W/m^2 K).

R is a square mean of the pellet and cladding roughnesses:

$$R=\left(\frac{R_f^2+R_c^2}{2}\right)^{\frac{1}{2}}, \tag{3.83}$$

t_0 is thickness of the gas layer contained in the roughnesses (m), given empirically by

$$t_0=1.98(R_f+R_c)\exp(-1.81\times10^{-7}P_i). \tag{3.84}$$

The terms g_1 and g_2 are temperature jump distances at the fuel and cladding surfaces (m), respectively, and the sum of the two is given by

$$g_1+g_2=3757\left[\frac{\mu}{P}\left(\frac{T}{M}\right)^{\frac{1}{2}}\right] \tag{3.85}$$

where P is gas pressure (Pa); T is gas temperature (K); μ is gas viscosity (kg/m s); M is the molecular weight of the gas stom. k_m is an average of fuel and cladding thermal conductivities at the surfaces defined by

$$\frac{1}{k_m}=\frac{1}{2}\left(\frac{1}{k_f}+\frac{1}{k_c}\right). \tag{3.86}$$

In the original definition, the gap conductance as defined by (3.82) gives the average heat transfer coefficient along the circumference of a gap. But here its meaning is expanded to give the local heat transfer coefficient at a small part of the circumference. If we assume that a fraction F of the circumference has pellet fragments that have relocated outwards until they make soft-contact (P_i equals zero) with the cladding, and that the remaining $(1-F)$ has all fragments in the concentric position, then the average gap conductance is given by

$$\bar{h}_g=F\,h_g(t_0)+(1-F)h_g(t_g) \tag{3.87}$$

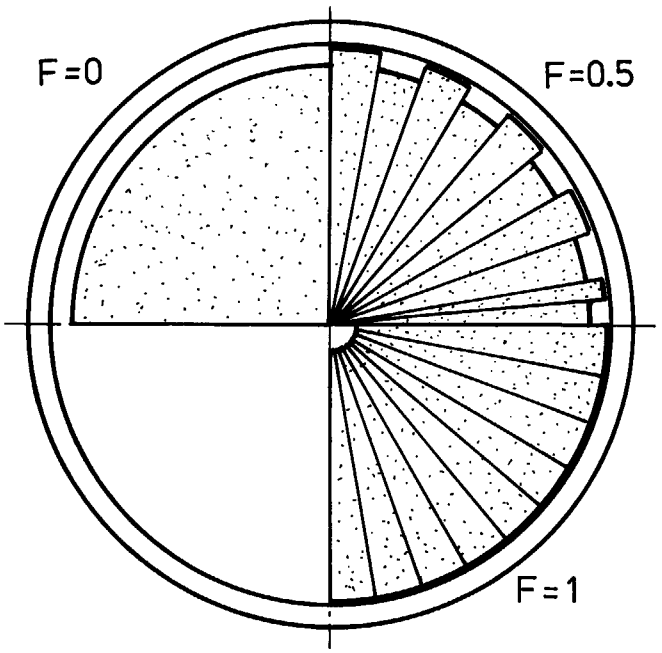

Fig. 10 Heterogeneous relocation model.

where $h_g(t)$ is the gap conductance given either by (3.82 a) or (3.82 b) depending on the value of t which is gap size (**Fig. 10**).

As a standard value, $F=0.1$ is stored in the code for use in all sectors of all fuel rods. By input however, different F values can be assigned to four sectors of a rod, so that directional relocation of pellet fragments toward one direction of the bundle may be simulated.

Radiative heat transfer is of minor importance at pellet-clad gap in most cases. Radiative heat flux is a function of fourth power of temperatures:

$$q_r=\sigma\left\{\frac{1}{\varepsilon_f}+\frac{A_f}{A_c}\left(\frac{1}{\varepsilon_c}-1\right)\right\}^{-1}\{T_f^4-T_c^4\} \tag{3.88}$$

where σ is Stefan-Boltzman constant (5.67×10^{-8} W/m^2 K^4); A is surface area (m^2); ε is emissivity and T is temperature (K). Subscripts f and c denote fuel and cladding, respectively. In order to include q_r into linear heat conduction equation, (3.88) is approximated as follows:

$$q_r=h_r(T_f-T_c) \tag{3.89}$$

where 'radiative heat transfer coefficient' h_r is defined using the temperature in the previous time step as

$$h_r=\sigma\left[\frac{1}{\varepsilon_f}+\frac{A_f}{A_c}\left(\frac{1}{\varepsilon_c}-1\right)\right]^{-1}(T_f^{old}+T_c^{old})[(T_f^{old})^2+(T_c^{old})^2]\,. \tag{3.90}$$

Material properties relevant to internal heat conduction are specific heats, emissivities and thermal conductivities of pellet and cladding, and gas thermal conductivity. MATPRO models[14] are used for them except for fuel thermal conductivity of UO_2 pellet, for which Lyons equation[15] is used with density correction term:

$$k=\frac{1.025}{0.95}\frac{D}{1+0.5(1-D)}\left(\frac{3824}{129.4+T}+6.1256\times10^{-11}T^3\right) \tag{3.91}$$

where k is thermal conductivity (W/m K), T is temperature (K) and D is density (fraction to theoretical density).

3.8 Reflood Heat Transfer

Rod surface heat transfer under (bottom) reflooding condition is calculated using the FLECHT correlation with some modifications. Two important parameters governing the phenomenological reflood heat transfer correlations are v_{in} , inlet reflooding velocity (m/s), and z_q , axial height of the quench front (m). The former, v_{in} , must always be input as an external variable when reflood calculation is required. The quench front position can be either input as a time-dependent variable, or computed by the code using the FLECHT quench front correlation[16].

The FLECHT correlation gives quench time as a function of quench front elevation when the inlet reflood rate is held constant. When the initial cladding temperature T_{init} is much higher than 204 °C, it is written as

$$t_q(z_q)=f\, t_{q,\,peak\ power}[Q_r+0.5\,Q_r \exp(-9Q_r^2)] \tag{3.92}$$

where $t_{q,\,peak\ power}$ is the quench time of the peak power elevation, which is a complex function of flooding rate, pressure, inlet subcooling and so forth, for detail see the original paper[16]. Q_r is the normalized power integral from the inlet to z_q

$$Q_r=\int_0^{z_q} q\,dz \Big/ \int_0^{z_{peak\ power}} q\,dz \tag{3.93}$$

where q is linear heat rating in W/m. f is a correction factor that accounts for the different fuel length and power profile between the fuel rod in problem and the FLECHT core as

$$f=z(Q_r)/[z(Q_r)]_{FLECHT\ cosine}\,. \tag{3.94}$$

Equation (3.92) gives quench time at an arbitrary elevation when v_{in} and other conditions are held constant. Under varying conditions, quench front velocity v_q can be defined as

$$v_q=\frac{(z_q+\Delta z_q)-z_q}{t_q(z_q+\Delta z_q)-t_q(z_q)} \tag{3.95}$$

in which the quench time t_q is derived from (3.83) using the new (after change) condition data. Then the new quench front elevation is derived as

$$z_q(t+\Delta t)=z_q(t)+v_q\,\Delta t\,. \tag{3.96}$$

Heat transfer coefficient in the region above the quench front is also given in the FLECHT as an empirical correlation. But it is primarily for the 'quasi-steady' period, and the correction term proposed for the preceding 'developing' period lacks generality. In the FRETA-B model, therefore, some modification had to be made for the 'developing period' during which the introduced water does not reach boiling point.

For the well-developed two-phase flow in the quai-steady period, FLECHT heat transfer coefficient is given as

$$h_{FL}=215.8\exp(-5.9v_{in})\exp[-3.937(z-z_q)]$$
$$+261.2[1-\exp(-9.84v_{in})]\left[0.714+0.286\left\{1-\exp\left(\frac{0.1684P}{v_{in}^2}\right)\right\}\right] \tag{3.97}$$

where heat transfer coefficient is in W/m^2 K, and P is pressure (MPa). The condition for the quasi-steady period is

$$z_q \geq z_s=0.558(39.37v_{in})^{**}(0.5466-1.677v_{in})\,. \tag{3.98}$$

In the FRETA-B model, another critical height z_s' is defined as

$$z_s' = \int_0^{t_c} v_{in}\, dt \tag{3.99}$$

where 'new critical time' t_c is given by

$$t_c = \frac{\rho C_p S (T_{sat} - T_{in})}{q} \tag{3.100}$$

where ρ is density (kg/m^3); S is flow area (m^2); C_p is specific heat (J/kg·K); q is linear heat rating (W/m); T_{sat} and T_{in} are saturation and inlet temperatures (K), respectively.

Before reflooding starts, dominant heat transfer modes are radiative heat transfer and convective heat transfer to superheated steam. Using the two critical heights defined above, a smooth linear interpolation is made between these pre-reflood modes and the well-developed reflood heat transfer as

$$\begin{aligned} &z_q < z_s' && \phi = \phi_r + h_0 (T_w - T_B), \\ &z_s' < z_q < z_s && \phi = (1-k)[\phi_r + h_0 (T_w - T_B)] + k\, h_{FL} (T_w - T_{sat}), \\ &z_s < z_q && \phi = h_{FL} (T_w - T_{sat}), \end{aligned} \tag{3.101}$$

where ϕ and ϕ_r are total and radiative heat fluxes, respectively; h_0 is pre-reflood convective heat transfer coefficient; T_w and T_B are wall and bulk temperatures, respectively; k is an interpolation factor given by

$$k = \frac{z_q - z_s'}{z_s - z_s'} . \tag{3.102}$$

In the region below the quench front, nucleate boiling condition is assumed.

3.9 Thermal Effect of Shroud

During a transient, shroud plates and other structural materials work as a heat source or sink. As stated in Chapter 2, all structural components in a bundle are idealized by the code as 'shroud', either tubular or planar. Tubular 'shroud' is used for simulating the control-rod guide tube in PWR, or the external wall of an experimental rig.

Geometries of shrouds are specified as a part of the input data for radiative heat transfer. Therefore a shroud plate is divided into face elements each facing different coolant subchannel. If, for example, a shroud face forms the external surfaces of four subchannels, it must be input as four independent face elements. Different properties (heat capacity, external temperature etc.) can be assigned to them.

Each face element is classified into either insulated shroud or conductive shroud. The former emits or absorbs heat only by heat capacity; it does not conduct heat out of the bundle. It is used for simulating the components completely contained within the bundle, or the external wall that is thermally insulated from outside. The conductive shroud model is used for the external wall of the bundle whose outside surface is cooled by external coolant, as is normally used in experimental rigs. In each case, the thermal effect is treated by simple one-point approximation of heat conduction equation. As a special case, shroud face elements can be assumed to be in thermal equilibrium with the coolant. In this case, even heat capacity of the shroud is neglected and the only thermal effect of the element is to completely reflect radiation.

(1) Insulated Shroud

This type of shroud, either tubular or planar, conducts heat on one side but has the

opposite side insulated. One-point approximation means in this case neglect of thermal resistance within the plate. The governing equation is

$$\frac{\rho C_p V}{\Delta t}(T^{n+1}-T^n)=-\phi-\phi_r \tag{3.103}$$

where T^{n+1} is wall temperature in the present step (K); T^n is its previous value; V is volume per unit surface area (m); ρ is density (kg/m^3); C_p is specific heat (J/kg·K); Δt is time step size (s); ϕ is convective heat flux; ϕ_r is radiative heat flux (both taken positive when they flow out of the plate) (W/m^2).

As in the thermal calculation of fuel rods, radiative heat flux ϕ_r is evaluated separately (explicitly) in the radiative heat transfer subcode. Hence unknowns in (3.103) are T^{n+1} and ϕ, so that (3.103) can be expressed in the form

$$A_1 T^{n+1}+B_1=\phi. \tag{3.104}$$

Equation (3.104) can be solved for T^{n+1} and ϕ simultaneously with one of the heat transfer correlations (3.77) or (3.78) depending on the coolant state, just as was done in the fuel rod thermal calculation. The obtained convective heat flux (positive in flowing-out side), together with the radiative heat flux, affects the coolant temperature in the next step.

(2) Conductive Shroud

This type of shroud transmits heat from the coolant inside bundle to the external coolant. One-point approximation at the bundle-side surface leads to the equation:

$$\frac{\rho C_p d}{\Delta t}(T_w^{n+1}-T_w^n)=-\phi+h_G(T_{Bo}-T_w^n)-\phi_r \tag{3.105}$$

where h_G is combined heat conductance (W/m^2·K) of internal thermal conductivity and heat transfer at the outside surface:

$$h_G=\frac{1}{1/h_{co}+d/k}, \tag{3.106}$$

and other variables are: h_{co} is heat transfer coefficient at the external surface (W/m^2·K); k is thermal conductivity of the wall (W/m·K); d is its thickness (m); T_{Bo} is temperature of the external coolant (K).

Taking the external coolant temperature as a boundary condition, (3.105) can also be expressed in the form of (3.104). Since the heat flow across shroud is merely a correction term for fuel behavior, the heat transfer coefficient h_{co} is not calculated by the code, but specified as the input data as well as other parameters ρ, C_p, d and T_{Bo}.

4. Cladding Oxidation Model

At high temperature, Zircaloy cladding tubes react with water (steam) as

$$Zr + 2\,H_2O \longrightarrow ZrO_2 + 2\,H_2\,. \tag{4.1}$$

The zirconia layer forms on the surface, and oxygen diffuses through the layer into the interior metal layer. Oxidation also proceeds from the inner surface after the cladding rupture. Calculation of cladding oxidation is made when the cladding temperature exceeded the input threshold value (default value 973 K).

Oxygen generally diffuses much faster in the oxide than in the metal layer. At the oxide-metal boundary, therefore, the oxygen atom flux coming from the oxide side is much larger than the flux away into the metal layer, and the difference is used for changing the metal into oxide, see **Fig. 11**. In this situation, oxide layer growth kinetics is determined by the oxygen diffusion in the (already-formed) oxide layer alone, independent of the diffusion in the metal layer.

Several empirical correlations have been proposed based on the diffusion-controled parabolic rate equation concept in the form:

$$h^2 = K\,t \tag{4.2}$$

where h is the thickness of oxide layer (m), and t is time (s). K is a temperature-dependent constant, for which FRETA-B uses the values reported by Cathcart[17]:

$$K = 1.13 \times 10^{-6}\left(-\frac{150.2}{RT}\right) \tag{4.3}$$

where R is gas constant (kJ/mol K) and T is temperature (K). Though the applicability of the Cathcart correlation is in fact limited to above 1000 °C, its use below 1000 °C does not make problem because the duration of LOCA is so short that no significant oxidation proceeds

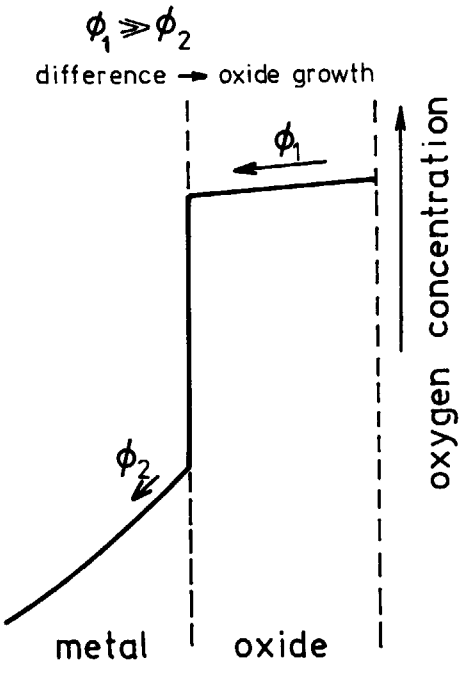

Fig. 11 Oxigen concentration in the cladding with oxide layer.

below 1000 °C.

Equation (4.2) describes the oxidation kinetics when the cladding temperature is kept constant throughout the process. For treating the kinetics with varying conditions, (4.2) can be used in incremental form:

$$(h^{n+1})^2-(h^n)^2=K\,\Delta t \tag{4.4}$$

where $n+1$ denotes the present time step whose size is Δt, and n the previous time step. Thus,

$$h^{n+1}=\sqrt{(h^n)^2+K\,\Delta t}\ . \tag{4.5}$$

Volume increment of the oxide layer in unit axial length is

$$\Delta V=\pi\{(r_0-h^n)^2-(r_0-h^{n+1})^2\} \tag{4.6}$$

where r_0 is the initial outer surface radius (m). Oxidation from the inner surface is calculated similarly.

Finally, reaction heat, given as follows, is added to linear heat rating of the rod (sector):

$$q_{react}=\rho\cdot\Delta V\cdot Q \tag{4.7}$$

where ρ is the density of the original metal, and Q is reaction heat (6500 J/g-Zr[18]).

Oxygen concentration in the metal affects the strength of the material. Hence, besides analyzing the oxide layer growth, diffusion of oxygen in the metal phase is calculated for determining the average oxygen concentration.

Assuming a diffusion constant independent of concentration, diffusion equation is written as

$$\frac{\partial c}{\partial t}=\frac{D}{r}\frac{\partial}{\partial r}\left(r\frac{\partial c}{\partial r}\right) \tag{4.8}$$

where c is oxygen concentration (kg/m^3), t is time (s), r is radial distance from the inner surface (m), and D is diffusion constant (m^2/s) given as[19]

$$D=3.923\times10^{-4}\exp\left(-\frac{213.4}{RT}\right) \tag{4.9}$$

with R denoting the gas constant (8.317 X 10^{-3} kJ/mol K). No differentiation is made between the alpha and beta phases concerning the oxygen diffusion.

The metal part is divided into four slabs with equal thicknesses and equation (4.8) is approximated by the finite difference method in the explicit way as

$$\frac{c_i^*-c_i}{\Delta t}=\frac{D}{r_i}\frac{1}{\Delta r}\left[\frac{r_i+r_{i+1}}{2}\left(\frac{c_{i+1}-c_i}{\Delta r}\right)-\frac{r_i+r_{i-1}}{2}\left(\frac{c_i-c_{i-1}}{\Delta r}\right)\right]$$

$$=\frac{D}{\Delta r^2}\frac{1}{r_i}[r_{R,i}c_{i+1}-(r_{L,i}+r_{R,i})c_i+r_{L,i}c_{i-1}] \tag{4.10}$$

where

$$r_{R,i}=\frac{1}{2}(r_i+r_{i+1})\quad\text{and}\quad r_{L,i}=\frac{1}{2}(r_i+r_{i-1})$$

and c_i^* denotes the concentration in the present time step. At the outer surface (interface with the oxide layer) of the metal phase, oxygen concentration is taken equal to the maximum oxygen solubility in the alpha-phase Zircaloy[20]:

$$c_N=c_{eq}=453.7\qquad \text{kg/m}^3\,.$$

At the inside surface, the same condition is used when the rod is ruptured and hence when oxidation proceeds from the inner surface too. When the rod is intact, the boundary condition at the inner surface is

$$\left.\frac{\partial c}{\partial r}\right|_{r=r_0} = 0 , \tag{4.11}$$

and the finite difference expression at the inside surface is

$$\frac{c_1^* - c_1}{\Delta t} = \frac{D}{\Delta r^2}\frac{1}{r_1}\left[\frac{r_1 + r_2}{2}(c_2 - c_1)\right]. \tag{4.12}$$

All the present-step concentration values c_1^* to c_N^* can be directly determined from the previous-step values c_i, provided that the time step size is sufficiently small. For stable calculation with the explicit method, given time step is divided into local sub-steps whose size is proportional to the ratio of the remaining metal layer thickness to the increment of oxide layer growth.

5 Mechanical Models

5.1 Scope

Fuel rod deformation modes considered in FRETA-B are thermal expansion of fuel pellets and the cladding; pellet-clad interaction (PCI); pressure-induced cladding deformation (ballooning). The restriction of excessive ballooning either by rod-rod contact or by rupture is also modeled. But no modeling has been made on bending of fuel rods, nor on interaction with grid spacers.

All mechanical calculations are made in subroutine DEFORM. The call for DEFORM is made separately for each rod and each axial segment. In each segment of a rod, stress-strain calculation at 20 azimuthal nodes is required to reproduce smooth profile of ballooning. Moreover, extremely rapid deformation in the final stage of ballooning requires very small time step for estimation of rupture strain. To save running time, therefore, sub-time step for mechanical calculation is used, which subdivides the input time step allowing coarse time meshing for other models, see **Fig. 4**.

The maximum strain increment in a time step is monitored, and when it is found to have exceeded a threshold value (0.05) in an axial segment of a rod, all the calculated results on the rod and the segment in problem are canceled and the time step is redivided into smaller ones. But in the other rods, this operation is not made; the undivided time step remains valid for those rods. Since rod deformation and internal pressure are closely related, the subdivided time step also applies to the calculation of internal gas pressure.

Figure 12 shows the flow of calculation within each call of DEFORM. Thermal expansion and gas pressure-induced deformation are calculated first, regardless of the gap size. In the two-dimensional modeling with four fuel sectors, check of the gap closure is made on two diagonal sectors simultaneously, and the pellet is shifted to realize equal gap size in the two sides. It is because pellet-cladding contact pressure in one side, if any, must be supported at the opposite side. When the two sides are found to have closed gaps, the preceding calculation results on pressure-induced deformation are canceled, and are replaced by the calculation of pellet-clad interaction.

5.2 Thermal Expansion

Complete cracking of pellet is assumed in calculating thermal expansion under irradiation: every fragment of a pellet is assumed to expand freely. Dividing a pellet into concentric rings, outward displacement of ring i is given by

$$u_i = \sum_{j=1}^{i} a(T_j)\,\Delta r_j \tag{5.1}$$

where T_j is the average temperature of j-th ring, Δr_j is its original thickness, and $a(T)$ is integrated linear thermal expansion from 25 °C to T (°C) which is given by the MATPRO model[14] as

$$[UO_2]\,a = -1.79\times10^{-4}+7.107\times10^{-6}T+2.581\times10^{-9}T^2+1.14\times10^{-13}T^3\ , \tag{5.2}$$

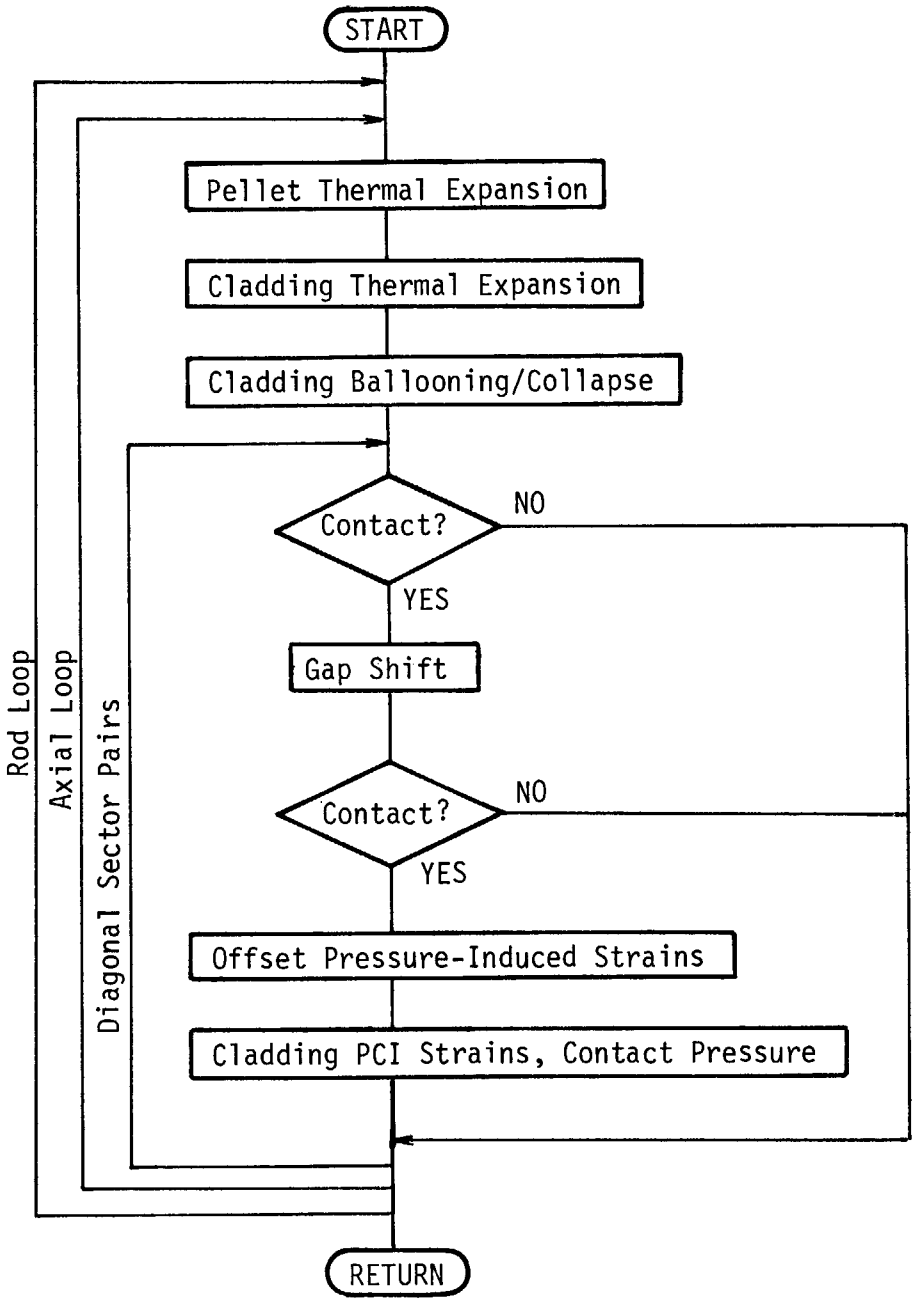

Fig. 12 Flow of mechanical calculation.

$$[PuO_2]a = -2.137\times10^{-4}+8.495\times10^{-6}T+2.151\times10^{-9}T^2+3.714\times10^{-16}T^3 \,. \tag{5.3}$$

For mixed oxide fuel, weighted average (by mole fractions) of the above two correlations is used. Eqn. (5.1) means that cracked fragments of a pellet are pushed outward successively from the center. If the fuel temperature was everywhere T_i, the radial displacement of ring i would have been

$$u_i^* = a(T_i)r_i \tag{5.4}$$

where r_i is mean radius of ring i. The difference between u_i and u_i^* represents the mismatch of cracked fragments, and hence determines crack volume. Total crack volume per unit fuel length is given by

$$V_c = 2\pi \sum_{i=1}^{N} (u_i - u_i^*) \Delta r_i (1 + a_i) \ . \tag{5.5}$$

where N denotes the outermost fuel ring.

Axial expansion of each fuel ring is obtained by multiplying the initial pellet height by the integrated thermal expansion a_i of the ring. The axial expansion of the pellet stack as a whole is determined by the expansion either at dish shoulder or pellet center (flat pellet). Thermal expansion of fuel pellet is evaluated successively and independently at four sectors of a fuel rod, so that four different values of axial stack expansion result. The average value is simply adopted as expressing the fuel stack state.

Thermal expansion of cladding is evaluated at one node in the radial direction, i.e. at midplane. Azimuthally, however, ballooning analysis requires 20 nodes, so that thermal expansion must also be evaluated at the 20 nodes. Since the result of thermal calculation is given at four positions per circumference, temperatures of the remaining 16 points are interpolated from the four values using a function of the form:

$$T(\theta) = A_0 + A_1 \sin(\theta) + A_2 \sin(2\theta) + A_3 \cos(\theta) \tag{5.6}$$

where θ is the azimuthal angle measured from a sector boundary, so that the four calculated data are given at $\frac{\pi}{4}$, $\frac{3}{4}\pi$, $\frac{5}{4}\pi$, and $\frac{7}{4}\pi$.

Texture-dependent thermal expansion of Zircaloy is treated in the MATPRO model by assuming a fixed texture. Axial and radial expansions are

$$\begin{aligned}
&\text{[axial]} \quad a = \frac{\Delta L}{L_0} = -1.199\times10^{-4} + 4.441\times10^{-6} T \quad (27^\circ C \leq T \leq 800^\circ C) \\
&\qquad\qquad = -8.3\times10^{-3} + 9.7\times10^{-6} T \quad (1000^\circ C \leq T) \\
&\text{[radial]} \quad a = -1.815\times10^{-4} + 6.721\times10^{-6} T \quad (27^\circ C \leq T \leq 800^\circ C) \\
&\qquad\qquad = -6.8\times10^{-3} + 9.7\times10^{-6} T \quad (1000^\circ C \leq T) \ .
\end{aligned} \tag{5.7}$$

Between 800 and 1000 °C, namely in the two-phase region of unoxidized zircaloy, thermal expansion is given by a discrete data table.

As in fuel pellet, azimuthally different values are obtained for the axial cladding expansion. By adopting the average value, it is implicitly assumed that larger or smaller expansions than the average value are converted to thermal stress under the plane-strain condition.

5.3 Deformation of Cladding Tube by Gas Pressure

As in other models, FRETA-B model for cladding deformation is two-dimensional in the transverse cross section: the rod state is assumed to be axially uniform within each axial segment.

Figure 13 shows the geometrical model of cladding deformation in the transverse cross section, which is azimuthally non-uniform. In each rod, cylindrical coordinate is used with the origin at the center of the original geometry. Variations of the midplane radius r and wall thickness h along the circumference are expressed by the Fourier series, with azimuthal angle θ, as

$$r(\theta) = r_0 + \sum_{n=1}^{N} [a_n \cos(n\theta) + b_n \sin(n\theta)] \ , \tag{5.8}$$

$$h(\theta) = h_0 + \sum_{n=1}^{N} [c_n \cos(n\theta) + d_n \sin(n\theta)] \ , \tag{5.9}$$

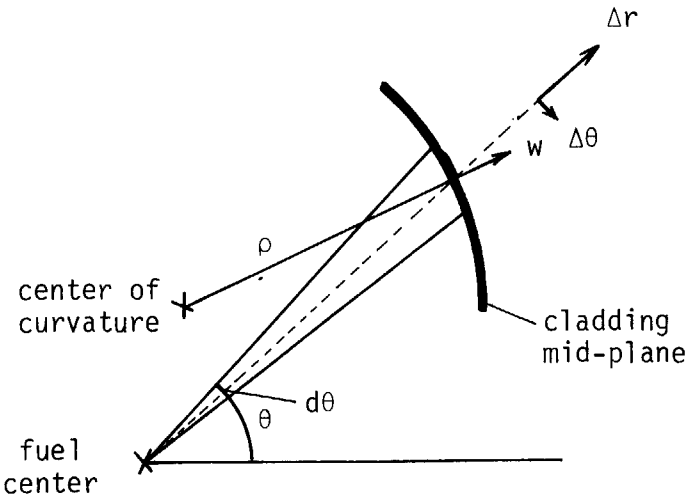

Fig. 13 Local curvature of the cladding midplane.

where N is normally taken to be 2 to 4. Using abbreviations

$$r'=\frac{dr}{d\theta} \quad \text{and} \quad r''=\frac{d}{d\theta}\left(\frac{dr}{d\theta}\right) ,$$

the curvature at a point (r, θ) is given by

$$\frac{1}{\rho}=k=\frac{r^2+2r'^2-r\cdot r''}{(r^2+r'^2)^{3/2}} . \tag{5.10}$$

Here a local coordinate is introduced, which is distinguished from the rodwise cylindrical coordinate by subscripts:

local	ρ	..... normal
	t	..... tangential
global (in a rod)	r	..... radial
	θ	..... azimuthal.

Z-axis is common to the two coordinates from the assumption.

With zero curvature in z-direction, the cladding hoop stress σ_t (Pa) is given by the membrane theory as

$$\sigma_t=\frac{\rho \Delta P}{h(\theta)} \tag{5.11}$$

where ρ is the radius of curvature (m^{-1}) and ΔP is derived from the rod internal and external pressures P_i and P_o (Pa), respectively, as

$$\Delta P=P_i-P_o . \tag{5.12}$$

Axial stress is assumed to be constant over a cross section and given by

$$\sigma_z=\frac{P_iS_i-P_o(S_i+S_c)}{S_c} \tag{5.13}$$

where S_i is the cross-sectional area of the rod internal volume and S_c is the area of the cladding cross section (m^2). They are calculated, using the Fourier expansion (5.8) and (5.9), as

$$\begin{aligned} S_i&=\frac{1}{2}\int_0^{2\pi}\left[r(\theta)-\frac{1}{2}h(\theta)\right]^2 d\theta \\ &=\pi\left(r_o-\frac{h_o}{2}\right)^2+\frac{\pi}{2}\sum_{n=1}^{N}\left[\left(a_n-\frac{c_n}{2}\right)^2+\left(b_n+\frac{d_n}{2}\right)^2\right] \end{aligned} \tag{5.14}$$

$$S_c = 2\pi r_0 h_0 (1+\bar{\varepsilon}_{th})^2 \tag{5.15}$$

where $\bar{\varepsilon}_{th}$ is average thermal strain. Variation of radial stress across the cladding is beyond the scope of the membrane theory; radial stress is approximated as everywhere equal to

$$\sigma_r = -\frac{1}{2}(P_i + P_o). \tag{5.16}$$

Using these stress components, elastic strains are calculated by

$$\begin{aligned}
\varepsilon_t^e &= \frac{1}{E}[\sigma_t - \nu(\sigma_z+\sigma_r)], \\
\varepsilon_z^e &= \frac{1}{E}[\sigma_z - \nu(\sigma_t+\sigma_r)], \\
\varepsilon_r^e &= \frac{1}{E}[\sigma_r - \nu(\sigma_t+\sigma_z)],
\end{aligned} \tag{5.17}$$

where E and ν are Young's modulus and Poisson's ratio, respectively.

Von Mises' equivalent stress for an anisotropic material is given in the form:

$$\sigma^{eq} = [F(\sigma_t-\sigma_r)^2 + G(\sigma_z-\sigma_r)^2 + H(\sigma_z-\sigma_t)^2]^{\frac{1}{2}} \tag{5.18}$$

where F, G, and H are Hill's anisotropy parameters. Dividing (5.18) with $\sqrt{G+H}$, we have

$$\sigma^Y = \frac{\sigma^{eq}}{\sqrt{G+H}} = [F'(\sigma_t-\sigma_r)^2 + G'(\sigma_z-\sigma_r)^2 + H'(\sigma_z-\sigma_t)^2]^{\frac{1}{2}} \tag{5.19}$$

where $F'=F/(G+H)$, $G'=G/(G+H)$ and $H'=H/(G+H)$.

Since G' plus H' equals unity, (5.19) indicates that σ^Y equals σ_z when the stress state is pure tension in z-direction. Hence σ^Y can be regarded as a kind of equivalent stress for reference to the uniaxial tensile testing data. Relationship between stress and strain rate in uniaxial creep tests, which will be described in more detail in 5.5, is now generalized to the relationship between σ^Y and generalized plastic strain increment (in a unit time) $\Delta\varepsilon_{eq}^p$. Then the Prandtl-Reuss flow rule for relating the strain components to the generalized strain is written in the form:

$$\begin{aligned}
\Delta\varepsilon_t^p &= \Delta\varepsilon_{eq}^p[F'(\sigma_t-\sigma_r)+H'(\sigma_t-\sigma_z)]/\sigma^Y, \\
\Delta\varepsilon_z^p &= \Delta\varepsilon_{eq}^p[H'(\sigma_z-\sigma_t)+G'(\sigma_z-\sigma_r)]/\sigma^Y, \\
\Delta\varepsilon_r^p &= \Delta\varepsilon_{eq}^p[G'(\sigma_r-\sigma_z)+F'(\sigma_r-\sigma_t)]/\sigma^Y.
\end{aligned} \tag{5.20}$$

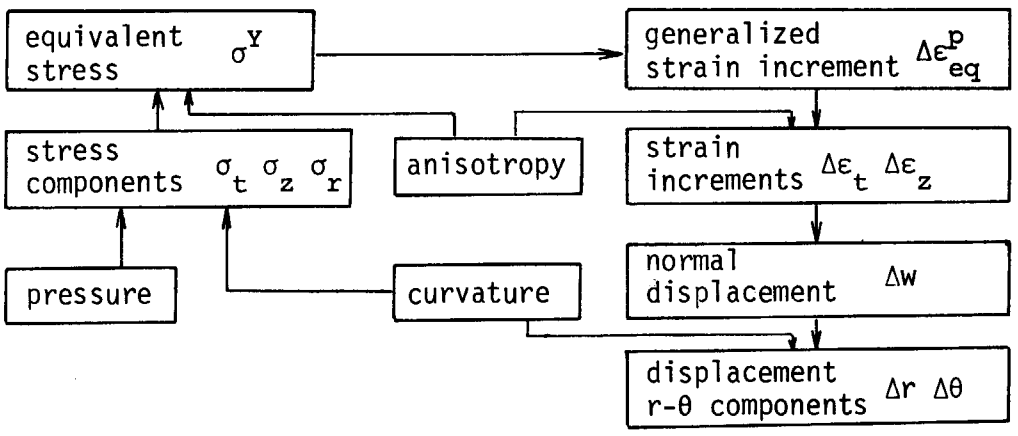

Fig. 14 Logic of calculating plastic strain increment.

Thus at the end of a time step, components ($i=t, z, r$) of total cladding strain are derived at each node as

$$\varepsilon_i=\varepsilon_i^e+(\varepsilon_i^p)_{old}+\Delta\varepsilon_i^p+\varepsilon_i^{th} \tag{5.21}$$

where the superscript th denotes thermal strain.

With the strain components, normal and axial components of the cladding local displacement are given by

$$\Delta w_\rho=\rho\,\Delta\varepsilon_t\ , \tag{5.22}$$

$$\Delta L=\Delta z\,\Delta\varepsilon_z\ , \tag{5.23}$$

where Δz is the axial segment length. In this model, displacement in a cross section occurs only along the radius of curvature, so that it has no tangential component.

The normal displacement Δw_ρ is decomposed into (r, θ) components in the rod global coordinate by

$$\Delta r=\frac{r\,\Delta w_\rho}{\sqrt{r'^2+r^2}}\ , \tag{5.24}$$

$$\Delta\theta=\frac{-r'}{\sqrt{r'^2+r^2}}\frac{\Delta w_\rho}{r}\ . \tag{5.25}$$

The wall thickness increment is simply given by

$$\Delta h=h\,\Delta\varepsilon_r\ . \tag{5.26}$$

Thus, new cladding geometry has been defined by a set of new geometrical data (midplane radius, azimuthal angle, wall thickness) as

$$(r_{i,old}+\Delta r_i',\ \theta_{i,old}+\Delta\theta_i',\ h_{i,old}+\Delta h_i)\quad (i=1,\ 20).$$

This data set is expressed by the Fourier series for the new step. This process of calculating the local strain increment is made independently at each azimuthal node. However, the calculated displacements determines the local curvature at nearby nodes, hence local stresses in the next step through (5.11). Thus the present ballooning model is two-dimensional as a whole through the interference effect appearing in the next step.

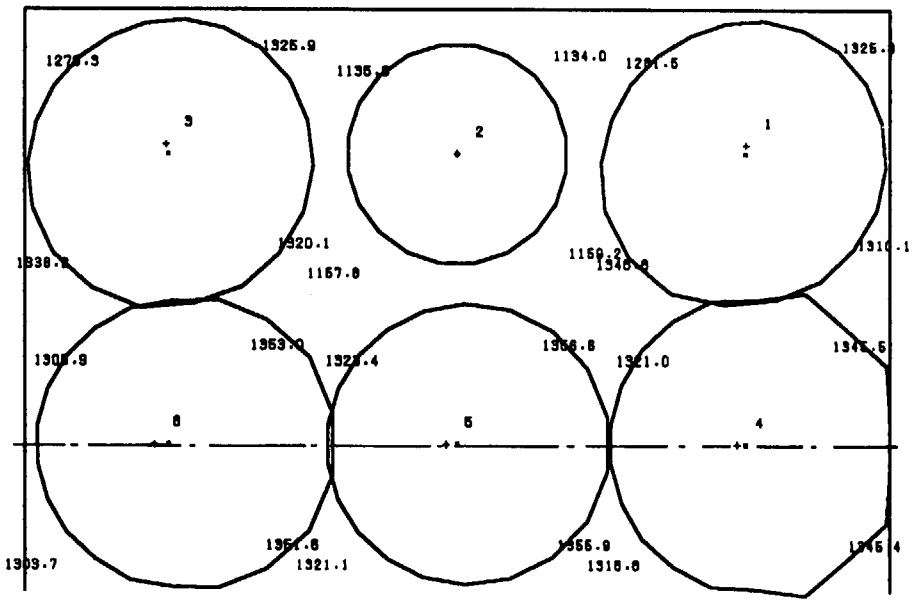

Fig. 15 Example of multi-rod ballooning calculation.

An example of ballooning calculation is shown in **Fig. 15**. In this case, five pressurized fuel rods are on the course of ballooning. Circles indicate cladding midplanes; attached numerical data show the sectowise cladding surface temperature in K.

5.4 Pellet-Clad Interaction

Differently from the case of ballooning, the calculation of pellet-clad gap state and interaction is made at one azimuthal point in each sector, hence directly using the results of thermal analysis. As was shown in **Fig. 12**, the gap closure in each step is examined after a series of calculation on thermal expansions and pressure-induced cladding deformation.

The gap state is first determined independently in each sector. Open or closed gap state is judged by the sign of the radial gap size given by

$$t_g = r_{ci} - (r_{fo} + \bar{\mu}) \tag{5.27}$$

where $\bar{\mu} = 1.98(\mu_f + \mu_c)$,

and r is radius, μ is surface roughness with subscripts f and c denoting fuel and cladding, respectively, i and o denoting inner and outer surfaces, respectively.

When t_g is positive in all four sectors, the gap is open and the already calculated pressure-induced deformation is confirmed as showing the present geometry. If, on the other hand, t_g is found to be negative in a sector i, the gap size is averaged over the two opposite sectors:

$$\bar{t}_g(i, i+2) = \frac{1}{2}\{(t_g)_i + (t_g)_{i+2}\} \ , \tag{5.28}$$

and the sign of $\bar{t}_g$ is checked again.

Thus gap closure is defined as the state of a couple of fuel sectors diagonal to each other, and PCI is calculated for the couple. The code is prepared for the situation that the gap is closed along one diagonal of a rod, whereas open along the other one.

Even in a general case, the magnitude of interaction is different between two diagonal sector couples. But the interaction in each sector is treated as if it is axisymmetric, to enable the use of the thin-shell model. The following assumptions are made for simplification:

1) fuel pellet behaves as a rigid body,
2) PCI in each axial segment is determined by local pellet and cladding dimensions alone, and
3) after contact, no slipping occurs between pellet and cladding.

Assumption 1) means that only cladding deforms by excessive thermal expansion of pellet, and that the dimension of pellet is not affected by PCI. Therefore the output of the PCI calculation is not dimensions nor total strains, but contact pressure and the cladding plastic strains.

The PCI-induced stress-strain history of the cladding is treated by the model for stress relaxation under fixed displacement. For this purpose, given time step size Δt is divided into 2 to 30 sub-steps depending on the differential thermal expansion of pellet and cladding:

$$\Delta t = \delta t_1 + \delta t_2 + \cdots\cdots\cdots + \delta t_N. \tag{5.29}$$

The excess thermal expansion of pellet is assumed to be accomodated entirely by elastic strains of the cladding at the start of the step Δt. Then gradually with sub-steps δt, elastic strain is replaced by plastic strain lowering the stress.

From the thin-shell model (neglecting radial stress), the elastic strain increments are related to stress increments by

$$\Delta\varepsilon_\theta^e=\frac{1}{E}(\Delta\sigma_\theta-\nu\Delta\sigma_z),$$

$$\Delta\varepsilon_z^e=\frac{1}{E}(\Delta\sigma_z-\nu\Delta\sigma_\theta), \tag{5.30}$$

$$\Delta\varepsilon_r^e=-\frac{\nu}{E}(\Delta\sigma_\theta+\Delta\sigma_z).$$

From assumptions 1) and 3), once gap is closed, differential deflections of pellet and cladding (both radial and axial) can be calculated from thermal expansions. These deflections are expressed as strains by dividing with the gap radius and designated as G and H, which can be determined as

$$G=\Delta\varepsilon_\theta^{th}(fuel)-\Delta\varepsilon_\theta^{th}(clad)=\Delta\varepsilon_\theta^e-\frac{h}{2r_m}\Delta\varepsilon_r^e, \tag{5.31}$$

$$H=\Delta\varepsilon_z^{th}(fuel)-\Delta\varepsilon_z^{th}(clad)=\Delta\varepsilon_z^e, \tag{5.32}$$

where r_m is midplane radius and h is wall thickness of the cladding.

$\Delta\varepsilon_\theta^{th}$ and $\Delta\varepsilon_z^{th}$ (fuel) are thermal strain increments at the outer surface of the pellet which are in fact equal (isotropic expansion).

Substituting (5.30) into (5.31) and (5.32), we obtain

$$\frac{1}{E}(\Delta\sigma_\theta-\nu\Delta\sigma_z)+\frac{\nu h}{2r_m\cdot E}(\Delta\sigma_\theta+\Delta\sigma_z)=G\ , \tag{5.33}$$

$$\frac{1}{E}(\Delta\sigma_z-\nu\Delta\sigma_\theta)=H. \tag{5.34}$$

Solving (5.33) and (5.34), we have

$$\Delta\sigma_\theta=\frac{G+\nu(1-B)H}{(1+\nu)(1-\nu+\nu B)}E\ , \tag{5.35}$$

$$\Delta\sigma_z=\frac{\nu G+(1+\nu B)H}{(1+\nu)(1-\nu+\nu B)}E\ , \tag{5.36}$$

where $B=\dfrac{h}{2r_m}$.

Substituting (5.35) and (5.36) into (5.30), the 'initial' elastic strain of the time step Δt are calculated as

$$\varepsilon_\theta^{e,init}=\frac{(1-\nu^2)G-\nu(1+\nu)BH}{(1+\nu)(1-\nu+\nu B)}+\varepsilon_\theta^{e,old}\ , \tag{5.37}$$

$$\varepsilon_z^{e,init}=\frac{[(1-\nu^2)+\nu(1+\nu)B]H}{(1+\nu)(1-\nu+\nu B)}+\varepsilon_z^{e,old}. \tag{5.38}$$

The initial stress components are obtained by adding $\Delta\sigma_\theta$ and $\Delta\sigma_z$ to the corresponding stress components at the end of the previous step. Using these stresses, the equivalent stress for reference to uniaxial tensile data is obtained using (5.19) as in the case of pressure-induced deformation. Then the generalized strain increment $\delta^1\varepsilon_{eq}^p$ in the first sub-step δt_1 is calculated with the uniaxial creep correlation. Its three components are derived by the Prandtl-Reuss flow rule, (5.20).

At the end of the sub-step, the plastic strain increments are compensated by the reduction of elastic strain components:

$$\delta^1\varepsilon_i^e=-\delta^1\varepsilon_i^p \tag{5.39}$$

where the superscript 1 indicates that the increment is for the first sub-step.

Then solving (5.30) for σ, the stress increments (actually reduction) due to relaxation are calculated as

$$\delta^1\sigma_\theta=\frac{E}{1-\nu^2}\,(\delta^1\varepsilon_\theta^e+\nu\delta^1\varepsilon_z^e),$$
$$\delta^1\sigma_z=\frac{E}{1-\nu^2}\,(\delta^1\varepsilon_z^e+\nu\delta^1\varepsilon^e), \tag{5.40}$$

and subtracted from the 'initial' stresses.

The procedure from (5.39) to (5.40) is repeated in subsequent sub-steps to the last one δt_N, and the stress components and the strain components, both elastic and plastic, are finally determined as the end state of the whole time step Δt as

$$\sigma_i=\sigma_i^{old}+\Delta\sigma_i^{init}+\sum_j^N(\delta\sigma_i)_j, \tag{5.41}$$

$$\varepsilon_i^e=\varepsilon_i^{e,init}+\sum_j^N(\delta\varepsilon_i^e)_j, \tag{5.42}$$

$$\varepsilon_i^p=\varepsilon_i^{p,old}+\sum_j(\delta\varepsilon_i^p)_j. \tag{5.43}$$

The pellet-cladding contact pressure is calculated by

$$P_c=\frac{r_{co}P_o+h\sigma_\theta}{r_{ci}}-P_i \tag{5.44}$$

where P_o and P_i are external and internal pressures, respectively.

A situation can occur that, as in **Fig. 16**, the pellet-clad gap is closed along one diagonal while it is open along the other diagonal. Since the cladding displacement in the closed-gap sector is evaluated at one (central) node in the sector and the result is allocated to all the nodes in the sector, a discontinuity can arise at the sector boundary. The dicontinuous cladding strains due to this discontinuity, however, can be diminished by the smoothing effect of the Fourier-series fitting of midplane radii.

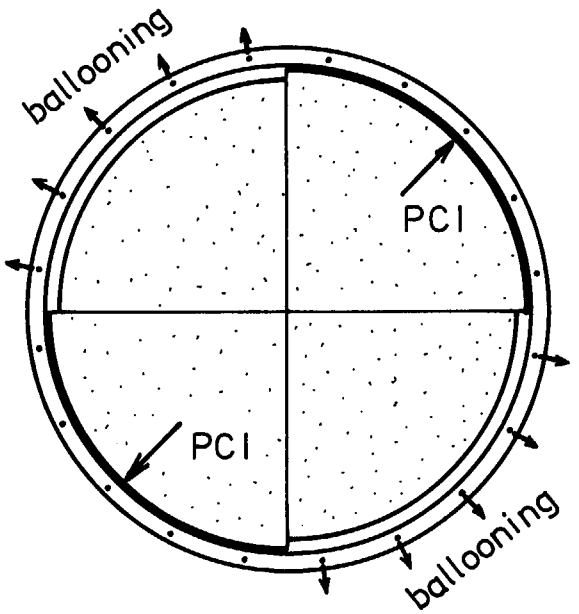

Fig. 16 Different gap states between two diagonal sets of fuel sectors.

5.5 Plasticity-Creep Correlation and Anisotropy of Zircaloy

(1) Uniaxial Equation

Strength data of Zircaloy have been mostly taken from uniaxial tensile or creep testings in the longitudinal direction of either tube or sheet specimen. Strictly speaking, this longitudinal strength depends on the texture of particular tube or sheet. For practical analysis of fuel behavior during accident, however, it is convenient to postulate a typical longitudinal strength which represents such tensile and creep data, and also to postulate a typical anisotropy factor to apply the uniaxial results to bi-axial problems. This idealized longitudinal strength corresponds to σ^y in eqn. (5.19).

The equation dealing with the non-elastic straining is written in general form as

$$\sigma = f(\dot{\varepsilon}, \varepsilon) \tag{5.45}$$

where $\dot{\varepsilon}^p$ is non-elastic (plastic or creep) strain rate (s^{-1}). This general form is written in more explicit forms, depending on which of the strain and the strain rate is more important, either in creep type:

$$\dot{\varepsilon}^p = A\sigma^n, \tag{5.46}$$

or in plasticity (strain hardening) type:

$$\sigma = K\varepsilon^\nu \ . \tag{5.47}$$

In the temperature range relevant to the ballooning, creep-type equation well describes the deformation process. But in the lower temperature range, the plasticity type of equation must be used, so that some discontinuity at the boundary is unavoidable.

In the following descriptions, stress and strain are given as true stress and true strain.

a) low temperature range of alpha-phase Zircaloy ($T < 730$ K)

The MATPRO-09 model[14] is used, in which strain-hardening curve is expressed in the form of (5.47). The coefficient K and stress exponent ν are given, when the unit of stress σ is MN/m^2, by

$$K = (1.075\times10^3 - 0.9996\cdot T)\cdot(1-0.546w) \ , \tag{5.48}$$

$$\nu = (-0.0186 + 7.11\times10^{-4}T - 7.721\times10^{-7}T^2)\cdot Y\cdot Z \ , \tag{5.49}$$

$$Y = 0.847\exp(-39.2w) + 0.153 - 0.0916w + 0.229w^2 \ ,$$

$$Z = \exp[-(\phi t)^{1/3}/(3.73\times10^7 + 2\times10^8 w)] \ ,$$

where T is temperature (K), w is cold work (m^2/m^2), ϕ is fast neutron flux (n/m^2 s) and t is time (s).

For calculating the plastic strain increment, yielding of the material must be checked. It is made by comparing the strains ε_1 and ε_2, which are determined by the stress σ and the old plastic strain ε^p_{old} as

$$\varepsilon_1 = \varepsilon^p_{old} + \frac{\sigma}{E} \ ,$$

$$\varepsilon_2 = \left(\frac{\sigma}{K}\right)^{1/\nu} \ , \tag{5.50}$$

and if $\varepsilon_1 \geq \varepsilon_2$, the material is elastic and $\varepsilon = \varepsilon_1$,

if $\varepsilon_1 \leq \varepsilon_2$, the material is plastic and $\varepsilon = \varepsilon_2$.

In the first case, there is no plastic strain increment, whereas in the second case, the increment is given by

$$\Delta\varepsilon^{p}=\varepsilon-\varepsilon^{p}_{old}\,. \tag{5.51}$$

b) high-alpha region (730 K $\leq T \leq$ 1073 K)

The uniaxial creep rate proposed by Rosinger et al[21] is used:

$$\dot{\varepsilon}_{\alpha}=2000\,\sigma^{5.32}\exp\left(-\frac{34220}{T}\right) \tag{5.52}$$

where σ is stress (MPa), and $\dot{\varepsilon}$ is true strain rate (s^{-1}).

c) beta-phase range ($T \geq$ 1273 K)

Also given by Rosinger et al as

$$\dot{\varepsilon}_{\beta}=8.1\,\sigma^{3.79}\exp\left(-\frac{17110}{T}\right)\,. \tag{5.53}$$

d) two-phase region (1073 $< T <$ 1273)

Interpolation is made using the creep rate equations (5.52) and (5.53),

$$\dot{\varepsilon}_{\alpha\beta}=\left\{1-\left(\frac{T-1073}{200}\right)^{4}\right\}\dot{\varepsilon}_{\alpha}+\left(\frac{T-1073}{200}\right)^{4}\dot{\varepsilon}_{\beta}\,. \tag{5.54}$$

(2) Anisotropy Factors

The creep rate equations (5.51) to (5.53) are regarded as relating the generalized strain increment (in unit time) to the equivalent stress referenced to the longitudinal direction, i.e. H' in (5.19). For calculating three components of a strain, the anisotropy factors σ^{Y}, F', G' must be numerically determined. The only existing study of anisotropy in the temperature range relevant to the LOCA condition seems to be that performed in PNWL[22]. It estimated the ratios between the factors in the range:

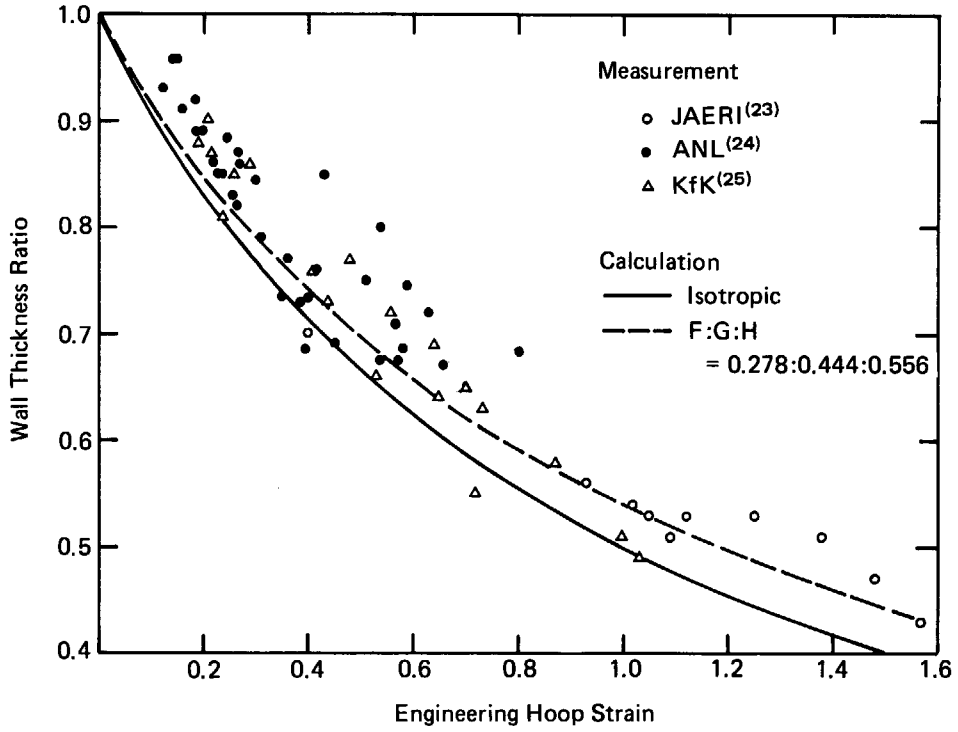

Fig. 17 Relationship between radial and hoop strains by closed-end tube burst.

$$R=\frac{H}{G}=1.25\sim2.50\ ,$$
$$P=\frac{H}{F}=2.0\ \ \sim4.0\ . \tag{5.55}$$

Use of the smallest fractions from the above ranges, hence the smallest anisotropy seems to match the wall-thinning and axial shrinkage data in closed-end burst experiments, see **Fig. 17**. Then the anisotropy factors after division by $(G+H)$, see 5.3, are obtained as $F'=0.278$, $G'=0.444$, $H'=0.556$.

(3) Effect of Oxidation on the Cladding Strength

It is assumed that oxide layers do not contribute to the strength of a cladding tube, so that the oxide thicknesses are subtracted from the cladding wall thickness for use in the mechanical calculation:

$$h_m=h_0-(d_1+d_2) \tag{5.56}$$

where d_1 and d_2 are oxide thicknesses at inside and outside surfaces. They oxygen atoms dissolved in the metal decrease the creep rate. The effect of uniform oxygen concentration is expressed in the usual creep rate equation form as

$$\dot{\varepsilon}=F A\sigma^n \tag{5.57}$$

where $\dot{\varepsilon}$ and σ are strain rate and stress, respectively, and A and n are coefficient and stress exponent, respectively, for unoxidized zircaloy appearing in (5.46). The coefficient F stands for the effect of oxygen concentration as[26)]

$$F=\exp(-342C) \tag{5.58}$$

where C is oxygen concentration (weight fraction) minus normal oxygen concentration in unoxidized Zircaloys (1×10^{-3}).

The case with spacial distribution of oxygen concentration is handled by defining the local stress and strain rate for each of N sub-slabs as

$$N\sigma=\sigma_1+\sigma_2+\cdots\cdots\ +\sigma_N, \tag{5.59}$$

and

$$\dot{\varepsilon}=\dot{\varepsilon}_1=\dot{\varepsilon}_2=\cdots\cdots\ =\dot{\varepsilon}_N, \tag{5.60}$$

where σ is average or macroscopic stress and σ_i is local stress in the i-th slab. Assuming (5.57) type of rate equation for each sub-slab and solving for local stress,

$$\sigma_i=A^{-\frac{1}{n}}F_i^{-\frac{1}{n}}\dot{\varepsilon}_i^{\frac{1}{n}}. \tag{5.61}$$

Inserting (5.61) into (5.59), and using the relationship of (5.60), we have

$$N\sigma=A^{-\frac{1}{n}}\dot{\varepsilon}^{\frac{1}{n}}[F_1^{-\frac{1}{n}}+F_2^{-\frac{1}{n}}+\cdots+F_N^{-\frac{1}{n}}], \tag{5.62}$$

hence

$$\dot{\varepsilon}=A\sigma^n\left[\frac{N}{F_1^{-\frac{1}{n}}+F_2^{-\frac{1}{n}}+\cdots+F_N^{-\frac{1}{n}}}\right]^n. \tag{5.63}$$

We can thus define a coefficient for hardening due to dissolved oxygen as

$$F=\left[\frac{N}{F_1^{-\frac{1}{n}}+F_2^{-\frac{1}{n}}+\cdots+F_N^{-\frac{1}{n}}}\right]^n \tag{5.64}$$

for use in the macroscopic creep rate equation.

5.6 Fuel Rod Rupture

In FRETA-B, a ballooned fuel rod is judged to have ruptured when the local hoop strain at any azimuthal node has exceeded the threshold value. The threshold value was so determined as to give a reasonable estimate of azimuthal-average rupture strain when used with the approximate model of ballooning by the membrane theory.

According to metallographic examinations of ruptured cladding tubes, wall thickness near the rupture point is sometimes found to have decreased to one-fifth of the original thickness[24]. It amounts to a local radial (true) strain of -1.6. But such a microscopic value cannot be applied to the local strains calculated by the (modified) thin-shell theory of the code, because the theory is in fact not applicable to such a large strain range.

The use of the thin-shell theory until rod rupture occurs is quite approximate. Therefore, the rupture criterion must be determined empirically so that it may compensate the error in the strain calculated by the approximate model. For use in FRETA-B, average rupture hoop strain data were collected from the out-pile ballooning experiments with small temperature ramp rate, as shown in **Fig. 18**. These hoop strain values are not local ones, but circumferential-average values. However, under the experimental conditions as stated above, temperature distribution is fairly uniform and hence the difference between local and average rupture strains is fairly small. Thus the use of the upper envelope of such data as a local rupture criterion compensates the inadequate treatment of strain localization by the thin-shell model, and enables reasonable estimate of average hoop strain.

The envelope, indicated by the broken line in **Fig. 18**, is expressed as a simplified function of temperature as

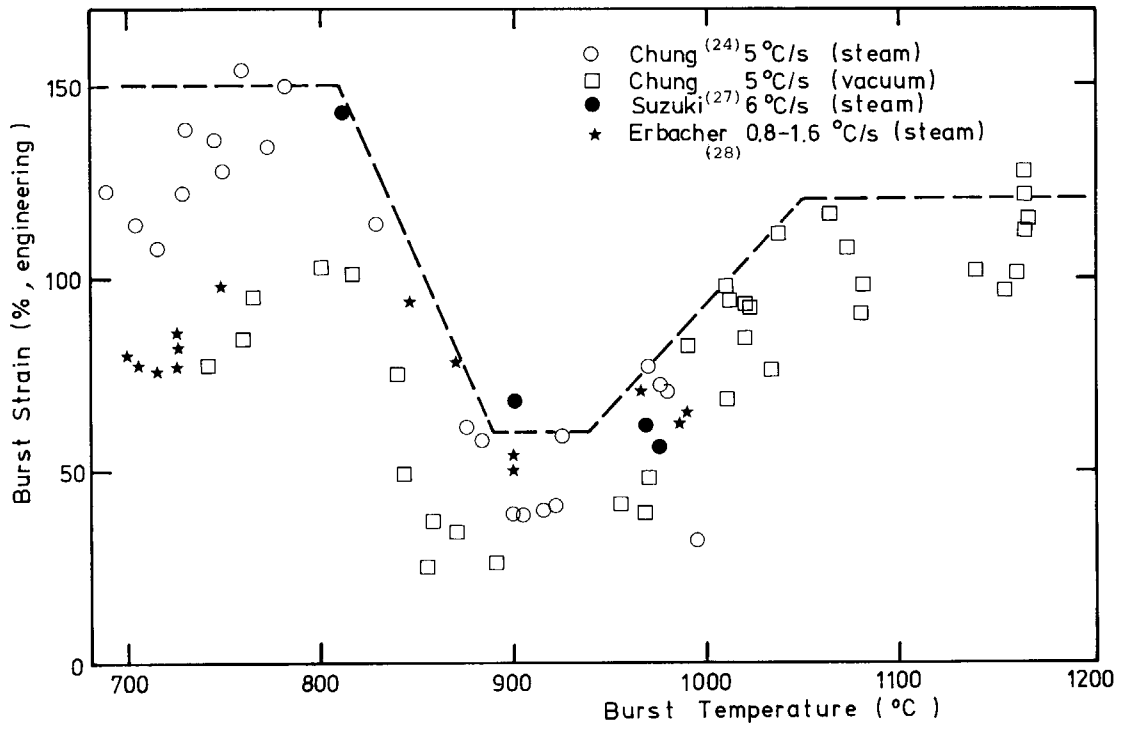

Fig. 18 Average burst strains in single-rod ballooning experiments.

$$
\begin{aligned}
\varepsilon_\theta(\text{true}) &= 1.0 && (T \leq 1123\,K)\ , \\
&= 0.3+0.014(1173-T) && (1123<T\leq 1173)\ , \\
&= 0.3 && (1173<T\leq 1223)\ , \\
&= 1.0+0.014(T-1273) && (1223<T\leq 1273)\ , \\
&= 1.0 && (1273<T)\ ,
\end{aligned}
\tag{5.65}
$$

In a rod that was judged to have ruptured at a node, the internal gas pressure is instantaneously set equal to the external pressure, so that the driving force for further deformation is lost automatically.

5.7 Rod-Rod or Rod-Shroud Contact

After a partial rod-rod contact, further ballooning is calculated only at free nodes not trapped by other fuel rods. Monitoring of the rod-rod contact is made by tracing the displacements of all the azimuthal nodes of all the fuel rods.

Let P in **Fig. 19** be an azimuthal node of a rod whose center (original geometry) is O_1. Likewise, let Q and R be two adjacent nodes of another rod whose center is O_2. Let S be the intersection of two lines QR and O_1P. The condition for that node P is trapped by the chord QR is:

1) point S is included in the span QR ($\vec{SQ}\cdot\vec{SR}<0$ in vector form) and
2) point S is included in the span O_1P ($\vec{SO_1}\cdot\vec{SP}<0$).

These conditions are checked for the combinations of all nodes and all chords with two adjacent nodes. This method can be applied to the check of rod-to-shroud contact by replacing the chord with the shroud face element.

When a node is judged to have been captured by another rod or shroud, the node is excluded from the calculation of further straining.

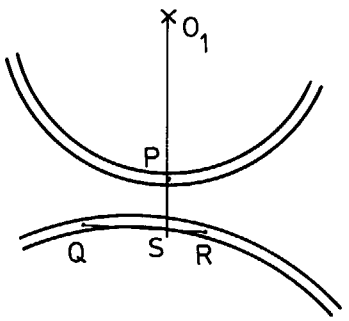

Fig. 19 Rod-rod contact model.

6. Fuel Rod Internal Gas Pressure Model

FRETA-B calculates the hot-state gas pressure and optionally transient gas flow through the pellet-cladding gap, based on the input cold-state gas pressure data. Gas composition (helium, fission gas, H_2O etc.) and total moles are fixed throughout the calculation run: composition change due for example to additional fission gas release is neglected. Gas pressure calculation in each rod is made until the rod is judged to have ruptured.

6.1 Uniform Gas Pressure in a Rod

Unless specified otherwise by input, gas pressure in a fuel rod is assumed to be everywhere uniform. Free volumes considered for pressure calculation are upper and lower plena, fuel-clad gap, center hole, dish, and crack volumes of fuel pellets. The ideal gas law is assumed in each volume element:

$$PV_i=n_iRT_i \tag{6.1}$$

where P is pressure (Pa), R is the gas constant (8.317 J/mole·K), and V_i, n_i, T_i, are the volume (m^3), gas moles, and the local temperature (K), respectively, of volume element i. The temperature of each volume element is approximated as follows:

1) upper and lower plenum temperatures are set equal to the outlet and inlet coolant temperatures, respectively,
2) pellet-clad gap temperature is set equal to the average of the fuel and the cladding surface temperatures,
3) fuel crack temperature is equal to the volumetric average temperature of fuel, whereas the temperatures at center hole and dish volume are taken equal to the respective local temperatures.

Thermal expansion of fuel stack reduces the plenum volumes. Reduction of the upper plenum volume is calculated by

$$V_{pu}=V_{pu0}\left(1-\delta\frac{\Delta h}{L_{pu0}}\right) \tag{6.2}$$

where L_{pu0} and V_{pu0} are the length (m) and volume (m^3), respectively, of the upper plenum in the cold state, and Δh is the differential thermal expansion of the fuel and the cladding (m). δ is a coefficient that depends on the lower end geometry:

$\delta=1$ (no lower plenum),

$\delta=\frac{1}{2}$ (with lower plenum).

The hot volume of the lower plenum is given by (6.2) with δ equals 1/2; that is, when gas plenum exists at both ends, they are assumed to equally accomodate the fuel stack elongation.

Equation (6.1) is written in the form:

$$\left(\frac{V}{T}\right)_i=n_i\frac{R}{P} \tag{6.3}$$

Since the gas pressure is uniform all over a fuel rod, (6.3) can be summed over whole void volumes. Hence,

$$P=nR/\sum_i \left(\frac{V}{T}\right)_i \tag{6.4}$$

where n is the total gas moles in a rod.

When the cladding has ruptured at an elevation, the gas pressure is instantaneously set equal to the current external pressure.

6.2 Transient Axial Gas Flow

Transient axial pressure gradient and gas flow occur as a result of sudden change of local gas temperature or void volume. From the viewpoint of fuel behavior analysis under LOCA, this effect can be important in connection with the kinetics of ballooning (direct effect of gas pressure on fuel temperature is negligible). If a fuel rod swells at an elevation, and if considerable flow resistance exists between the position and the gas plenum, the ballooning results in reduced local pressure which works as a negative feed-back mechanism for further deformation. The transient gas flow calculation is made as an input option: unless specified, instantaneous pressure equilibrium is assumed in each rod as described in 6.1.

With cracked and relocated pellets, actual geometry of gas flow path in a rod is extremely complex, being composed of pellet-cladding gap and pellet cracks. To simplify the problem, however, relocation of cracked pellets is neglected, and the gas is assumed to flow through the idealized concentric fuel-cladding gap space. This approximation reduces the calculated flow resistance. The induced error is adjusted by setting a numerical constant so that the calculated gas flow rate in simulation experiments may fit to the measurement.

The gas flow is assumed to be Poiseulle flow. Molecular gas flow rate through an annular path from axial position $i+1$ to i is given by

$$F=\frac{\pi g^3 r\cdot(P_{i+1}^2-P_i^2)}{12\mu RTl} \tag{6.5}$$

where F is flow rate (moles/s); g and r are the width and midplane radius of the annulus (m), respectively; P is pressure (Pa); μ is dynamic viscosity (kg/m s); l is the distance between the two positions (m).

Equation (6.5) transforms to the form:

$$F\cdot R^f=P_{i+1}^2-P_i^2 \tag{6.6}$$

where

$$R^f=\frac{12\mu RTl}{\pi g^3 r} \ . \tag{6.7}$$

Here let the two subscripts $i+1$ and i indicate two successive axial segments. If we give the variables in the right-hand side of (6.7) representative values of segment i, then the resultant value R_i^f gives the flow resistance over segment i. The flow resistance between the centers of segments $i+1$ and i is given by

$$R_{i,i+1}^f=\frac{1}{2}(R_i^f+R_{i+1}^f) \ . \tag{6.8}$$

Then using $R_{i,i+1}^f$, (6.6) can be rewritten as

$$R_{i,i+1}^f\cdot F_{i+1,i}=P_{i+1}^2-P_i^2 \tag{6.9}$$

where $F_{i+1,i}$ is molecular gas flow rate from segment $i+1$ to i (moles/s).

Gas mole increase in segment i in a given time step Δt is determined as

$$\Delta n_i = \left[\frac{P_{i+1}^2 - P_i^2}{R_{i,i+1}^f} + \frac{P_{i-1}^2 - P_i^2}{R_{i,i-1}^f} \right] \Delta t \ . \tag{6.10}$$

Thus, if the segmentwise flow resistance is large enough, or the time step size is small enough, new gas moles hence new gas pressure in each segment is explicitly obtained using the previous-step pressures.

Such a situation is, however, exceptional: given time step size (which is determined from the stability of thermal or mechanical calculation) is usually too large to explicitly calculate inter-segment gas flow. Procedures normally taken to cope with such a numerical instability is either to redivide the given time step into sub-steps, or to solve the flow equation by implicit method. In this code, however, neither procedure is taken. It is because gas pressure and flow calculation in a fuel code is made merely as a step to calculate fuel rod deformation. As stated before, the time step size given to the gas flow subcode is determined from the stability of thermal or mechanical calculation. In other words, the step size represents the characteristic time of heat transfer or rod deformation. Then, the transient gas flow calculation is worth undergoing only when the characteristic time for gas flow is longer than the thermal or mechanical characteristic time. Otherwise, the assumption of instantaneous pressure equilibrium stated in 6.1 can save running time without affecting the accuracy of calculated fuel temperature and deformation.

Thus, the policy of FRETA-B is basically to calculate transient gas flow only when the explicit solution (6.10) does not invite numerical instability under the given time step size. It can however occur that some axial segments have large enough gap size, while others have narrow gaps and make considerable flow barrier between the large-gap zone and the gas plenum. To generally handle any combination of segmentwise gap sizes, the code monitors the segmentwise flow resistances and integrates the segments with small resistances into a larger control volume. Since flow resistance and contained gas moles are additive quantities for serial flow segments, this procedure can be easily undertaken and leads consistently to the extreme case of instantaneous pressure equilibrium throughout a rod (**Fig. 20**).

Quantities determining the numerical stability are time step size, flow resistance and the gas moles contained in the volume (inventory). An instability factor is defined as follows:

$$f = \frac{\Delta t}{n \cdot R^f} \ . \tag{6.11}$$

Integration of segments increases the denominator of the f-factor.

First, the gas mole inventory and flow resistance of the lowermost segment, n_1 and R_1^f, are substituted into (6.11) together with the current time step size. If the resultant value is greater than a limiting value, segment 1 is judged to be unstable by itself and segments 1 and 2 are integrated into a single control volume whose pressure is calculated by (6.4). The limiting value for f was determined to be 10^{-7} $(\mathrm{MPa})^{-2}$ from the experience of test calculations as a value preventing numerical instability. Then the f-factor is evaluated for the combination of segments 1 and 2 with added gas moles and flow resistances. This operation is continued until, by integration of segments 1 to j, the f-factor becomes small enough.

Thus the first integrated control volume has been defined, and integration into the next volume is started from segment $j+1$ upward in the same way. The last volume includes the upper gas plenum. Total number and the composition of the integrated volumes can change from time step to step.

The gas pressure in an integrated volume V_m is calculated by (6.4) taking all the axial segments and their volume elements that belong to V_m. Flow resistances are converted to the values for the path between the centers of the integrated volumes. Then (6.5) is applied to

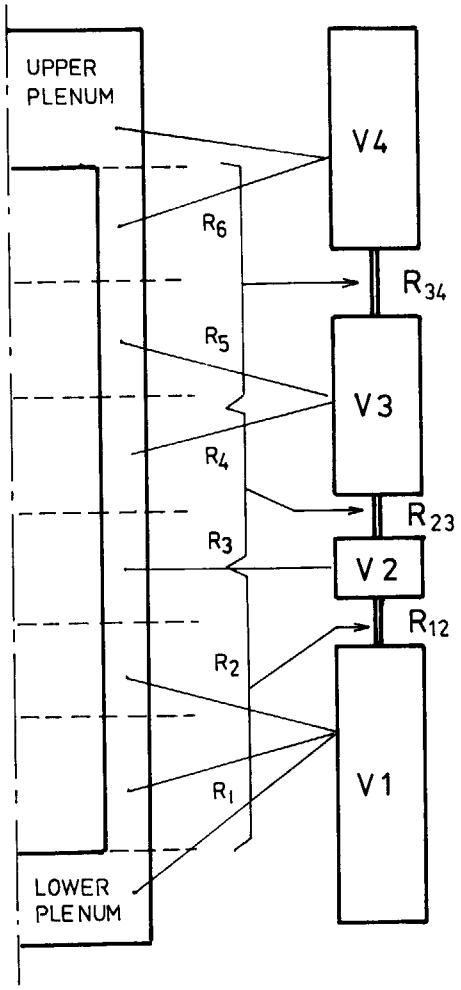

Fig. 20 Integration of axial segments into uniform-pressure zones.

the inter-integrated volume gas flow, and from the obtained gas mole increase Δn_m in volume m, new gas pressure is derived as

$$P_m=(n_m+\Delta n_m)R/\sum_{i\in V_m}\left(\frac{V}{T}\right)_i \tag{6.12}$$

where the summation is made for all segments that belong to V_m. The pressure P_m is common to all the segments that belong to V_m, so that the new gas inventory in each segment is calculated by

$$n_i=P_m\left(\frac{V}{T}\right)_i/R\ . \tag{6.13}$$

These procedures apply to the gas flow through an idealized concentric gap space. For considering more realistic complex flow path, (6.5) is rewritten in the form

$$F=\frac{\pi}{Ha}\bar{D}\cdot D_H^3\frac{P_{i+1}^2-P_i^2}{2\mu RTl} \tag{6.14}$$

where $\bar{D}$ is the midplane diameter of the flow path, D_H is equivalent hydraulic diameter and Ha is a numerical constant called Hagen number. The present annular flow path case corresponds to the values: $\bar{D}=2r$, $D_H=2g$, $Ha=96$, where g is radial gap size. The complex flow path in irradiated fuel is considered by changing the Ha value. According to an out-pile experiment[29], the Ha number is greater than 200 for irradiated fuel rod at cold state. The code leaves the Hagen number for input by user, with a default value of 200.

7. Code Assessment

Assessment of the code's capability, particularly accuracy check of the analytical results, has been made through many post-test calculations of various fuel behavior simulation experiments. Some results of these calculations have been published[30)-32)].

Model for heat conduction in fuel rod, basic part of the code, was assessed through the calculations on fuel irradiation experiments with center thermocouples performed in Halden HBWR reactor. For this assessment, the first startup data were adopted for comparison because the complex interaction of fuel temperature and fission gas release during long-term irradiation is completely out of the scope of the code. After determining the standard value of the relocation factor (factor F in (3.87)) to be 0.1, fuel center temperature for various design and operation conditions could be predicted to the relative error (with respect to center temperature minus input coolant temperature) within about 2%. This standard value was also applicable to fuel rods irradiated in the PBF reactor in INEL (**Fig. 21**).

Transient fuel temperature calculation was checked using the data on fuel center temperature response to reactor scram. This check was made through participation to a benchmarking program performed by the Halden Project. Though the result was not published, the blind test result by FRETA-B was evaluated by the project to be 'accurate' as other (normal operation)

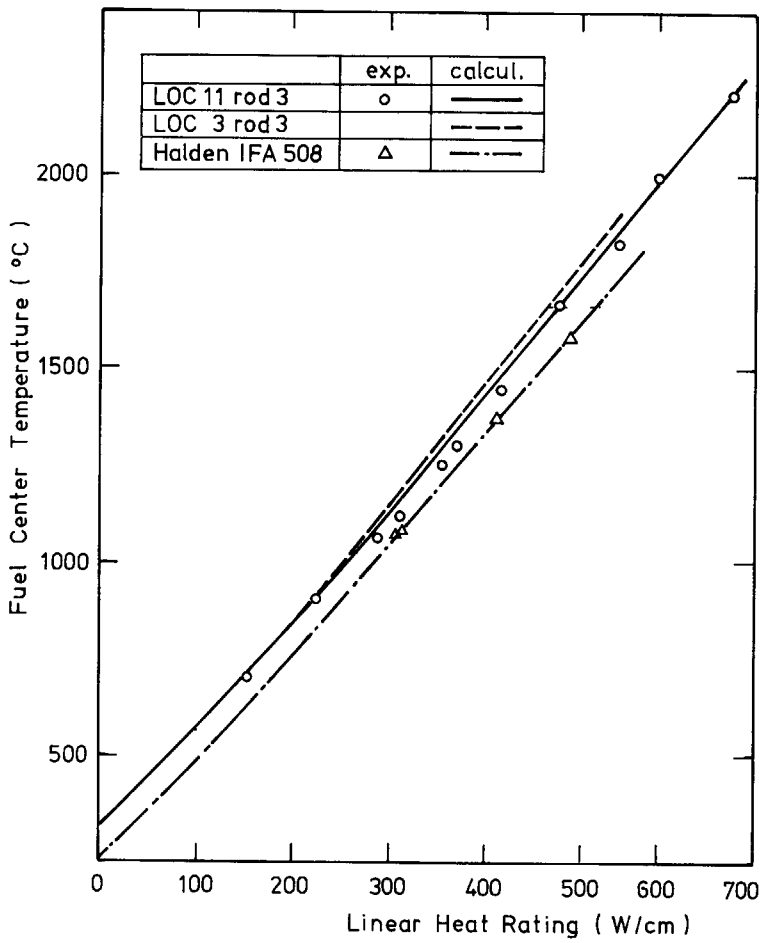

Fig. 21 FRETA-B prediction of fuel center temperatures in irradiation experiments with fresh fuel rods (ref. 32).

code results.

The ballooning model was first assessed using out-pile, single-rod ballooning experiment data. Most of these have simple experimental conditions: empty cladding tube, containing fixed gas moles or being pressurized to a constant pressure, is heated directly by electric current which is controled to achieve nearly constant temperature ramp rate. Therefore, these experiments were analyzed not by the whole code, but by the mechanical subcode DEFORM giving the cladding temperature and gas pressure as input values. Under nearly constant temperature ramp rate, 'rupture temperature', which is defined as the cladding temperature at the moment of sharp drop of internal gas pressure, offers a benchmarking for the validity of mechanical model and creep rate correlation. Some of the results have been published[30] together with the results of more integral analysis of in-pile experiment.

The gas flow model was assessed through the analysis of the post-irradiation gas flow experiment performed by Dagbjartsson[29]. This experiment has been analyzed by Dagbjartsson himself using the basically same model. Therefore the check calculation was made to reconfirm his results and to check the consistency of the added segment-integration procedure.

Out of the subcodes for the two rod-surface heat transfer modes, radiative and convective, the radiative heat transfer subcode was separately assessed through the analysis of a rod-bundle heat transfer experiment in Hitachi and the result was published[31]. On the other hand, the convective heat transfer calculation was always made as a part of analyses of integral LOCA simulation experiments. In such integral calculations, consistencies of both thermal and mechanical results were simultaneously checked.

The LOC-series experiments in the PBF reactor is unique in very rich instrumentation for coolant conditions. Out of the LOC-series, LOC-11 and 3 experiments were analyzed by FRETA-B[32]. Four fuel rods in each experiment were contained in separate shrouds, so that they were analyzed as single rods. The rich instrumentation enabled the estimation of local coolant conditions for input of segmentwise boundary condition (MODSHT = 5). Therefore the validity of thermal calculations could be checked in a fairly separated manner for each subcode in terms of onset of dryout, peak cladding temperature and fuel center temperature at different periods of an experiment. The calculated ballooning was basically consistent with the observation.

To check the code capability to handle fuel rod bundle, out-pile multi-rod ballooning experiment in JAERI was first taken up for analysis, and then the in-pile experiment MT-1 in the NRU reactor (Chalk River) was analyzed. The MT series experiments have used 6 × 6 rod bundle with removed four corner rods and with one empty tube in the center. These experiments had no blowdown phase: fuel rods at low power were cooled by steam from the beginning. The transient was initiated by reducing the steam flow and terminated by the quench of all rods by reflooding, whose temperature history is shown in **Fig. 22**.

In this analysis, all necessary input data were not afforded by the published data, so that some guess of input parameters (for example rod-to-rod power distribution) to 'tune' to the experimental results was unavoidable. However, the basic agreements with experimental data obtained for many parameters, i.e. cladding temperature histories of many fuel rods at various elevations, rod rupture times, final rod expansions and flow channel blockage ratio, justities the use of minimum number of arbitrary assumptions. The result was published together with some analyses of out-pile ballooning experiments[30] as a proof that out-pile and in-pile balloonings can be predicted by the same model consistently with thermal analysis.

Since the expansion of the code into multi-rod two-dimensional version, the greatest emphasis in the development work has been placed on suppression of running time. This target was pursued through

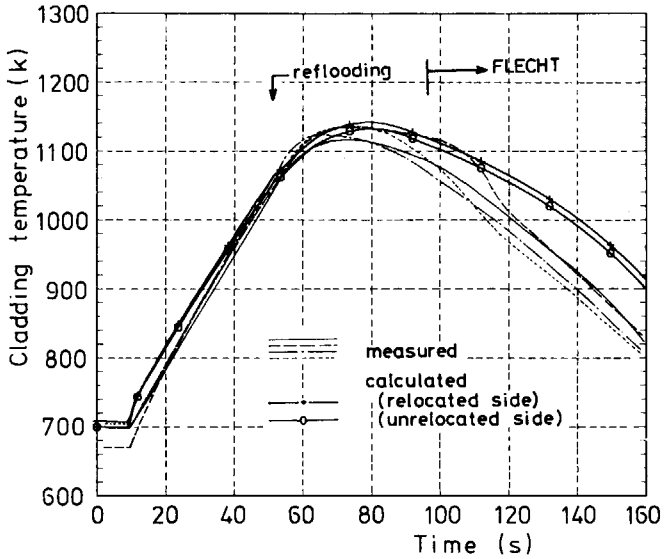

Fig. 22 Measured and calculated cladding temperatures in NRU MT-1 unpressurized fuel rods (ref. 30).

1) use of fast-running submodels,
2) automatic time step redivision capability,
3) explicit logic for the whole calculation (for example, fuel rod deformation is reflected to heat conduction not in the present step but in the next step.),
4) use of local time steps for phenomena that proceeds much faster than others,
5) bypass of subcodes in which the expected state change is negligible,
6) balancing the accuracy of model calculation with the inherent uncertainty in accident analysis,

and other minor measures.

These measure have certainly served to suppress the running time of FRETA-B. It is however difficult to quantitatively state the effects because these measures have been strengthened keeping step with the expansion of the calculational capability. It is also difficult to give the running time of an analysis in terms of its external size (total nodes and time span for analysis) alone. What can be said is that a LOCA simulation experiment with the most complex bundle geometry performed until now could be analyzed in reasonable running time. The analysis of the NRU MT-1 experiment mentioned before, which considered the behavior of 17 fuel rods with five axial segments up to 160 s, took about five minutes on the FACOM M-380 computer. This running time is felt fairly small for the apparent size of the analysis.

However, it must also be pointed out that the cooling condition of the MT-1 experiment contributed to suppress the running time: it had no blowdown phase and the steam flow was reduced to nearly zero before reflooding, so that time-consuming coolant enthalpy calculation could be skipped. Otherwise, the running time would have increased several times.

Considering all these, for a calculation run to be possible within reasonable running time (routine running is possible in the daytime on most computer systems), a rough figure of the largest bundle size for analysis would be that number of rods times number of axial segments equals about 100 for typical LOCA events. If local coolant conditions are input as boundary condition, this number would be increased several times, possibly enabling analysis of a half bundle of 8 X 8 BWR fuel rod bundle. The maximum number of rods is fixed to 17 in the present FRETA-B code (not variable dimension), but a measure has been taken to enable expansion into larger number with minimum modifications.

8. Concluding Remarks

A multi-rod fuel behavior analysis code FRETA-B was developed to analyze the fuel state changes during accidents, particularly LOCA. The code analyzes heat transfer, cladding oxidation, gas pressure and deformation in individual rods of a bundle, and also considers the rod-rod and rod-shroud interactions. Efforts have been made to minimize the increase of running time due to handling of many fuel rods. The development work was successful in that, though analysis of a whole PWR or BWR fuel bundle was not possible, the most complex fuel bundle in LOCA simulation experiments to date could be analyzed with reasonable accuracy.

The above 'reasonable accuracy' means that, in analyzing a simulation experiment, principal features of the experiment could be consistently reproduced after parametrically changing some input variables within the realistic range. This limitation is partly due to inadequateness of the FRETA-B code, but is for the greater part due to inherent uncertainties in defining the boundary conditions of accident conditions even in simulation experiments. For example, 30 K difference in cladding temperature sometimes brings the difference in cladding deformation from unvisible swelling to fully developed ballooning with rod-rod contact. Even if the heat transfer model was elaborated to achieve an accuracy of ±15 K, how can one define the coolant condition to assure such an accuracy?

It means that if the code were to be used for fuel behavior analysis of commercial fuel rod bundle (it is possible if the bundle size is reduced by using structural symmetry relationship), the calculation should be made principally in the form of parametric study. For instance, the effect of fuel design changes or minor changes in normal operation condition (large changes induce the change in entire thermal hydraulic condition) on fuel behavior during LOCA could be studied by using the code.

If the code were to be used for post-test analysis of a simulation experiment, the user should take even freer standpoint. Since the empirical correlations used in the FRETA-B submodels have generally limited applicability, the user should replace some of them on reasonable grounds with other models to consistently reproduce the essential feature of his experiment. The authors wish the code is extensively used as such a 'tool' for analysis.

Acknowledgements

The authors are grateful to Dr. M. Nozawa, Vice Director of Tokai Research Establishment and Dr. M. Ichikawa, Chief, Fuel Reliability Lab. I, for their encouragement of the work. The authors also acknowledge the useful suggestions by Mr. M. Suzuki on the ballooning and metal-water reaction models. They are also indebted to Dr. J. Nakamura for some of the code assessment works.

References

1) Uchida M., Harayama Y. and Otsubo N. : "FREG-3T: A Computer Program to Analyze LWR Fuel Behavior under Accident Conditions", JAERI-M 8482 (1979) (in Japanese).
2) Siefken L.J., et al. : "FRAP-T6: A Computer Code for the Transient Analysis of Oxide Fuel Rods", EGG-2104 (1981).
3) Bowring R.W., Cooper C.A. and Haste T.J. : "MABEL-2: A Code to Analyses Cladding Deformation in a Loss-of-Coolant Accident: Part 1: Short Description", AEEW-R 1529 (1982).
4) Uchida M., Nakamura J. and Otsubo N. : "FRETA-B: A Computer Code for the Analysis of Fuel Rod Bundle Behaviors under Accident Conditions", JAERI-M 9495 (1981).
5) Revised ANS Standard (ANS 5.1), "Decay Heat Power in Light Water Reactors for Shutdown Times Less than 10^4 Seconds", (1978).
6) Ransom V.H., et al. : "RELAP5/MOD1 Code Manual Volume 1: System Models and Numerical Methods", NUREG/CR-1826 (EGG-2070), (1980).
7) Bjornard T.A. and Griffith P. : "PWR Blowdown Heat Transfer", ASME Symposium on the Thermal and Hydraulic Aspects of Nuclear Reactor Safety, Vol.1, (1977).
8) Hottel H.C. : "Radiant Heat Transmission", Chapter 4 of "Heat Transmission", (ed. McAdams W.H.) McGraw-Hill, (1954).
9) Schack A. : Arch. Eisen Hüttenwesen, 241 (1939).
10) Finlayson B.A. : "The Method of Weighted Residuals and Variational Principles", Academic Press, New York (1972).
11) Wheeler C.L., et al. : "COBRA-IV-I : An Interim Version of COBRA for Thermal Analysis of Rod Bundle Nuclear Fuel Elements and Cores", BNWL-1962 (1976).
12) Ross A.M. and Stoute R.L. : "Heat Transfer Coefficient Between UO_2 and Zircaloy-2", CRFD-1075, (1962).
13) Beyer C.E., et al. : "GAPCON-THERMAL-2: A Computer Program for Calculating the Thermal Behavior of an Oxide Fuel Rod", BNWL-1898 (1975).
14) MacDonald P.E. and Thompson L.B. : "MATPRO-VERSION 09: A Handbook of Materials Properties for Use in the Analysis of Light Water Reactor Fuel Rod Behavior", TREE-NUREG-1005 (1976).
15) Lyons M.F., et al. : "UO_2 Pellet Thermal Conductivity from Irradiation with Central Melting", GEAP-5591 (1964).
16) Yeh H-C., Dodge C.E. and Hochreiter L.E. : "Reflood Heat Transfer Correlation", Nucl. Technol., Vol.46, 473 (1979).
17) Cathcart J.V. : "Zirconium Metal-Water Oxidation Kinetics", ORNL/NUREG/TM-41 (1976).
18) USDOC : "JANAF Thermochemical Tables", (1971).
19) Pawel R.E. : "Oxygen Diffusion in Oxide and Alpha Zircaloy Phases", ORNL/NUREG-5, (1976).
20) Chung H.M., Garde A.M. and Cassner T.F. : "Pseudobinary Zircaloy-Oxygen Phase Diagram", ANL-75-58, p.56, (1975).
21) Rosinger H.E., Bera P.C. and Clendening W.R. : "Steady-State Creep of Zircaloy-4 Fuel Cladding from 940 to 1873 K", J. Nucl. Mater., 82 (1979) 286.
22) Hann C.R., et al. : "Transient Deformation Properties of Zircaloy for LOCA Simulation, Final Report, Volume 1", EPRI-NP-526 (Vol.1) (1977).
23) Furuta T., et al. : "Factors Influencing Deformation and Wall Thickness of Fuel Rods under a Loss-of-Coolant Accident", JAERI-M 6542 (1976).
24) Chung H.M. and Kassner T.F. : "Deformation Characteristics of Zircaloy Cladding in Vacuum and Steam under Transient-Heating Conditions: Summary Report", ANL-77-31 (1978).
25) Karb E.H., et al. : "KfK In-Pile Tests on LWR Fuel Rod Behavior During the Heatup Phase of a LOCA", KfK 3028 (1980).
26) Hagrman D.L., et al. : "MATPRO-VERSION 11 (Revision 1) A Handbook of Materials Properties for Use in the Analysis of Light Water Reactor Fuel Rod Behavior", TREE-1280, Rev 1 R3 and R4 (1980).
27) Suzuki M. : "High Temperature Deformation and Burst Behavior of Internally Pressurized Zircaloy-4 Tubes", JAERI-M 8523 (1979) (in Japanese).
28) Erbacher F.J. : "LWR Fuel Cladding Deformation in a LOCA and its Interaction with Emergency Core Cooling", Proceedings of ANS-ENS Topical Meeting on Reactor Safety Aspects of Fuel Behavior, August 2-6, 1981, Sun Valley, Idaho.
29) Dagbjartsson S.J., et al. : "Axial Gas Flow in Irradiated PWR Fuel Rods", TREE-NUREG-1158 (1977).

30) Uchida M. : "Application of a Two-Dimensional Ballooning Model to Out-Pile and In-Pile Simulation Experiments", Nucl. Eng. Des., 77 (1984) 37.
31) Uchida M. and Nakamura J. : "Matrix Calculation of Radiant Heat Transfer in LWR Fuel Bundles under Accident Conditions", Nucl. Eng. Des., 65 (1981) 63.
32) Uchida M. : "Post-Test Analysis of Fuel Behaviors in PBF LOCA Experiments by FRETA-B Code", JAERI-M 82-189 (1982).

Appendix A Input Manual

A1. Definition of Bundle Geometry

(1) Fuel Rod Number and Subchannel Number

For visualization of the descriptions in this section, readers are refered to **Fig. 3** of the main text.

When multiple fuel rods are to be analyzed, those rods must be identified by sequential numbers. The sequence can be in arbitrary order. In this case, subchannels must also be given sequential numbers, again in arbitrary order. Even in single rod calculation, subchannel number is necessary if radiative heat transfer from fuel rod is to be calculated, or if different coolant conditions are to be considered in four subchannels surrounding the single rod.

Each fuel rod is divided into four azimuthal sectors. They must be given sequential numbers 1 to 4. Sector 1 should be the upper-right sector in each rod, and the subsequent numbers be given in counter-clockwise order. Even when a sector of a rod is located completely outside of a symmetry face (it can occur when geometry for analysis is reduced by symmetry relationship as sector 2 of rod 1 in **Fig. 3**), the sequence must include such a 'unseen' sector.

(2) Fuel Rod Position and Shroud Position

These data are used only for monitoring rod-rod or rod-shroud contact, and for two-dimensional plotting purposes. Informations necessary for other calculations such as radiative heat transfer are supplied through other input data. These positional data can therefore be skipped when the expected fuel rod deformation is small and two-dimensional plotting is not required.

Fuel rod position in the square lattice is specified by giving the (x,y) coordinate of their centers through the array ZAH(I,N) where I=1 gives x and I=2 gives y coordinates; N denotes rod number. Distance is normalized by the rod-rod pitch. For example, two rods with coordinates (0, 1.0) and (1.0, 1.0) are the nearest-neighbors to each other in the lattice. Origin of the coordinate can be arbitrary, but in the two-dimensional plotting the rod with its center at (0, 0) comes to the left-bottom of the paper.

Shroud position is specified by giving the coordinates of the two ends of a line element in the transverse cross section, whose total number is specified by the variable NSHRBD. This information is input through the array SHZAR(I,J,N) where I=1 or 2 denotes the (x,y) coordinate as in the fuel rod array; J=1 and 2 denote the two ends of the line element whose number is given by N.

(3) Sequential Number of Face Elements

When radiative heat transfer is to be calculated, or subchannelwise different coolant states are to be considered, all the face elements in contact with the coolant must be given sequential numbers. The 'face' here includes those imaginary ones such as boundary between subchannels and symmetry face. The term 'element' is used in such a meaning as that a normal coolant subchannel is bounded by eight face elements, four out of which are the surfaces of four surrounding fuel rods and the other four are subchannel boundaries.

All the face elements are grouped into four according to their nature: (a) fuel rod surface, (b) shroud (structural material) surface, (c) symmetry face, (d) boundary face. The sequence in each group can be arbitrary, but group (a) must come first and then group (b). In **Fig. 3**,

faces 1 to 7 are fuel rod surfaces; 8 to 15 are shroud surfaces; 16 to 18 are symmetry faces; 19 to 24 are boundary faces.

(4) Subchannel Type and Local Face Element Index

These data are used in combination with the face element number, and therefore necessary when radiative heat transfer or subchannelwise enthalpy calculation is required. Infinite square lattice is simply the repetition of Type IV in **Fig. A1**. All other types are provided for simulating the peripheral part of a bundle, or the subchannels intersected by symmetry face. The face elements forming a subchannel have indices to show the geometrical relationship between them. For defining bundle geometry, subchannel type must be specified for each subchannel, and the correspondence between the sequential face number and local face element index must be established.

The actual dimensions of the subchannel types in **Fig. A1** are determined only by rod-rod pitch and cladding outer radius. It is assumed that the straight face elements (e.g. index 6 of Type II, or index 4 of Type V) are located at half-pitch distance from the nearest rod center. In actual bundle, the external shroud can be located at arbitrary distance from the outermost rod row. Subchannel types to simulate those situations are not provided.

It can also occur that a test fuel bundle has a special geometry in the periphery not covered by the subchannel type stock of the code. In such a case, the actual geometry must be approximated by the combination of the prepared subchannel types, an example of which is shown in **Fig. A2**. Discrepancy of the flow area caused by such approximation can be corrected by inputting subchannel flow areas to the array FAREAH(I) in the card group of **Table A2**.

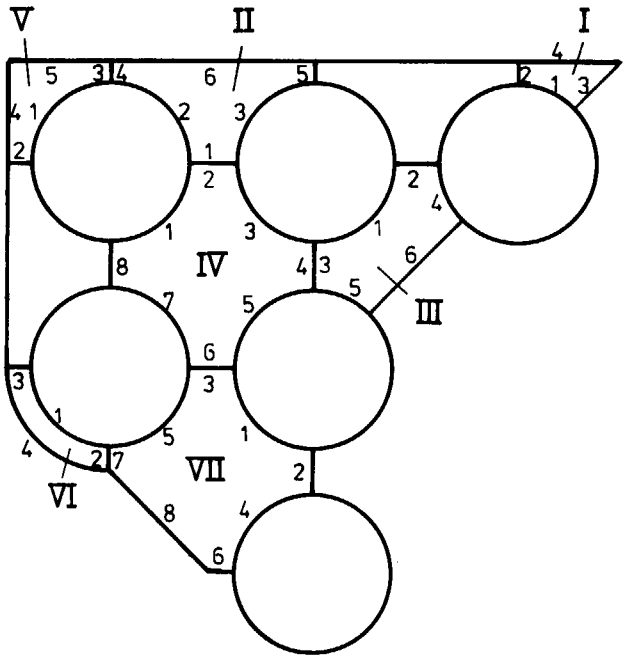

Fig. A1 Subchannel types prepared in the code (Roman numerals are subchannel type numbers and Arabic numerals are local face element indices).

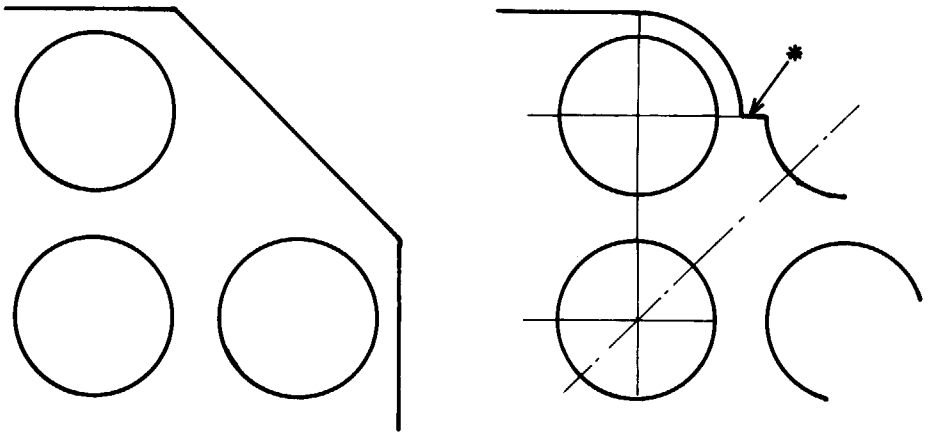

(a) actual geometry (b) approximated geometry

Fig. A2 Approximation of diverse geometries in the periphery of bundle using sub-channel types prepared by the code (In this example, a discontinuity exists at the boundary marked by asterisk. It does not, however, cause any problem except for the accuracy of approximation).

A2. Input Card Arrangement

(1) File Requirement

Some calculational results of the code are written on either tentative or permanent discs. Therefore, discs (or tapes) must be allocated to the logical machine number (NF in READ(NF), WRITE(NF)) which is specified in the input cards.

1) files for historical output data storage

Tentative files must be prepared for storage of historical output data. Positions where such historical data output is made are specified by the array NPRHIS(I) in namelist input data NAM. The total number of the tentative files must be equal to the number of non-zero data of NPRHIS. For example, if NPRHIS = 10101, 30501, 40503, 0, 0, ..., three tentative files must be prepared and they must be allocated to the logical machine numbers starting from 50: in this case 50, 51 and 52. At least one file (allocated to 50) is necessary even if NPRHIS positional data are all zero.

2) file for plotting data storage

If plotting is to be made by other code (off-line plotting), a permanent file must be allocated to logical machine number 70 for storage of data.

3) file for coolant data input

By option, voluminous coolant condition data can be input not from cards but from disc or tape. This option is taken when a value other than 0 and 5 is given to the input variable ICTAPE in namelist NAM. The logical machine number of the file must be equal to ICTAPE (READ(ICTAPE)).

(2) Input Data

Input data are grouped into four parts, the last two of which may be skipped depending on the option. The input cards must be arranged in the following order.

1) tytle card (18A4)

2) namelist /NAM/

Variables in this namelist are described in **Table A1**. **Table A1** classifies these varia-

bles into nine groups, but it is only for convenience of explanation: variables in this namelist can be written in arbitrary order.

3) fixed-format cards for bundle geometry definition

Described in **Table A2**. This group can be skipped in the case of single-rod calculation without radiative heat transfer.

4) fixed-format cards for coolant condition data

These cards are necessary in a special condition (ICTAPE = 5) specified in /NAM/. When ICTAPE $\neq$ 0 or 5, these cards are replaced by disc or tape which is allocated to logical machine number ICTAPE, according to the format shown in **Table A3**.

A sample input card image is shown in **Table A4**.

Table A1 Namelist /NAM/

Name	Description	Stored Value
[GROUP 1] Fuel Specifications (common to all rods)		
TEMPØ	Initial fuel temperature (K). Dimensional data are input at this temperature.	298.15
RFIP	Fuel inner radius (m)	0.0
RFOP	Fuel outer radius (m)	0.0046597
RCIP	Cladding inner radius (m)	0.0047422
RCOP	Cladding outer radius (m)	0.0053594
RDISH	Dish shoulder radius (m). Axial thermal expansion is calculated at this radius.	0.0
DDEPTH	Pellet dish depth (m). For one-end dish, negative value is input.	0.0
HPELT	Pellet height (m)	0.015
ZFUEL	Pellet stack height (m)	3.6576
ZCLAD	Cladding length (m). Unnecessary when VPLNUØ is input.	0.0
FRDEN	Fuel density (fraction to theoretical density)	0.95
PITCH	Fuel rod pitch (m)	0.0143
DEQ	Equivalent hydraulic diameter of the coolant channel (m). If zero, calculated from PITCH.	0.0
FAREA	Coolant flow area (m^2). If zero, calculated from PITCH. (Used for single-rod, 1-D case only.)	0.0
ROUF	Pellet surface roughness (m)	4.E-6
ROUC	Cladding surface roughness (m)	2.E-6

Table A1 Namelist /NAM/ (Continued)

Name	Description	Stored Value
FRPUO2	Weight fraction of PuO_2 in fuel	0.0
MATCLD	Cladding material (=2: zry-2, =4: zry-4)	4
COLDW	Cold work of cladding (m^2/m^2)	0.2
RHOC	Cladding density (kg/m^3)	6550.
TMELT	Fuel melting temperature (K)	3073.15
	[GROUP 2] Space Mesh Data	
NROD	Number of fuel rods to be analyzed	1 (<18)
KRADC	Option for two-dimensional calculation. KRADC must be 1 when 1) radiative heat transfer is to be calculated, or 2) NROD is not equal 1, or 3)four coolant subchannels around a single rod have different states.	0
NODF	Number of radial nodes in fuel pellet	4(< 6)
NODS	The radial node number at which pellet axial expansion is to be evaluated. If zero, evaluated at dish shoulder; if no-dish, evaluated at RFOP/2.	0
NDIV	Option for radial mesh. = 0 : rings with equal thickness = 1 : rings with equal volume.	0
NAXIN	Number of axial nodes for pellet stack. Gas plena are not included. If positive, pellet stack is equally divided; if negative, segment lengths are input by HL	1 (< 10)
HL(J),J=1, -NAXIN	Necessary when NAXIN is negative. Lengths of pellet stack segments from bottom.	

Table A1 Namelist /NAM/ (Continued)

Name	Description	Stored Value
NOCHAN	Necessary when KRADC is non-zero. Number of coolant subchannels.	1(< 30)
NSURF	Necessary when KRADC is non-zero. Number of face elements (includes such imaginary faces as symmetry face and subchannel boundaries.)	0 (< 150)
NBPOIN	Number of azimuthal nodes in a rod for two-dimensional ballooning calculation. Either 4, or 12 or 20.	20
NFORDR	Order of Fourier series for expressing azimuthal distribution of strains. (< NBPOIN/2 - 1)	2
NSYMSF	Necessary when KRADC is non-zero and symmetry is utilized to reduce the geometry. Number of fuel sectors that are completely outside the symmetry face(s). Used only for those fuel rods whose centers are on the symmetry face.	0 (< 31)
NSHRBD	Necessary when planar shrouds are to be drawn in two-dimensional plotting, or when rod-shroud contact is to be calculated. Number of planar shroud elements. Here, 'element' means any straight part of shroud (an element here can include several face elements in the subchannel model).	0 (< 51)
ZAH(I,N) I=1,2 N=1, NROD	Necessary when two-dimensional plotting is to be made, or when rod-rod or rod-shroud contact is to be calculated. Coordinates of fuel rod centers. ZAH(1,N) : x-coordinate of rod N ZAH(2,N) : y-coordinate of rod N Distance is normalized by fuel rod pitch (PITCH) and the position (0.0, 0.0) comes to the left-bottom of the paper.	

Table A1 Namelist /NAM/ (Continued)

Name	Description	Stored Value
SHZAH(K,I,J) K=1,2, I=1,2 J=1, NSHRBD	Necessary when NSHRBD is non-zero. SHZAH(1,1,J) : x-coordinate of an end of shroud element J SHZAH(2,1,J) : y-coordinate SHZAH(1,2,J) : x-cordinate of another end of J SHZAH(2,2,J) : y-coordinate Unit and origin is the same as for ZAH.	
	[GROUP 3] Rodwise Fuel State	
HOXID(K,L,J,N) K=1,2, L=1,4 J=1,NAXIN N=1,NROD	Initial oxide layer thickness of cladding (m). K=1 : inside surface, =2: outside surface. L is azimuthal sector number; J is axial segment; N is fuel rod number	0.0, 0.0
DSWEL(L,J,N) L=1,4 J=1,NAXIN N=1,NROD	Initial displacement of pellet surface at each node (m). Used for swelling and relocation.	0.0
EPSØ(K,L,J,N) K=1,3 L=1,NBPOIN J=1,NAXIN N=1,NROD	Initial cladding strain at each node (true strain, dimensionless) K=1: hoop, =2: axial, =3: radial	0.0
EPSPO(K,L,J,N)	Initial cladding plastic strain (same as EPSØ)	0.0
FRELOC(L,J,N) L=1,4 J=1,NAXIN N=1,NROD	Fractional relocation of pellet fragment	0.1

Table A1 Namelist /NAM/ (Continued)

Name	Description	Stored Value
	[GROUP 4] Gas Plenum Data	
IOPTGF	Option for transient gas flow calculation (= 0: uniform pressure; =1: gas flow calculated)	0
VPLNUØ(N) N=1,NROD	Upper gas plenum volume (m^3). If zero, calculated from the difference of ZFUEL and ZCLAD.	0.0
VPLNLØ(N)	Lower gas plenum volume (m^3)	0.0
GASPRS(N) N=1,NROD	Gas pressure at initial temperature (N/m^2). If zero, calculated from GASMOL	0.0
GASMOL(N) N=1, NROD	Total gas moles in a fuel rod (mole). Unnecessary if GASPRS is non-zero.	0.0
GASMIX(K,N) K=1,7 N=1, NROD	Plenum gas composition (K=1: helium, =2: argon =3: kripton, =4: xenon, =5: hydrogen, =6: air, =7: steam) If all (seven) zero values are input for a rod, the GASMIX values for rod 1 are used.	1.0, 6x0.0
	[GROUP 5] Time Step and Power Data	
TMAX	Time span for analysis (end time - start time) (s)	0.0
DT	Uniform time step size (s). Unnecessary when the size is time-dependent. It is not advisable to use a size greater than 2 s.	1.0
NTSTP	Length of TVSDT (time step size vs. time) table. If zero, uniform step size DT is used.	0 (< 51)
TVSDT(I,M) I=1,2 M=1, NTSTP	Time step size table. TVSDT(1,M): time (s) TVSDT(2,M); step size (s) Linear interpolation is made between time M and M+1 (same for all the arrays of this type).	

Table A1 Namelist /NAM/ (Continued)

Name	Description	Stored Value
DTSFMX	Maximum allowable temperature jump (pellet and cladding surfaces) in a time step (K). If DTSFMX is exceeded, time step is re-divided.	6.0
POWERØ(N) N=1, NROD	Average linear heat rating at time zero (W/m)	40000.0
NPOWER	Length of POWER (relative power vs. time) table. If NPOWER >0, POWER must be input. NPOWER= -1, ANS+20% table for LOCA is used. NPOWER= -2, ANS table plus delayed fission heat.	0 (< 104)
POWER(I,M) I=1, 2 M=1, NPOWER	Relative power history table. Omit if NPOWER < 0. POWER(1,M): time (s) POWER(2,M): relative power Common to all fuel rods. POWER(1,1) should be zero (initial power). Average linear heat rate of rod N at M-th period is given by POWERØ(N) x POWER(2,M).	
FRTPW(L,N) L=1, 4 N=1, NROD	Azimuthal power fraction. Given for four sectors in each rod. Unnecessary for uniform case.	4 x 1.0
NRPOW	Length of FRPDR (radial power distribution) table. If zero, uniform heat generation.	0 (< 53)
FRPDR(I,K) I=1,2 K=1, NRPOW	Radial power distribution FRPDR(1,K): radius (m) FRPDR(2,K): relative power(normalization is unnecessary) FRPDR data can be given at arbitrary radii in increasing order.	
RSCR M	Scram reactivity. Necessary when NPOWER= -2.	0.03

Table A1 Namelist /NAM/ (Continued)

Name	Description	Stored Value
FAPPO(J) J=1, NAXIN	Axial power distribution (relative value, normalization is unnecessary)	1.0
[GROUP 5] Coolant Condition Data		
MODSHT	Option for setting boundary condition in thermal calculation MODSHT = 1: cladding temperature is input, 2: uniform coolant enthalpy is input, 3: inlet (or outlet) enthalpy is input, 4: coolant temperature and heat transfer coefficient are input, 5: enthalpy is input at multiple axial nodes.	2
NCPRS	Length of TVCPRS (coolant pressure vs. time table).	1 (< 101)
NMFL	Length of TVMFL (mass flux table). Unnecessary when MODSHT is 1 or 4.	1 (< 101)
NHIN	Length of TVHIN (inlet enthalpy table). Necessary when MODSHT is 2, or 3 or 5.	0 (< 101)
NHOT	Length of TVHOT (outlet enthalpy table). Necessary only when MODSHT is 3 and the coolant flow can be reversed.	0 (< 101)
NHAV	Length of TVHAV (average enthalpy table). Necessary when MODSHT is 2.	0 (< 101)
TVCPRS(I,M) I=1, 2 M=1, NCPRS	Coolant pressure history table TVCPRS(1,M): time (s) TVCPRS(2,M): coolant pressure (N/m^2)	

Table A1 Namelist /NAM/ (Continued)

Name	Description	Stored Value
TVMFL(I,M) M=1, NMFL	Coolant mass flux history (axially uniform) TVMFL(1,M): time (s), TVMFL(2,M): mass flux(kg/m^2s)	
TVHIN(I,M) I=1, 2 M=1, NHIN	Coolant inlet enthalpy history. Rigorous value is required when MODSHT is 3; when MODSHT is 2 or 5, this data is used only for subcooled critical heat flux. TVHIN(1,M): time (s), TVHIN(2,M): enthalpy (J/kg)	
TVHOT(I,M) M=1, NHOT	Coolant outlet enthalpy history. Necessary when MODSHT is 3, and rigorous value is required only for the flow reversal periods. TVHOT(1,M): time (s), TVHOT(2,M): enthalpy (J/kg)	
TVHAV(I,M) M=1, NHAV	Coolant average enthalpy history. Necessary when MODSHT is 2. Similar to TVHIN and TVHOT.	
TIMREF	Reflood initialtion time (s). Ignore if reflood heat transfer is not to be calculated. Reflood calculation can be made only with MODSHT = 3.	1.0E5
NVIN	(Reflood calculation) Length of TVSVIN (reflood rate table).	0 (< 51)
TVSVIN(I,M) I=1,2 M=1, NVIN	(Reflood calculation) Reflood rate history. TVSVIN(1,M): time (s) TVSVIN(2,M): reflood rate (m/s)	
NQUEN	(Reflood calculation) Length of TVQUEN (quench front elevation table). If zero, quench front is calculated using FLECHT correlation.	0 (< 51)
TVQUEN(I,M) I=1,2 M=1, NQUEN	(Reflood calculation) Quench front history. TVQUEN(1,M): time (s), TVQUEN(2,M): quench front position from stack bottom (m)	
NTVSCT	Length of TVSCT (boundary condition table for MODSHT =1 or 4 or 5). Ignore if MODSHT =2 or 3.	0 (< 51)

Table A1 Namelist /NAM/ (Continued)

Name	Description	Stored Value
MINTPC	Necessary when NTVSCT≠ 0, hence when MODSHT=1, 4, or 5. Unnecessary if thermal boundary conditon data are input at every axial segment. MINTPC=0: when boundary condition data are input at selected axial segments, the condition of an unspecified segment is set equal to the next (upper) specified segment. MINTPC=1: condition of unspecified segment is determined by interpolation from upper and lower specified segments.	0
JCCND(I) I=1, N (N <NAXIN)	Necessary when NTVSCT≠0, and used in combination with MINTPC. Specifies the axial segments for which boundary condition data are to be input. JCCND array must end with NAXIN (top end segment). [ex.] JCCND = 1, 3, 6 (=NAXIN)	1, 2, 3, 4, 5, 6, 7, 8, 9,
TVSCT(I,M) M=1, NTVSCT	Thermal boundary condition data. Necessary when MODSHT=1, 4, or 5, and used in different meanings depending on the MODSHT value. Following abbreviations are made for explanation: t_i=time (s) T_s= cladding surface temperature (K), T_c= coolant temperature, h= heat transfer coefficient (W/m^2 K), p= coolant pressure (N/m^2), G= mass flux (kg/m^2 s), H= enthalpy (J/kg). when MODSHT = 1 TVSCT(1,1)= t_1 TVSCT(2,1)= T_s --- at JCCND(1) TVSCT(n+1,1)= T_s --- at JCCND(n) (=NAXIN) TVSCT(1,2) = t_2 TVSCT(2,2) = T_s --- at JCCND(1) TVSCT(n+1,2)= T_s --- at JCCND(n)	

Table A1 Namelist /NAM/ (Continued)

Name	Description	Stored Value
TVSCT(I,M) (continued)	when MODSHT = 4 TVSCT(1,1) = t_1 TVSCT(2,1) = T_c TVSCT(3,1) = h --- at JCCND(1) TVSCT(4,1) = T_c TVSCT(5,1) = h --- at JCCND(2) TVSCT(2n,1) = T_c TVSCT(2n+1,1) = h --- at JCCND(n) TVSCT(1,2) = t_2 TVSCT(2,2) = T_c when MODSHT = 5 (If ICTAPE≠0, TVSCT data can be input not here but at the end by fixed format). TVSCT(1,1) = t_1 TVSCT(2,1) = p TVSCT(3,1) = G TVSCT(4,1) = H --- at JCCND(1) TVSCT(5,1) = p TVSCT(6,1) = G TVSCT(7,1) = H --- at JCCND(2) TVSCT(3n-1,1) = p --- at JCCND(n) TVSCT(1,2) = t_2 TVSCT(2,2) = p	
ICTAPE	Used when MODSHT=5. When large amount of TVSCT data must be input, they can be input either at the end or from disc in fixed format. ICTAPE=0: TVSCT is input here (namelist NAM) =5: TVSCT is input at the end in fixed format by card, =30: same as ICTAPE=5, but by disc or tape through logical machine number 30 (READ(30)).	0

Table A1 Namelist /NAM/ (Continued)

Name	Description	Stored Value
ICHSUM	Used when MODSHT=3. Option for coolant enthalpy calculation. =0: all subchannels are at the same condition, =1: heat balance in each subchannel is independently calculated.	0
	[GROUP 7] Miscellaneous Data	
ICNTCT	Specifies the pellet-clad contact condition at time zero. =0: no effect, =1: contact condition is anticipated at time zero and careful setting of initial condition is made by the code.	0
TLOWMW	Lowest temperature that metal-water reaction is to be calculated (K).	973.15
RATEMW	Metal-water reaction heat (J/kg-Zr)	6.512E6
COEFMW(I) I=1,2	Metal-water reaction rate contants (weight gain) w^2= COEFMW(1) exp[-COEFMW(2)/RT] unit: $(kg\text{-}Zr)^2/m^4s$, cal/mole	1.13E-6 3.59E4
HAINP	Hagen number for axial gas flow calculation	200.0
IlDIM	Option for axisymmetric temperature calculation used when the conditon is axisymmetric in single-rod calculation for saving calculation time. =0: r-θ 2-dimensional, =1: axisymmetric	0

Table A1 Namelist /NAM/ (Continued)

Name	Description	Stored Value
	[GROUP 8] Lineprinter Output Control Three subroutines PRIN2D, PRINT1 and PRINT2 are provided for printout whose functions are: PRIN2D: outputs the results at specified time steps in all sectors, axial segments and rods (possible to cut unnecessary data). PRINT1: supplementary to PRIN2D. Used to printout the axial (or radial) variation of selected arrays in selected rods (one sector in each rod). PRINT2: History table of important variables at selected positions (about 200 periods are recorded automatically).	
MTSS	If MTSS=1, initial cold condition printout is skipped. (input card image is always output).	0
NTPRIN	Total number of printout periods with PRIN2D and PRINT1 (length of TPRINT table)	1 (< 51)
TPRINT(I) I=1,NTPRIN	Printout time (s)	
IPRND(L,J,N) L=1,4 J=1, NAXIN N=1, NROD	Flag for PRIN2D printout. If zero, output at that position is skipped.	1
LPRNT1(N) N=1, NROD	Positional flag for PRINT1 output. If zero, no PRINT1 output is made for the rod; if 1, 2, 3, or 4, printout is made for the corresponding fuel sector in the rod. Must not be greater than 4.	0
IPRCAT(I) I=1, 7	Flag to specify the array set to be output in PRINT1. If zero, printout is not made. By 1 to 7, following data sets are provided:	6x0, 1

Table A1 Namelist /NAM/ (Continued)

Name	Description	Stored Value
IPRCAT(I) (continued)	I=1 to 7 correspond to the following data sets: I=1: time, power, time step size etc., =2: center and surface temperatures of pellet and cladding, surface heat flux etc., =3: coolant conditions, =4: variables related to gap heat transfer, =5: stress and strain of cladding, =6: fuel rod dimensions, =7: radial temperature distribution. [ex.] If NROD=3, LPRNT1=0,0,4, and IPRCAT=3x0,1,3x0, then only the gap states of sector 4 of rod 3 are output in all axial segments by PRINT1.	
KPRHIS	Specifies the variables sets to be output in PRINT2 history table: =0: power, temperature and thermal variables, =1: power, dimension, stress, strain.	0
NPRHIS(I) I=1,10	Specifies the positions that PRINT2 output is to be made. NPRHIS data are also used to specify the positions of historical plot. Each NPRHIS value must be given as an integer determined by NPRHIS(I)= Nx10000 + Jx100 + L where N is rod number, J is axial segment, and L is sector number. PRINT2 output is made at max. 10 positions.	10x0
	[GROUP 9] Plot Specifications Two subroutines for plotting are provided: FTPLOT: history graph type plotting, whose position is specified by NPRHIS in group 8.	

Table A1 Namelist /NAM/ (Continued)

Name	Description	Stored Value
	PL2D : two-dimensional plotting. It produces a cladding deformation map of all rods at the specified elevation of the bundle and specified time. Rod surface temperatures are indicated on the map.	
IPLOT	Option for plotting. (=0: no plot, =1: plot)	0
NTPLOT	Total time periods that PL2D plotting is made.	0 (< 51)
TPLOTN(I) I=1,NTPLOT	Time periods that PL2D plotting is to be made.	
IPL2DJ(I) I=1,K (K≤ NAXIN)	Axial segment numbers that PL2D plotting is made. =0: no plot =J: plot at segment J with rod surf. temperature =-J: plot at segment J without temperature.	0
IPLOTM(I) I=1, 15	Flags to specify the variable for FTPLOT plot (=0: no plot, =1: plot , =-1: plot on the previous plot). I=1 to 15 correspond to the following y-axis variables (x-axis is time). I=1: linear heat rating (W/m) =2: cladding outer surface temperature (K) =3: cladding inner surface temperature (K) =4: pellet outer surface temperature (K) =5: pellet inner surface temperature (K) =6: coolant temperature (K) =7: coolant quality =8: heat transfer coefficient (W/m^2 K) =9: cladding hoop strain =10: cladding plastic hoop strain =11: cladding plastic axial strain =12: fuel rod gas pressure (N/m^2) =13: coolant pressure (N/m^2) =14: critical heat flux (W/m^2) =15: surface heat flux (W/m^2)	15x1

Table A1 Namelist /NAM/ (Continued)

Name	Description	Stored Value
WXAX	Length of x-axis in FTPLOT history plot (mm)	150.0
WYAX	Length of y-axis (mm)	200.0
TBLX(K) K=1,3	K=1: minimum value of x-axis (s), =2: maximum value of x-axis (s), =3: scale interval (s).	0., 50., 10.,
TBLY(K,I) K=1, 3 I=1, 15	Specifies y-axis in a similar way with TBLX. Index I corresponds to the variables of IPLOTM(I). Stored values are (units shown for IPLOTM): I= 1: K=1 0.0, K=2 6.0E4, K=3 1.0E4 I= 2 to 5: K=1 0.0, K=2 2500., K=3 500. I= 6: K=1 200., K=2 800., K=3 100. I= 7: K=1 0.0, K=2 1.0, K=3 0.2 I= 8: K=1 0.0, K=2 8.0E4, K=3 2.0E4 I= 9 to 11: K=1 0.0, K=2 0.05, K=3 0.01 I=12 to 13: K=1 0.0, K=2 2.0E7, K=3 6.0E6 I=14 to 15: K=1 0.0, K=2 1.0E7, K=3 2.0E6	
MPTAP	Used when the historical output data are to be stored in disc or tape for off-line plotting. If zero, no effect. If non-zero, data storage is made by WRITE(MPTAP), so that a file must be allocated to logical machine number of MPTAP. When MPTAP ≠ 0, all the variables (I=1 to 15) are stored regardless of the IPLOTM input values, but the positions are specified by NPRHIS(I) of group 8.	70

Table A2 Fixed-Format Card Group 1 Bundle Geometry Data
Necessary when KRADC = 1, and put after namelist NAM cards.

Column	Variable	Description
Card 1 Channel Data (NOCHAN cards are successively input.) Specifies from which faces each subchannel is composed (surrounded).		
1 - 3		comment field
4 - 10	ITYP(I)	channel type
11 - 15	ISUF(1,I)	sequential (whole bundle) face number for local face index 1 of subchannel I
16 - 20 ⋮ 46 - 50	ISUF(2,I) ⋮ ISUF(8,I)	sequential face number for local face index 2 sequential face number for local face index 8
51 - 60 (E10.3)	FAREAH(I)	subchannel flow area (m^2). If zero, calculated by the code. Used for correction of the approximated bundle geometry.
Card 2 Fuel Rod Surface Element Data (One card for each face element in order of face element sequential number)		
1 - 3	NSF1	sequential face number of face element I
4 - 6	blank	
7 - 9	MATER	must be 2, which shows that the element is rod surface.
10 - 12	IROD(1,I)	fuel sector number that the element I belongs to.
13 - 15	IROD(2,I)	fuel rod number that the element I belongs to.
16 -20	EMISSF	emmissivity of face I (F5.0)
Card 3 Shroud Surface Element Data One card describes a group of face elements with the same property and with continuous sequential numbers.		
1 - 3	NSF1	sequential face number of the first face of the group
4 - 6	NSF2	sequential face number of the last face of the group

Table A2 Fixed-Format Card Group 1 (Continued)

Column	Variable	Description
7 - 9	MATER	must be 1, which shows that the element is shroud surface.
10 - 12	IROD(1,I)	shroud type of group I elements. =0: shroud temperature is set equal to that of coolant, =1: no heat flow across shroud (heat capacity only) =2: heat flow across shroud (used for periphery).
13 - 15	blank	
16 - 20	EMISSF	emmissivity of the face element group (F5.0)
21 - 30	SHRTBL(1,I)	necessary when IROD(1,I)=1 or 2. SHRTBL(1,I) = $\rho C_p d$ where ρ is density (kg/m^3); C_p is specific heat (J/kg); d is thickness (m). (E10.4)
31 - 70	SHRTBL(L,I) L=2, 5	necessary only when IROD(1,I)= 2. (4E10.4) SHRTBL(2,I) = d ; (3,I) = thermal conductivity (W/m K) (4,I) = external coolant tempearature (K) (5,I) = heat transfer coefficient to external coolant (W/m^2 K)
Card 4 Imaginary Face Element Data Normally two cards are necessary: one for boundary faces and the other for symmetry faces. Whichever of the two may come first if it has younger sequential numbers.		
1 - 3	NSF1	sequential number of the first (boundary or symmetry) face element
4 - 6	NSF2	sequential number of the last face element of the group.
7 - 9	MATER	=0 for symmetry face (group); =3 for boundary face.
Card 5 Symmetry Relationship Data Omit if NSYMSF=0. FORMAT(16(I3,2I1)), (NSYMSF/16 + 1) cards are necessary.		
2 - 3	ISYMSF(1,1)	rod number (located on symmetry face)
4	ISYMSF(2,1)	fuel sector number completely outside the symmetry face.
5	ISYMSF(3,1)	fuel sector number with which ISYMSF(2,1) is symmetrical.

Table A3 Fixed-Format Card Group 2 Coolant Condition Data

This group of cards is necessary when MODSHT = 5 and ICTAPE = 5 or 30. When ICTAPE = 5, the following data are input by cards; when ICTAPE = 30, they are input by disc or tape from logical machine number 30 according to the same format.

Card	Format	Variable	Description
1	E10.4	TVSCT(1,1)	time (s) (first data point)
1-1	3E10.4	TVSCT(2,1) TVSCT(3,1) TVSCT(4,1)	coolant pressure (N/m^2) mass flux (kg/m^2 s) enthalpy (J/kg) — first axial block (JCCND(1))
1-2	3E10.4	TVSCT(5,1) TVSCT(6,1) TVSCT(7,1)	pressure (N/m^2) mass flux (kg/m^2 s) enthalpy (J/kg) — second axial block (JCCND(2))

1-n	3E10.4	TVSCT(3n-1,1) to TVSCT(3n+1,1)	pressure, mass flux, enthalpy — top block (JCCND(n))
2	E10.4	TVSCT(1,2)	time (s) (second data point)
2-1	3E10.4	TVSCT(2,2) to (4,2)	pressure, mass flux, enthalpy (JCCND(1))
---			
m	E10.4	TVSCT(1,m)	time (s) (last data point m=NTVSCT)
---			
m-n		TVSCT(3n+1,m)	enthalpy (J/kg) (JCCND(n))

Table A4 Sample input card image
(The bundle geometry of this sample problem is based on Fig. 3)

```
                1         2         3         4         5         6         7         8
CARD NO. ....5....0....5....0....5....0....5....0....5....0....5....0....5....0....5....0
 1. //JCLG JOB                                                                  00000100
 2. // EXEC JCLG                                                               00000200
 3. //SYSIN DD DATA,DLM='++'                                                    00000300
 4. // JUSER 84742179,MA.UCHIDA,0937.200                                       00000400
 5.    W.1 T.6 C.6 P.0 I.4                                                     00000500
 6.   GRP                                                                      00000600
 7.   OPTP MSGCLASS=0                                                          00000700
 8.   OPTP PASSWORD=18518                                                      00000800
 9. /*JOBPARM S=SYSC                                                          00000900
10. // EXEC FORTHE,SO=J2179.FRE2S,A='ELM(*),NOS,FLAG(W)',REGION=1500K          00001000
11. // EXEC LKEDCT,LM=J2179.FRBL83T,GRLIB=PNL,UNIT=TSSWK                       00001100
12. // EXEC LMGO,LM=J2179.FRBL83T,OBSIZE=137                                   00001200
13. // EXPAND GRNLP                                                           00001300
14. // EXPAND DISK,DDN=FT50F001}---------- (two files for two non-zero values  00001400
15. // EXPAND DISK,DDN=FT51F001}           of NPRHIS)                         00001500
16. // EXPAND DISK,DDN=FT70F001 ---------(a file for plotting data)            00001600
17. //SYSIN DD *                                                              00001700
18.  SAMPLE PROBLEM WITH MODSHT=3 AND WITH REFLOODING                         00001800
19.  &NAM  HPELT=0.00953, ZFUEL=2.743, ZCLAD=2.943,                           00001900
20.   GASPRS=2*3.2E6, POWERO=1553.0, 1412.0,                                  00002000
21.   RFOP=0.00413, RCIP=0.004205, RCOP=0.004815, RDISH=0.,PITCH=0.0127,      00002100
22.   TMAX=90., DTSFMX=25.0, MTSS=1 TIMREF=50.,                               00002200
23.   NOCHAN=6, NROD=2,NSURF=24,NAXIN=-5,NBPOIN=20,NVIN=1,NQUEN=0,            00002300
24.   NRPOW=0,NCPRS=1,NMFL=2,NHIN=1,NHOT=1, NTSTP=5,                          00002400
25.   NPOWER=1,NTPRIN=2, MODSHT=3, NSHRBD=2, NFORDR=6,                        00002500
26.   NPRHIS=10302, 10402, 8*0, LPRNT1=2, 2,                                  00002600
27.   KPRINT=01,KPRHIS=0,ICNTCT=0,KRADC=1,NSYMSF=1, IPRCAT=6*0,1,             00002700
28.   IPLOT=1, IPLOTM=15*0, IPLOTM(3)=1, IPL2DJ=2,3,4, NTPLOT=3,              00002800
29.   WXAX=180., WYAX=140., TBLX=0.0, 180., 20.,TBLY(1,3)=500., 1200., 100.,  00002900
30.   ZAH=2.0, 2.0,  1.0, 2.0,   SHZAH=2.5,2.5, 0.5,2.5, 0.5,2.5, 0.5,0.5,   00003000
31.   FAPPO=0.884,1.259, 1.224, 0.918, 0.554,                                 00003100
32.   HL=0.909, 0.534, 0.533, 0.534, 0.233,                                   00003200
33.   TPLOTN=60., 70., 80.,  TPRINT=60., 80.,                                 00003300
34.   TVCPRS=0., 2.76E5, TVMFL=9.,97., 10.,1.0, TVHOT=0.,5.E6,                00003400
35.   TVHIN=0., 2.824E6, TVSVIN=50., 0.051, POWER=0.,1.0,                     00003500
36.   IPRND=612*0,IPRND(1,2,1)=12*1, IPRND(1,2,2)=12*1,                       00003600
37.   TVSDT=8.0,1.0, 8.99,0.10, 10.0,0.10, 15.0,1.0, 20.0,2.0,               00003700
38.   FRELOC(1,1,1)=1.0,3*0.0, 1.0,3*0.0, 1.0,3*0.0, 1.0,3*0.0,              00003800
39.   FRELOC(1,1,2)=2*0.,1.0,3*0.0, 1.0,3*0.0, 1.0,3*0.0, 1.0,3*0.0, 1.0,0.,  00003900
40.  &END                                                                     00004000
41. CH1      1    1   19   16   11                    }                       00004100
42. CH2      2   21    2    4   19   20   12          }                       00004200
43. CH3      6    5   20   22   13                    } -------- (subchannel data) 00004300
44. CH4      3    7   21   23    3    8   17          }                       00004400
45. CH5      2   23    5    9   22   24   14          }                       00004500
46. CH6      1   10   24   18   15                    }                       00004600
47.   1     2  1  1 0.75                               }                      00004700
48.   2     2  4  1 0.75                               }                      00004800
49.   3     2  3  1 0.75                               } -------- (face element data) 00004900
50.   4     2  1  2 0.75                               }                      00005000
51.   5     2  4  2 0.75                               }                      00005100
52.   6     2  3  2 0.75                               }                      00005200
53.   7     2  2  2 0.75                               }                      00005300
54.   8 10  1  0    0.75                               }                      00005400
55.  11 15  1  2    0.3   31000.      0.015      15.0       523.      10000. 00005500
56.  16 18  0                                          }                      00005600
57.  19 24  3                                          }                      00005700
58.   124   ---------------- (symmetry relationship)                          00005800
59. ++                                                                        00005900
60. //                                                                        00006000
    ....5....0....5....0....5....0....5....0....5....0....5....0....5....0....5....0
```

Appendix B Sample Output

An example of FRETA-B output is shown in **Table B1**. Single rod calculation was selected for minimizing the amount of output pages. Subroutines PRIN2D and PRINT2 (see **Table A1**) were used.

Table B1 Sample output

```
HALDEN SHUTDOWN TEMPERATURE RESPONSE (D3 ROD, MODSHT=3)          CPU TIME=   0.045    PAGE( 1/   1)
                                 **********************
                                 * INPUT VALUES (NAM)  *
                                 **********************

        COLD STATE TEMPERATURE OF FUEL ROD                    293.15(DEG.K)              TEMPO
        FUEL INNER RADIUS (AT TEMPO)                    0.0       ( M )                  RFIP
        FUEL OUTER RADIUS (AT TEMPO)                    5.335E-03( M )                   RFOP
        CLAD INNER RADIUS (AT TEMPO)                    5.450E-03( M )                   RCIP
        CLAD OUTER RADIUS (AT TEMPO)                    6.390E-03( M )                   RCOP
        PELLET HEIGHT     (AT TEMPO)                    1.300E-02( M )                   HPELT
        LENGTH OF PELLET STUCK(AT TEMPO)                   0.5450( M )                   ZFUEL
        LENGTH OF FUEL ROD (AT TEMPO)                      1.0000( M )                   ZCLAD
        PELLET DISH DEPTH (AT TEMPO)                    0.0       ( M )                  DDEPTH
        PELLET DISH SHOULDER RADIUS (AT TEMPO)          0.0       ( M )                  RDISH
        FRACTIONAL FUEL DENSITY TO THEORETICAL DENSITY     0.95000(FRACTION)           FRDEN
        ROD PITCH                                       1.630E-02( M )                   PITCH
        EQIVALENT DIAMETER                              1.369E-02( M )                   DEQ
        COOLANT FLOW AREA                               1.374E-04(M**2)                  FAREA
        FUEL SURFACE ROUGHNESS                          4.000E-06( M )                   ROUF
        CLADDING SURFACE ROUGHNESS                      2.000E-06( M )                   ROUC

        WEIGHT FRACTION OF PUO2                           0.0     (FRACTION)            FRPUO2
        OPTION FOR CLADDING MATERIAL                            2                       MATCLD
        COLD WORK                                         0.20000(M**2/M**2)            COLDW
        PELLET MELTING TEMPERATURE                     3073.14990(DEG.K)              TMELT
        CLADDING DENSITY                                  6550.00(KG/M3)              RHOC

ROD( 1) DATA
        PLENUM VOLUME (UPPER)                           4.246E-05(CUB. M)              VPLNUO
                      (LOWER)                           0.0       (CUB. M)             VPLNLO
        PLENUM TEMPERATURE                              293.14990(DEG.K)               TPLEN
        GAP GAS PRESSURE (AT TEMPO)                     1.000E+05(N/M2)                GASPRS
        GAS MOLES IN GAP AND PLENUM (AT TEMPO)          0.0018285(MOLES)               GASMOL
        FILL GAS COMPOSITION
                MOLE FRACTION HELIUM                    0.1000000                      GASMIX(1)
                MOLE FRACTION ARGON                     0.0                            GASMIX(2)
                MOLE FRACTION KRYPTON                   0.0                            GASMIX(3)
                MOLE FRACTION XENON                     0.9000000                      GASMIX(4)
                MOLE FRACTION HYDROGEN                  0.0                            GASMIX(5)
                MOLE FRACTION AIR                       0.0                            GASMIX(6)
                MOLE FRACTION WATER VAPOR               0.0                            GASMIX(7)
```

```
HALDEN SHUTDOWN TEMPERATURE RESPONSE (D3 ROD, MODSHT=3)          CPU TIME=   0.047    PAGE( 2/   2)
        NUMBER OF CHANNEL                                  1                           NOCHAN
        NUMBER OF ROD                                      1                           NROD
        TOTAL NUMBER OF SOLID FACE ELEMENT                 0                           NSURF
        NUMBER OF AXIAL NODES                              3                           NAXIN
        NUMBER OF NODES IN FUEL                            5                           NODF
        NUMBER OF NODE IN CLADDING                         1                           NODC
        NODE NUMBER FOR CALC. AXIAL ELONGATION             3                           NODS
        OPTION FOR FUEL RADIAL MESH (=0: EQUIDIST.,=1: EQUIVOL.)   0                  NDIV
        NUMBER OF CIRCUMFERENTIAL NODE POINT FOR BALLOONING CAL.  20                   NBPOIN
        NUMBER OF ORDER FOR BALLOONING FITTING FUNCTION    2                           NFORDR
        NUMBER OF FUEL SECTOR OUTSIDE THE PARTIAL BUNDLE   0                           NSYMSF

        INITIAL TIME OF TRANSIENT CALCULATION            0.0(SECONDS)                  TIMEO
        THE DURATION OF THE TRANSIENT                   30.00(SEC)                     TMAX
        THE REFLUDDING TIME                          100000.00(SEC)                    TIMREF
        TIME STEP SIZE                                1.000E-02( SEC )                 DT
        NUMBER OF TIME-TIME STEP SIZE PAIRS                9                           NTSTP
        MAXIMUM TEMPERATURE CHANGE AT CLADDING OUTER SURFACE   6.0000                 DTSFMX
        NUMBER OF TIME-POWER(LINEAR HEAT RATE) PAIRS       4                           NPOWER
        INITIAL POWER (LINEAR HEAT RATE) FOR ROD(I)          (W/M)                     POWERO(I)
          28000.
        ACCUMULATED BURNUP UP TO START TIME FOR ROD(I)       (MWD/KGU)                 BURNO(I)
          0.0
        NUMBER OF RADIUS-POWER FRACTION PAIRS              4                           NRPOW
        RADIAL POWER PROFILE(PAIRS OF RADIUS AND POWER FRACTION)                       FRPDR(2,NRPOW)
          0.0       ,1.08000 1.778E-03,1.13500 3.557E-03,1.30000 5.335E-03,1.57000
        CIRCUMFERENTIAL POWER PROFILE FOR ROD(I)                                       FRTPW(4,1)
        1.000 1.000 1.000 1.000
        SCRAM REACTIVITY                                0.03000                        RSCRM

        OPTION FOR SETTING THE BOUNDARY CONDITION          3                           MODSHT
        NUMBER OF TIME-COOLANT PRESSURE PAIRS              2                           NCPRS
        NUMBER OF TIME-MASS FLUX PAIRS                     2                           NMFL
        NUMBER OF TIME-INLET ENTHALPY PAIRS                2                           NHIN
        NUMBER OF TIME-OUTLET ENTHALPY PAIRS               2                           NHOT
        NUMBER OF TIME-AVERAGE ENTHALPY PAIRS              0                           NHAV
        NUMBER OF TIME-COOLANT CONDITION(TVSCT) PAIRS      2                           NTVSCT
        INTERPOLATION OPTION FOR COOLANT INPUT DATA        1                           MINTPC
        UNIT NUMBER FOR COOLANT DATA READ(=0.NAMELIST INPUT)   0                       ICTAPE

        TRANSIENT GAS FLOW MODEL  (=1..ON, =0..OFF)        0                           IOPTGF
        TWO DIMENSIONAL RADIATION CALCULATION(=1.ON,=0.OFF)   0                        KRADC
        ONE DIMENSIONAL CALCULATION FLAG(=1.ON,=0.OFF)     0                           IIDIM
        PCI CALCULATION AT INITIAL STEP (=1..ON,=0..OFF)   1                           ICNTCT
        FLOW BLOCK.(=0.OFF,=1.WETTED PER.=ROD SURF,=2.ALL)   0                         KFLBLK
        LOWER LIMIT TEMPERATURE FOR METAL WATER REACTION   973.14(DEG.K)               TLOWMW
        REACTION HEAT RATE BY METAL WATER REACTION      6512000.0(J/KG.2IR.)           RATEMW
        COEFFICIENTS FOR METAL WATER REACTION EQUATION
              W = COEFMW(1)*EXP(-COEFMW(2)/(R*T) )         0.00000                     COEFMW(1)
                                                        35900.00                       COEFMW(2)
        COEFFICIENT HA FOR TRANSIENT FLOW CALCULATION     200.0                        HAINP
        PELLET THERMAL EXPANSION MODEL                       1                         MODEXP
        OPTION FOR COOLANT ENTHALPY CALC.(=0.AV.,=1.EACH)    0                         ICHSUM
        RELOCATION FACTOR  DISPRL=RELOCT*(RCI-RFO)        1.000                        RELOCT
```

Table B1 Sample output (Continued)

```
HALDEN SHUTDOWN TEMPERATURE RESPONSE (D3 ROD, MODSHT=3)                          CPU TIME=   0.052    PAGE( 3/   3)
       OPTION FOR PRINT OUT(=01(PRIN2D=ON),=10(PRINT1=ON)                  1                        KPRINT
       NUMBER OF PRINT OUT TIME                                            3                        NTPRIN
       NUMBER OF PLOT OUT TIME(PL2D)                                       2                        NTPLOT
       PRINT FLAG FOR PRINT1 CATEGORY(=1.ON,=0.OFF)
          0    0    0    0    0    0    1    0    0    0                                            IPRCAT(I)
       TYPE OF TIME STEP TABLE                                             0                        KPRHIS
       NODE NUMBER FOR TIME STEP TABLE(ROD*10000+IAX*100+THET)
            10101      0      0      0      0      0      0      0      0                            NPRHIS(I)
       PRINT FLAG FOR PRIN2D(L,IAX,IROD)=1..ON,=0..OFF                                             IPRND(L,I,J)
        ( 1, 1,  1)=1( 2, 1,  1)=1( 3, 1,  1)=1( 4, 1,  1)=1( 1, 2,  1)=1( 2, 2,  1)=1( 3, 2,  1)=1( 4, 2,  1)=1
        ( 1, 3,  1)=1( 2, 3,  1)=1( 3, 3,  1)=1( 4, 3,  1)=1(                                     .

       OPTION FOR PLOT OUTPUT (=1..ON,=0..OFF)                             0                        IPLOT

       CRITICAL HEAT FLUX FUNCTION                                         0                        KCRITH
       CLADDING STRESS-STRAIN FUNCTION                                     0                        KSTRAN
       SKIP INPUT DATA LIST PRINT (=1.YES,=0.NO)                           0                        MTSS
       OPTION FOR DEBUGGING                                                0                        IDEBUG
```

```
     HALDEN SHUTDOWN TEMPERATURE RESPONSE (D3 ROD, MODSHT=3)                     CPU TIME=   0.054    PAGE( 4/   4)

AXIAL NODE NO.       =     1     2     3
AXIAL LEVEL(M)       = 0.091 0.272 0.454
AXIAL NODE LENGTH(M)= 0.182 0.182 0.182
AXIAL POWER PROFILE = 1.000 1.000 1.000

RADIAL NODE RADII(M)=   0.0       0.00127   0.00253   0.00380   0.00507   0.00533   0.00545   0.00639
RADIAL POWER PROFILE=    0.8142    0.8360    0.8989    1.0030    1.1483    1.1841


                              ***** TIME DEPENDENT VARIABLES *****
   POWER RATIO VS TIME   NPOWER( 6),POWER      POWER(W/M) =POWERO(IROD)*POWER(I)
            TIME       (SEC)   -101.0000 -100.0000    0.0       0.7000    1.0000   30.0000
            POWER RATIO              0.0       1.00      1.00      0.06      0.06      0.04


   TIME STEP SIZE   NTSTP( 9),TVSDT
            TIME       (SEC)   -101.0000  -99.0000  -95.0000  -20.0000   -0.0001    0.0       0.7000    1.0000   30.0000
            TIME STEP  (SEC)     0.10000   0.20000   4.00000   4.00000   2.00000   0.05000   0.05000   0.10000   2.00000


   PRINT OUT STEP       NTPRIN(  3)
          TPRINT(SEC)              0.0       1.000    30.000

   COOLANT PRESS.   NCPRS( 2),TVCPRS
            TIME       (SEC)       0.0       30.0000
            PRESSURE(N/M2)       3.40E+06  3.40E+06


   MASS FLUX        NMFL ( 2),TVMFL
            TIME       (SEC)       0.0       30.0000
          MASS FLUX(KG/M2-S)      2500.00   2500.00


   INLET ENTHALPY   NHIN ( 2),TVHIN
            TIME       (SEC)       0.0       30.0000
          ENTHALPY   (J/KG)     1040000.0 1040000.0


   OUTLET ENTHALPY  NHOT ( 2),TVHOT
            TIME       (SEC)       0.0       30.0000
          ENTHALPY   (J/KG)     1060000.0 1060000.0
```

Table B1 Sample output (Continued)

```
   HALDEN SHUTDOWN TEMPERATURE RESPONSE (D3 ROD, MODSHT=3)                    CPU TIME=   2.427    PAGE( 1/  5)

TIME                              0.0      (SECONDS)
TIME STEP SIZE(NEW,OLD)          2.16246     2.46249 (SECONDS)

ROD  ROD      FUEL     CLAD     PLENUM  TEMPERATURE   PLENUM VOLUME     ROD
NO.  POWER    LENGTH   LENGTH   UPPER     LOWER      UPPER    LOWER    RUPTURE
     (W/M)    ( M )    ( M )    (DEG.K)   (DEG.K)    (MM**3)  (MM**3)  FLAG
---  -------- -------- -------- -------- --------   -------- --------  -------
  1 28000.000    0.550    1.001   514.029     0.0     42027.3      0.0     0

ROD  AXIAL  THETA  LINEAR    FUEL      FUEL      CLAD      CLAD      GAPCON    HEAT       SURFACE   RADIANT   HEAT
                  HEAT      CENTER    SURFACE   INNER     OUTER     TOTAL     TRANSFER   HEAT      HEAT      TRANSFER
NO   NO.    NO.  RATE      TEMP.     TEMP.     TEMP.     TEMP.               COEFF      FLUX      FLUX      MODE
                  (W/M)     (DEG.K)   (DEG.K)   (DEG.K)   (DEG.K)   (W/M2-K)  (W/M2-K)   (W/M2)    (W/M2)
---  -----  -----  --------  --------  --------  --------  --------  --------  ---------  --------  --------  --------
  1      1      1   28000.0   1519.96    843.88    578.00    532.79    3166.8    37869.6   710544.7       0.0         2
  1      1      2   28000.0   1528.38    865.78    576.85    531.94    2893.4    39369.2   705040.4       0.0         2
  1      1      3   28000.0   1537.26    889.19    575.20    531.71    2575.6    38642.8   683211.4       0.0         2
  1      1      4   28000.0   1528.40    865.91    577.25    532.36    2895.4    38450.1   704661.4       0.0         2
  1      2      1   28000.0   1521.90    852.02    575.32    531.43    2958.9    39722.3   691076.5       0.0         2
  1      2      2   28000.0   1527.15    855.34    579.52    532.80    3156.2    38967.7   731434.9       0.0         2
  1      2      3   28000.0   1539.40    899.94    572.21    530.44    2365.9    40085.3   657855.1       0.0         2
  1      2      4   28000.0   1527.16    855.42    579.88    533.18    3158.9    38173.5   731000.2       0.0         2
  1      3      1   28000.0   1519.86    845.25    575.99    531.03    3108.3    41602.4   707149.7       0.0         2
  1      3      2   28000.0   1527.61    863.28    577.11    531.80    2947.7    39980.7   710399.7       0.0         2
  1      3      3   28000.0   1537.27    891.71    573.76    530.71    2516.2    40558.9   676480.8       0.0         2
  1      3      4   28000.0   1527.61    863.15    577.24    531.91    2950.8    39743.9   710723.3       0.0         2

 COOLANT CONDITION
INLET ENTHALPY  1.04E+06(J/KG)  OUTLET ENTHALPY  1.06E+06(J/KG)  AVERAGE ENTHALPY  1.08E+06(J/KG)  REFLOOD RATE 0.0    (M/SEC)

AXIAL CHAN.  COOLANT   SATU.     COOLANT    VOID       QUALITY   CRITICAL   COOLANT    MASS       CHANNEL    CHANNEL    HEATED     FLOW
                TEMP.     TEMP.     ENTHALPY   FRACTION         HEAT       PRESSURE   FLUX       FLOW       EQUI.      EQUI.      BLOCK
NO.  NO.                                                        FLUX                             AREA       DIAMETER   DIAMETER   RATIO
             (DEG.K)   (DEG.K)   (J/KG)                        (W/M2)     (N/M2)     (KG/M2-S)  (M2)       (M)        (M)
-----  -----  --------  --------  --------   --------   --------  --------   --------   --------   --------   --------   --------
    1      1   514.03    514.03   1047437.     0.1319     0.0032  3184830.   3400000.    2500.00  1.37E-04   0.01369    0.01369    1.00000
    2      1   514.03    514.03   1062310.     0.3594     0.0116  3134661.   3400000.    2500.00  1.37E-04   0.01369    0.01369    1.00000
    3      1   514.03    514.03   1077182.     0.4942     0.0201  3088142.   3400000.    2500.00  1.37E-04   0.01369    0.01369    1.00000

   HALDEN SHUTDOWN TEMPERATURE RESPONSE (D3 ROD, MODSHT=3)                    CPU TIME=   2.431    PAGE( 2/  6)

TIME                              0.0      (SECONDS)

ROD  AX  THET  SURFACE RADIUS(AT TRANSIENT)          GAP      OXIDE     OXYGEN     REACTION   FUEL       ROD CENTER SHIFT      ROD
                PELLET   PELLET    CLADDING   CLADDING  THICK.   FILM      CONTENT    HEAT AT   CENTER                           CROSS
NO   NO  NO     CENTER   SURFACE   INNER      OUTER     ( M )    THICK.               CLAD OUT  SHIFT      ( X )     ( Y )     SECTION
               ( M )    ( M )     ( M )      ( M )               (MICRONS) (KG/M3)    (W/M2)    ( M )      ( M )     ( M )     ( M2 )
---  --  ----  -------- --------  ---------- --------  -------- --------  ---------  --------  ---------  --------  --------  --------
  1   1     1   0.0      5.45E-03  5.46E-03   6.40E-03  1.19E-05  0.0      6.55E+00   0.0       1.04E-06   0.0       0.0       1.29E-04
  1   1     2   0.0      5.45E-03  5.46E-03   6.40E-03  1.19E-05  0.0      6.55E+00   0.0       3.73E-09
  1   1     3   0.0      5.45E-03  5.46E-03   6.40E-03  1.19E-05  0.0      6.55E+00   0.0      -1.04E-06
  1   1     4   0.0      5.45E-03  5.46E-03   6.40E-03  1.19E-05  0.0      6.55E+00   0.0      -3.73E-09
  1   2     1   0.0      5.45E-03  5.46E-03   6.40E-03  1.19E-05  0.0      6.55E+00   0.0       1.09E-06   0.0       0.0       1.29E-04
  1   2     2   0.0      5.45E-03  5.46E-03   6.40E-03  1.19E-05  0.0      6.55E+00   0.0      -1.12E-08
  1   2     3   0.0      5.45E-03  5.46E-03   6.40E-03  1.19E-05  0.0      6.55E+00   0.0      -1.09E-06
  1   2     4   0.0      5.45E-03  5.46E-03   6.40E-03  1.19E-05  0.0      6.55E+00   0.0       1.12E-08
  1   3     1   0.0      5.45E-03  5.46E-03   6.40E-03  1.19E-05  0.0      6.55E+00   0.0       1.06E-06   0.0       0.0       1.29E-04
  1   3     2   0.0      5.45E-03  5.46E-03   6.40E-03  1.19E-05  0.0      6.55E+00   0.0      -9.31E-09
  1   3     3   0.0      5.45E-03  5.46E-03   6.40E-03  1.19E-05  0.0      6.55E+00   0.0      -1.06E-06
  1   3     4   0.0      5.45E-03  5.46E-03   6.40E-03  1.19E-05  0.0      6.55E+00   0.0       9.31E-09

ROD  AXIAL  THETA  RUPTURE  AXIAL      AXIAL ELONGATION      PELLET    PELLET    PELLET    GAP       CONTACT    RUPTURE
                   FLAG     NODE       PELLET    CLAD       CRACK     DISH      CHANFER   GAS       PRESSURE   FLAG
NO.  NO.    NO.             LENGTH     ( M )     ( M )      VOLUME    VOLUME    VOLUME    PRESSURE  (N/M2)
                            ( M )                           (M3)      (M3)      (M3)      (N/M2)
---  -----  -----  -------  --------   --------  --------   --------  --------  --------  --------  --------  --------
  1      1      1        0     0.1834   0.00171   0.00030   1.62E-08  0.0       6.21E-09  1.85E+05  7.19E+06         0
  1      1      2        0     0.1834   0.00175   0.00019   1.60E-08  0.0       6.23E-09  1.85E+05  5.34E+06         0
  1      1      3        0     0.1835   0.00179   0.00016   1.58E-08  0.0       6.18E-09  1.85E+05  4.75E+06         0
  1      1      4        0     0.1834   0.00175   0.00019   1.60E-08  0.0       6.23E-09  1.85E+05  5.34E+06         0
  1      2      1        0     0.1834   0.00171   0.00031   1.61E-08  0.0       6.15E-09  1.85E+05  7.99E+06         0
  1      2      2        0     0.1834   0.00175   0.00019   1.62E-08  0.0       6.32E-09  1.85E+05  4.63E+06         0
  1      2      3        0     0.1835   0.00180   0.00017   1.56E-08  0.0       6.09E-09  1.85E+05  5.59E+06         0
  1      2      4        0     0.1834   0.00175   0.00019   1.62E-08  0.0       6.32E-09  1.85E+05  4.64E+06         0
  1      3      1        0     0.1834   0.00171   0.00030   1.62E-08  0.0       6.20E-09  1.85E+05  7.40E+06         0
  1      3      2        0     0.1834   0.00175   0.00019   1.60E-08  0.0       6.24E-09  1.85E+05  5.16E+06         0
  1      3      3        0     0.1835   0.00179   0.00017   1.57E-08  0.0       6.16E-09  1.85E+05  4.96E+06         0
  1      3      4        0     0.1834   0.00175   0.00019   1.60E-08  0.0       6.25E-09  1.85E+05  5.17E+06         0

ROD  AXIAL  THETA ANGLE     CLADDING    CLADDING TOTAL STRAIN              CLADDING PLASTIC STRAIN          CLADDING  STRESS
                            OUTER
NO.  NO.    NO.             RADIUS      HOOP       AXIAL      RADIAL      HOOP       AXIAL      RADIAL     HOOP      AXIAL     EQUIVALENT
                   (RAD.)   ( M )       (M/M)      (M/M)      (M/M)       (M/M)      (M/M)      (M/M)      (N/M2)    (N/M2)    (N/M2)
---  -----  -----  -------  --------    --------   --------   --------    --------   --------   --------   --------  --------  --------
  1      1      3   0.7854   0.005931    0.0019     0.0017     0.0015      0.0        0.0        0.0        2.50E+07  4.73E+07  3.66E+07
  1      1      8   2.3562   0.005931    0.0019     0.0011     0.0017      0.0        0.0        0.0        1.34E+07 -4.73E+06  1.55E+07
  1      1     13   3.9270   0.005931    0.0019     0.0009     0.0018      0.0        0.0        0.0        9.65E+06 -1.78E+07  2.46E+07
  1      1     18   5.4978   0.005931    0.0019     0.0011     0.0017      0.0        0.0        0.0        1.34E+07 -4.59E+06  1.54E+07
  1      2      3   0.7854   0.005931    0.0020     0.0017     0.0015      0.0        0.0        0.0        3.01E+07  5.16E+07  3.97E+07
  1      2      8   2.3562   0.005931    0.0019     0.0010     0.0018      0.0        0.0        0.0        8.93E+06 -8.69E+06  1.53E+07
  1      2     13   3.9270   0.005931    0.0020     0.0009     0.0017      0.0        0.0        0.0        1.50E+07 -1.27E+07  2.38E+07
  1      2     18   5.4978   0.005931    0.0019     0.0010     0.0018      0.0        0.0        0.0        8.96E+06 -8.58E+06  1.53E+07
  1      3      3   0.7854   0.005931    0.0019     0.0017     0.0015      0.0        0.0        0.0        2.64E+07  4.85E+07  3.75E+07
  1      3      8   2.3562   0.005931    0.0019     0.0010     0.0017      0.0        0.0        0.0        1.22E+07 -5.93E+06  1.55E+07
  1      3     13   3.9270   0.005931    0.0019     0.0009     0.0018      0.0        0.0        0.0        1.10E+07 -1.66E+07  2.44E+07
  1      3     18   5.4978   0.005931    0.0019     0.0010     0.0017      0.0        0.0        0.0        1.23E+07 -5.86E+06  1.55E+07
```

Table B1 Sample output (Continued)

```
   HALDEN SHUTDOWN TEMPERATURE RESPONSE (D3 ROD, MODSHT=3)                    CPU TIME=   4.411    PAGE( 1/  11)

 TIME                          30.00000 (SECONDS)
 TIME STEP SIZE(NEW,OLD)        1.10593     1.80902 (SECONDS)

 ROD  ROD       FUEL      CLAD      PLENUM  TEMPERATURE   PLENUM VOLUME     ROD
 NO.  POWER     LENGTH    LENGTH    UPPER     LOWER      UPPER     LOWER    RUPTURE
      (W/M)     ( M )     ( M )     (DEG.K)   (DEG.K)    (MM**3)   (MM**3)  FLAG
 ---  --------  --------  --------  --------  --------   --------  --------  --------
   1  1133.347     0.546     1.001   514.029     0.0     42382.4       0.0     0

 ROD  AXIAL  THETA  LINEAR    FUEL      FUEL      CLAD      CLAD      GAPCON    HEAT      SURFACE   RADIANT   HEAT
 NO   NO.    NO.    HEAT      CENTER    SURFACE   INNER     OUTER     TOTAL     TRANSFER  HEAT      HEAT      TRANSFER
                     RATE      TEMP.     TEMP.     TEMP.     TEMP.               COEFF     FLUX      FLUX      MODE
                     (W/M)     (DEG.K)   (DEG.K)   (DEG.K)   (DEG.K)   (W/M2-K)  (W/M2-K)  (W/M2)    (W/M2)
 ---  -----  -----  --------  --------  --------  --------  --------  --------  --------  --------  --------  --------
   1      1      1    1133.3    611.43    575.18    520.04    516.12    1280.1   25683.7   60008.0       0.0         2
   1      1      2    1133.3    611.44    575.21    520.06    516.14    1280.1   25450.5   59979.0       0.0         2
   1      1      3    1133.3    611.44    575.19    520.06    516.14    1280.1   25464.1   60011.0       0.0         2
   1      1      4    1133.3    611.43    575.20    520.05    516.14    1280.1   25444.2   59974.0       0.0         2
   1      2      1    1133.3    611.51    575.31    520.27    516.36    1280.3   25661.2   59899.0       0.0         2
   1      2      2    1133.3    611.51    575.32    520.26    516.35    1280.3   25829.7   59870.0       0.0         2
   1      2      3    1133.3    611.51    575.31    520.26    516.35    1280.3   25817.2   59904.0       0.0         2
   1      2      4    1133.3    611.52    575.33    520.26    516.35    1280.3   25821.3   59882.0       0.0         2
   1      3      1    1133.3    611.45    575.28    520.24    516.33    1280.3   25955.8   59839.0       0.0         2
   1      3      2    1133.3    611.45    575.27    520.24    516.34    1280.3   25945.7   59860.0       0.0         2
   1      3      3    1133.3    611.45    575.27    520.25    516.34    1280.3   25948.1   59872.0       0.0         2
   1      3      4    1133.3    611.46    575.27    520.25    516.34    1280.3   25947.1   59876.0       0.0         2

 COOLANT CONDITION
INLET ENTHALPY  1.04E+06(J/KG)  OUTLET ENTHALPY  1.06E+06(J/KG)  AVERAGE ENTHALPY  1.04E+06(J/KG)  REFLOOD RATE 0.0     (M/SEC)

 AXIAL CHAN. COOLANT  SATU.    COOLANT   VOID      QUALITY   CRITICAL  COOLANT   MASS      CHANNEL   CHANNEL   HEATED    FLOW
 NO.   NO.   TEMP.    TEMP.    ENTHALPY  FRACTION            HEAT      PRESSURE  FLUX      FLOW      EQUI.     EQUI.     BLOCK
                                                             FLUX                          AREA      DIAMETER  DIAMETER  RATIO
       (DEG.K)  (DEG.K)  (J/KG)                 (W/M2)    (N/M2)    (KG/M2-S) (M2)      (M)       (M)
 -----  -----  --------  --------  --------  --------  --------  --------  --------  --------  --------  --------  --------
     1      1   513.78    514.03   1040677.    0.0      -0.0007  3208767.  3400000.   2500.00  1.37E-04  0.01369   0.01369   1.00000
     2      1   514.03    514.03   1042030.    0.0049    0.0001  3203921.  3400000.   2500.00  1.37E-04  0.01369   0.01369   1.00000
     3      1   514.03    514.03   1043381.    0.0399    0.0009  3199109.  3400000.   2500.00  1.37E-04  0.01369   0.01369   1.00000


   HALDEN SHUTDOWN TEMPERATURE RESPONSE (D3 ROD, MODSHT=3)                    CPU TIME=   4.415    PAGE( 2/  12)

 TIME                          30.00000 (SECONDS)

ROD AX THET  SURFACE RADIUS(AT TRANSIENT)                GAP      OXIDE    OXYGEN    REACTION  FUEL          ROD CENTER SHIFT          ROD
NO  NO NO    PELLET   PELLET    CLADDING   CLADDING      THICK.   FILM     CONTENT   HEAT AT   CENTER        ( X )     ( Y )     CROSS
             CENTER   SURFACE   INNER      OUTER         ( M )    THICK.             CLAD OUT  SHIFT                               SECTION
             ( M )    ( M )     ( M )      ( M )                  (MICRONS) (KG/M3)   (W/M2)    ( M )     ( M )     ( M )     ( M2 )
--- -- ----  -------- --------  --------   --------      -------- -------- --------  --------  --------  --------  --------  --------
  1  1    1  0.0      5.41E-03  5.46E-03   6.40E-03      4.86E-05 0.0      6.55E+00  0.0       -7.45E-08 0.0       0.0       1.29E-04
  1  1    2  0.0      5.41E-03  5.46E-03   6.40E-03      4.86E-05 0.0      6.55E+00  0.0        3.73E-09
  1  1    3  0.0      5.41E-03  5.46E-03   6.40E-03      4.86E-05 0.0      6.55E+00  0.0        7.45E-08
  1  1    4  0.0      5.41E-03  5.46E-03   6.40E-03      4.86E-05 0.0      6.55E+00  0.0       -3.73E-09
  1  2    1  0.0      5.41E-03  5.46E-03   6.40E-03      4.86E-05 0.0      6.55E+00  0.0       -4.84E-08 0.0       0.0       1.29E-04
  1  2    2  0.0      5.41E-03  5.46E-03   6.40E-03      4.86E-05 0.0      6.55E+00  0.0        3.73E-09
  1  2    3  0.0      5.41E-03  5.46E-03   6.40E-03      4.86E-05 0.0      6.55E+00  0.0        4.84E-08
  1  2    4  0.0      5.41E-03  5.46E-03   6.40E-03      4.86E-05 0.0      6.55E+00  0.0       -3.73E-09
  1  3    1  0.0      5.41E-03  5.46E-03   6.40E-03      4.86E-05 0.0      6.55E+00  0.0       -5.40E-08 0.0       0.0       1.29E-04
  1  3    2  0.0      5.41E-03  5.46E-03   6.40E-03      4.86E-05 0.0      6.55E+00  0.0       -3.73E-09
  1  3    3  0.0      5.41E-03  5.46E-03   6.40E-03      4.86E-05 0.0      6.55E+00  0.0        5.40E-08
  1  3    4  0.0      5.41E-03  5.46E-03   6.40E-03      4.86E-05 0.0      6.55E+00  0.0        3.73E-09

 ROD  AXIAL  THETA  RUPTURE  AXIAL      AXIAL ELONGATION          PELLET    PELLET    PELLET    GAP       CONTACT   RUPTURE
 NO.  NO.    NO.    FLAG     NODE       PELLET     CLAD           CRACK     DISH      CHANFER   GAS       PRESSURE  FLAG
                             LENGTH     ( M )      ( M )          VOLUME    VOLUME    VOLUME    PRESSURE  (N/M2)
                             ( M )                                (M3)      (M3)      (M3)      (N/M2)
 ---  -----  -----  -------  --------   --------   --------       --------  --------  --------  --------  --------  --------
   1      1      1        0    0.1821   0.00044    0.00017        6.23E-10  0.0       2.48E-10  1.81E+05  0.0           0
   1      1      2        0    0.1821   0.00044    0.00017        6.23E-10  0.0       2.46E-10  1.81E+05  0.0           0
   1      1      3        0    0.1821   0.00044    0.00017        6.23E-10  0.0       2.48E-10  1.81E+05  0.0           0
   1      1      4        0    0.1821   0.00044    0.00017        6.23E-10  0.0       2.48E-10  1.81E+05  0.0           0
   1      2      1        0    0.1821   0.00044    0.00017        6.22E-10  0.0       2.48E-10  1.81E+05  0.0           0
   1      2      2        0    0.1821   0.00044    0.00017        6.22E-10  0.0       2.48E-10  1.81E+05  0.0           0
   1      2      3        0    0.1821   0.00044    0.00017        6.23E-10  0.0       2.48E-10  1.81E+05  0.0           0
   1      2      4        0    0.1821   0.00044    0.00017        6.22E-10  0.0       2.48E-10  1.81E+05  0.0           0
   1      3      1        0    0.1821   0.00044    0.00017        6.22E-10  0.0       2.48E-10  1.81E+05  0.0           0
   1      3      2        0    0.1821   0.00044    0.00017        6.22E-10  0.0       2.48E-10  1.81E+05  0.0           0
   1      3      3        0    0.1821   0.00044    0.00017        6.22E-10  0.0       2.48E-10  1.81E+05  0.0           0
   1      3      4        0    0.1821   0.00044    0.00017        6.22E-10  0.0       2.48E-10  1.81E+05  0.0           0

 ROD AXIAL THETA ANGLE     CLADDING    CLADDING TOTAL STRAIN              CLADDING PLASTIC STRAIN            CLADDING  STRESS
                           OUTER
 NO. NO.   NO.             RADIUS      HOOP       AXIAL      RADIAL       HOOP       AXIAL      RADIAL      HOOP      AXIAL     EQUIVALENT
                   (RAD.)  ( M )       (M/M)      (M/M)      (M/M)        (M/M)      (M/M)      (M/M)       (N/M2)    (N/M2)    (N/M2)
 --- ----- -----  --------  --------    --------   --------   --------     --------   --------   --------    --------  --------  --------
   1     1     3    0.7854  0.005927    0.0013     0.0010     0.0016       0.0        0.0        0.0     -2.03E+07 -8.59E+06 1.38E+07
   1     1     8    2.3562  0.005927    0.0013     0.0010     0.0016       0.0        0.0        0.0     -2.03E+07 -8.59E+06 1.38E+07
   1     1    13    3.9270  0.005927    0.0013     0.0010     0.0016       0.0        0.0        0.0     -2.03E+07 -8.59E+06 1.38E+07
   1     1    18    5.4978  0.005927    0.0013     0.0010     0.0016       0.0        0.0        0.0     -2.03E+07 -8.59E+06 1.38E+07
   1     2     3    0.7854  0.005927    0.0013     0.0010     0.0016       0.0        0.0        0.0     -2.03E+07 -8.59E+06 1.38E+07
   1     2     8    2.3562  0.005927    0.0013     0.0010     0.0016       0.0        0.0        0.0     -2.03E+07 -8.59E+06 1.38E+07
   1     2    13    3.9270  0.005927    0.0013     0.0010     0.0016       0.0        0.0        0.0     -2.03E+07 -8.59E+06 1.38E+07
   1     2    18    5.4978  0.005927    0.0013     0.0010     0.0016       0.0        0.0        0.0     -2.03E+07 -8.59E+06 1.38E+07
   1     3     3    0.7854  0.005927    0.0013     0.0010     0.0016       0.0        0.0        0.0     -2.03E+07 -8.59E+06 1.38E+07
   1     3     8    2.3562  0.005927    0.0013     0.0010     0.0016       0.0        0.0        0.0     -2.03E+07 -8.59E+06 1.38E+07
   1     3    13    3.9270  0.005927    0.0013     0.0010     0.0016       0.0        0.0        0.0     -2.03E+07 -8.59E+06 1.38E+07
   1     3    18    5.4978  0.005927    0.0013     0.0010     0.0016       0.0        0.0        0.0     -2.03E+07 -8.59E+06 1.38E+07
```

Table B1 Sample output (Continued)

HALDEN SHUTDOWN TEMPERATURE RESPONSE (D3 ROD, MODSHT=3) CPU TIME= 4.310 PAGE(3/ 9)

ROD(1) 1AXIAL NODE 1 CIRCUM NODE

STP	TIME (SEC)	MH RUPT	L.H.R (W/M)	TCO (DEG.K)	TCI (DEG.K)	TFO (DEG.K)	TFI (DEG.K)	TB (DEG.K)	QUALT OR ZQ (M)	HCOEFF (W/M2.K)	GAPCON TOTAL (W/M2.K)	HEAT FLUX (W/M2)	RAD. FLUX (W/M2)	INNER PRESSURE (MN/M2)	COOLANT PRESSURE (MN/M2)	MASS FLUX (KG/M2/S)
76	-7.361	2 00	28000.	532.73	578.43	840.46	1518.88	514.03	0.003	38391.	3249.	718148.	0.	0.1849	3.4000	2500.
77	-4.625	2 00	28000.	532.75	578.00	844.10	1520.45	514.03	0.003	38006.	3168.	711378.	0.	0.1849	3.4000	2500.
78	-2.162	2 00	28000.	532.70	578.53	839.77	1518.96	514.03	0.003	38582.	3268.	720310.	0.	0.1849	3.4000	2500.
79	0.0	2 00	28000.	532.79	578.00	843.88	1519.96	514.03	0.003	37870.	3167.	710545.	0.	0.1849	3.4000	2500.
83	0.200	2 00	21455.	532.75	578.01	840.93	1517.89	514.03	0.003	38007.	3183.	711657.	0.	0.1849	3.4000	2500.
87	0.400	2 00	13975.	532.13	575.11	839.37	1511.79	514.03	0.003	37505.	2952.	679013.	0.	0.1849	3.4000	2500.
91	0.600	2 00	6495.	530.90	569.87	840.29	1501.51	514.03	0.003	36611.	2558.	617575.	0.	0.1849	3.4000	2500.
95	0.808	2 00	1820.	529.06	562.42	845.49	1487.11	514.03	0.002	35250.	2047.	529892.	0.	0.1849	3.4000	2500.
98	1.000	2 00	1820.	527.15	555.03	856.55	1473.23	514.03	0.002	33957.	1538.	445496.	0.	0.1848	3.4000	2500.
100	1.166	2 00	1817.	526.22	552.49	860.16	1460.89	514.03	0.002	33760.	1540.	411660.	0.	0.1848	3.4000	2500.
102	1.395	2 00	1812.	526.00	551.93	860.56	1443.54	514.03	0.002	33681.	1540.	403174.	0.	0.1847	3.4000	2500.
104	1.655	2 00	1806.	525.92	551.63	858.07	1423.55	514.03	0.001	33604.	1539.	399478.	0.	0.1846	3.4000	2500.
106	1.950	2 00	1799.	525.80	551.16	853.64	1400.18	514.03	0.001	33487.	1536.	394066.	0.	0.1845	3.4000	2500.
107	2.112	2 00	1795.	525.72	550.85	850.90	1387.10	514.03	0.001	33413.	1534.	390523.	0.	0.1845	3.4000	2500.
108	2.285	2 00	1791.	525.62	550.50	847.86	1373.15	514.03	0.001	33333.	1531.	386545.	0.	0.1844	3.4000	2500.
109	2.469	2 00	1787.	525.52	550.12	844.55	1358.50	514.03	0.001	33245.	1528.	382140.	0.	0.1844	3.4000	2500.
110	2.665	2 00	1782.	525.41	549.70	840.99	1342.88	514.03	0.001	33149.	1525.	377358.	0.	0.1843	3.4000	2500.
111	2.875	2 00	1777.	525.29	549.26	837.23	1326.24	514.03	0.001	33045.	1522.	372219.	0.	0.1843	3.4000	2500.
112	3.097	2 00	1772.	525.17	548.79	833.37	1308.92	514.03	0.001	32936.	1518.	366873.	0.	0.1842	3.4000	2500.
113	3.335	2 00	1767.	525.04	548.31	829.20	1290.98	514.03	0.001	32820.	1515.	361331.	0.	0.1842	3.4000	2500.
114	3.588	2 00	1761.	524.90	547.80	824.74	1271.97	514.03	0.001	32694.	1511.	355464.	0.	0.1841	3.4000	2500.
115	3.857	2 00	1754.	524.75	547.25	819.99	1252.28	514.03	0.001	32569.	1507.	349192.	0.	0.1840	3.4000	2500.
116	4.145	2 00	1748.	524.59	546.66	814.92	1232.16	514.03	0.001	32439.	1502.	342513.	0.	0.1839	3.4000	2500.
117	4.451	2 00	1740.	524.41	546.04	809.52	1211.20	514.03	0.001	32298.	1498.	335412.	0.	0.1839	3.4000	2500.
118	4.777	2 00	1733.	524.23	545.37	803.77	1189.55	514.03	0.001	32147.	1493.	327896.	0.	0.1838	3.4000	2500.
119	5.124	2 00	1725.	524.03	544.67	797.66	1167.54	514.03	0.001	31988.	1488.	319954.	0.	0.1837	3.4000	2500.
120	5.494	2 00	1716.	523.82	543.93	791.19	1144.66	514.03	0.001	31821.	1482.	311595.	0.	0.1836	3.4000	2500.
121	5.889	2 00	1707.	523.60	543.14	784.35	1121.58	514.03	0.001	31645.	1476.	302805.	0.	0.1835	3.4000	2500.
122	6.309	2 00	1697.	523.36	542.32	777.20	1097.95	514.03	0.001	31457.	1470.	293583.	0.	0.1834	3.4000	2500.
123	6.757	2 00	1686.	523.12	541.47	770.02	1073.63	514.03	0.001	31260.	1463.	284130.	0.	0.1833	3.4000	2500.
124	7.234	2 00	1675.	522.87	540.62	762.37	1049.49	514.03	0.001	31052.	1457.	274624.	0.	0.1832	3.4000	2500.
125	7.742	2 00	1663.	522.61	539.72	754.35	1024.55	514.03	0.001	30850.	1450.	264675.	0.	0.1831	3.4000	2500.
126	8.284	2 00	1651.	522.33	538.77	745.97	999.79	514.03	0.001	30635.	1442.	254211.	0.	0.1830	3.4000	2500.
127	8.861	2 00	1637.	522.04	537.79	737.23	974.75	514.03	0.000	30409.	1435.	243486.	0.	0.1829	3.4000	2500.
128	9.477	2 00	1623.	521.73	536.77	728.16	949.57	514.03	0.000	30171.	1427.	232391.	0.	0.1828	3.4000	2500.
129	10.132	2 00	1607.	521.41	535.73	718.80	924.75	514.03	0.000	29925.	1418.	221030.	0.	0.1827	3.4000	2500.
130	10.830	2 00	1591.	521.09	534.66	709.78	899.63	514.03	0.000	29670.	1410.	209454.	0.	0.1826	3.4000	2500.
131	11.574	2 00	1574.	520.78	533.66	700.29	875.46	514.03	0.000	29406.	1401.	198658.	0.	0.1825	3.4000	2500.
132	12.367	2 00	1555.	520.45	532.60	690.65	851.26	514.03	0.000	29158.	1393.	187311.	0.	0.1824	3.4000	2500.
133	13.212	2 00	1535.	520.11	531.53	680.86	827.71	514.03	0.000	28895.	1384.	175858.	0.	0.1822	3.4000	2500.
134	14.112	2 00	1514.	519.77	530.45	670.96	804.96	514.03	0.000	28623.	1375.	164445.	0.	0.1821	3.4000	2500.
135	15.071	2 00	1492.	519.41	529.36	661.03	782.44	514.01	-0.000	28342.	1366.	153140.	0.	0.1820	3.4000	2500.
136	16.093	2 00	1468.	519.04	528.26	651.68	761.41	513.98	-0.000	28059.	1356.	141938.	0.	0.1819	3.4000	2500.
137	17.182	2 00	1443.	518.70	527.28	642.30	741.11	513.96	-0.000	27777.	1348.	131859.	0.	0.1818	3.4000	2500.
138	18.342	2 00	1415.	518.36	526.27	633.08	721.38	513.93	-0.000	27520.	1339.	121710.	0.	0.1817	3.4000	2500.
139	19.578	2 00	1386.	518.02	525.30	624.05	703.38	513.91	-0.000	27256.	1331.	111885.	0.	0.1816	3.4000	2500.
140	20.895	2 00	1356.	517.68	524.35	615.33	686.32	513.89	-0.000	26996.	1323.	102377.	0.	0.1815	3.4000	2500.
141	22.298	2 00	1323.	517.36	523.44	606.94	670.10	513.87	-0.000	26744.	1314.	93368.	0.	0.1813	3.4000	2500.
142	23.794	2 00	1288.	517.05	522.58	598.96	655.06	513.85	-0.000	26501.	1306.	84873.	0.	0.1813	3.4000	2500.
143	25.387	2 00	1251.	516.76	521.78	591.96	641.78	513.83	-0.001	26269.	1299.	76942.	0.	0.1812	3.4000	2500.

+++ TIMTEM (S)= 2.84 TIMDEF (S)= 0.94

HALDEN SHUTDOWN TEMPERATURE RESPONSE (D3 ROD, MODSHT=3) CPU TIME= 4.410 PAGE(4/ 10)

ROD(1) 1AXIAL NODE 1 CIRCUM NODE

STP	TIME (SEC)	MH RUPT	L.H.R (W/M)	TCO (DEG.K)	TCI (DEG.K)	TFO (DEG.K)	TFI (DEG.K)	TB (DEG.K)	QUALT OR ZQ (M)	HCOEFF (W/M2.K)	GAPCON TOTAL (W/M2.K)	HEAT FLUX (W/M2)	RAD. FLUX (W/M2)	INNER PRESSURE (MN/M2)	COOLANT PRESSURE (MN/M2)	MASS FLUX (KG/M2/S)
144	27.085	2 00	1211.	516.51	521.10	585.11	629.41	513.81	-0.001	26050.	1292.	70313.	0.	0.1811	3.4000	2500.
145	28.894	2 00	1169.	516.26	520.43	578.77	617.94	513.80	-0.001	25862.	1286.	63785.	0.	0.1810	3.4000	2500.
146	30.000	2 00	1133.	516.12	520.04	575.18	611.43	513.78	-0.001	25684.	1280.	60008.	0.	0.1809	3.4000	2500.

+++ TIMTEM (S)= 2.89 TIMDEF (S)= 0.96